Spring 1-1-2021

Synthesis, Characterization, And Catalytic And Biological Activities of A Mixed-ligand Cobalt(ii) Bipyridyl/diphenylazodioxide Complex

Kylin A. Emhoff
Cleveland State University

Recommended Citation

Emhoff, Kylin A., "Synthesis, Characterization, And Catalytic And Biological Activities of A Mixed-ligand Cobalt(ii) Bipyridyl/diphenylazodioxide Complex" (2021). *ETD Archive*. 1205.
https://engagedscholarship.csuohio.edu/etdarchive/1205

SYNTHESIS, CHARACTERIZATION, AND CATALYTIC AND BIOLOGICAL ACTIVITIES OF A MIXED-LIGAND COBALT(II) BIPYRIDYL/DIPHENYLAZODIOXIDE COMPLEX

KYLIN A. EMHOFF

Bachelor of Science in Chemistry
Cleveland State University
May 2016

Submitted in partial fulfillment of requirements for the degree
DOCTOR OF PHILOSOPHY IN CLINICAL-BIOANALYTICAL CHEMISTRY
at the
CLEVELAND STATE UNIVERSITY
May 2021

We hereby approve this dissertation for

KYLIN ALICE EMHOFF

Candidate for the Doctor of Philosophy in Clinical-Bioanalytical Chemistry degree

for the Department of Chemistry

and CLEVELAND STATE UNIVERSITY'S

College of Graduate Studies by

Committee Chairperson, W. Christopher Boyd
Department of Chemistry, April 13, 2021

Thesis Committee Member, Dr. Mekki Bayachou
Department of Chemistry, April 13, 2021

Thesis Committee Member, Dr. Andrew Resnick
Department of Physics, April 13, 2021

Thesis Chairperson, Dr. Bin Su
Department of Chemistry, April 13, 2021

Thesis Committee Member, Dr. Xue-Long Sun
Department of Chemistry, April 13, 2021

Thesis Committee Member, Dr. Aimin Zhou
Department of Chemistry, April 13, 2021

Student's Date of Defense: April 13, 2021

DEDICATION

Dedicated to my parents

In loving memory of my father Lee Strmac,

who would have been proud to see me pursue my dreams

and

my grandmother Bunny Becker,

who was always loving and supportive of my accomplishments

ACKNOWLEDGEMENTS

First and foremost, I would like to sincerely thank my advisor, Dr. Chris Boyd, for allowing me to gain valuable research experience in his lab first as an undergraduate and then as a Ph.D. student. Thank you for always being a dedicated, patient, supportive, and understanding mentor. I admire your immense passion for chemistry, which always motivated me to work hard in the lab and will continue to inspire me to grow as a scientist. I will value all the lessons you have taught me. Lastly, thank you for encouraging me to have more confidence in myself, especially during times when I would be self-critical.

I would also like to thank my dissertation committee members. Thank you to Dr. Mekki Bayachou and Dr. Aimin Zhou for their willingness to collaborate with us to help achieve certain goals of our research, which led to the publication of two papers. These collaborations have not only allowed me to gain collaborative skills but also gain experience in other disciplines of chemistry. Thank you to Dr. Andrew Resnick, Dr. Bin Su, and Dr. Xue-Long Sun for all their invaluable feedback they gave me in ways to improve my research and my writing skills. I feel I have greatly improved in my research and writing skills throughout the course of my Ph.D.

A special thank you goes out to the other collaborators of my research. Thank you to Dr. Wiley Youngs and his former Ph.D. student Dr. Michael Stromyer from The University of Akron for determining the crystal structure of my novel azodioxide complex, which led to my first paper publication. Thank you to Dr. David Tierney and Dr. Robert McCarrick from Miami University for allowing us to use their EPR spectrometer to acquire useful EPR spectra and for their EPR expertise in helping us interpret our EPR spectra. Thank you to Dr. Jerry Mundell for his willingness to collaborate with us in acquiring and interpreting electrochemical measurements. Lastly, thank you to Dr. Norah Alghamdi and Dr. Ruhan Wei, former Ph.D. students from Dr. Aimin Zhou's group, for conducting biological studies on my novel azodioxide complex.

I would also like to thank my labmates. A special thank you to Lakshmi for mentoring and befriending me in the Boyd lab when I was an undergraduate. Thank you to Ahmed for always willing to lend a helping hand. Thank you to former undergraduate labmates Sydney Simpson, Drew Kingery, and Teya Eshelman for assisting me in completing certain experiments for my research project.

A special thanks to my best friend, Kelsey, for always being loyal and believing in me, for our weekly facetime chats and our get-togethers, and for teaching me to always look at the positive side of any situation.

Lastly, I would like to give my sincerest gratitude to my family, especially my parents Rhonda and Paul. I truly appreciate them for putting up with me and for reminding me to take care of myself sometimes. Their continuous support and encouragement have and will continue to motivate me to keep growing as a scientist and to inspire women to pursue careers in STEM.

SYNTHESIS, CHARACTERIZATION, AND CATALYTIC AND BIOLOGICAL ACTIVITIES OF A MIXED-LIGAND COBALT(II) BIPYRIDYL/DIPHENYLAZODIOXIDE COMPLEX

KYLIN A. EMHOFF

ABSTRACT

Transition metal complexes have immense importance in the pharmaceutical industry. These types of complexes can be useful catalysts in the synthesis of medicinal compounds and can act as anticancer drugs. In these pharmaceutical applications, 1st-row transition metal-containing complexes offer certain advantages compared to their 2nd and 3rd-row transition metal counterparts. Our motivation was to investigate pharmaceutical applications of transition metal complexes containing both a 1st-row transition metal *and* unusual ligands to expand the knowledge of a class of complexes that could potentially be beneficial in the pharmaceutical industry. A class of rare ligands that piqued our interest was that of the diaryl azodioxides, *cis*-Ar(O)NN(O)Ar, which belong to the wider class of organic derivatives of nitric oxide (NO). Our synthesis and pharmaceutical applications of the azodioxide complex salt $[Co(bpy)\{Ph(O)NN(O)Ph\}_2](PF_6)_2$ have been able to significantly expand the knowledge of azodioxide complexes by displaying an unusual trigonal prismatic coordination geometry for cobalt(II) with only bidentate ligands, showing evidence of ligand-based redox activity, acting as an active catalyst in allylic amination/C–C double-bond transposition reactions, and selectively inducing apoptosis in SK-HEP-1 human liver adenocarcinoma cells. Importantly, catalytic and biological studies of $[Co(bpy)\{Ph(O)NN(O)Ph\}_2](PF_6)_2$ are ongoing, and focused on its potential for use in the pharmaceutical industry as a drug or catalyst for drug synthesis. Future work will

involve comparing the catalytic and biological activities of $[Co(bpy)\{Ph(O)NN(O)Ph\}_2](PF_6)_2$ with other azodioxide complexes prepared by our group to identify structure-activity relationships and inform the design of more efficient catalysts and anti-cancer, pro-apoptotic agents.

TABLE OF CONTENTS

LIST OF TABLES

LIST OF FIGURES

CHAPTER I

INTRODUCTION

1.1 Transition Metal Complexes as Catalysts in the Pharmaceutical Industry

Transition metal complexes have immense importance in the pharmaceutical industry. In particular, some transition metal complexes can be useful catalysts for the synthesis of drugs or other medically relevant compounds. The benefits of catalysis include a smaller number of synthetic steps, a reduction in the amount of waste produced, and a decrease in both reaction times and the amounts of reagents used. It has been estimated that about 90% of commercially-derived pharmaceuticals in the industry are produced using catalysis, and catalysis allows a pharmaceutical company to strengthen its product worth while reducing the carbon footprint of its processes. Processes that involve catalysis by transition metal complexes have been applied widely in the pharmaceutical industry, for the past 30 years in particular. Examples of transition metal-catalyzed reactions in the pharmaceutical industry include (but are not limited to) asymmetric hydrogenation, alkene metathesis, carbon-carbon (C–C) or carbon-heteroatom (C–X, where "X" is a heteroatom) cross-coupling reactions, and allylic amination. Specifically, transition metal-catalyzed processes have been applied in both discovery syntheses and large-scale active pharmaceutical ingredient (API) syntheses. Transition metal catalysts allow for the highly efficient preparation of target molecules by imparting chemo-, regio-, and stereoselectivity to reactions.[1] An especially important distinguishing feature of transition metal catalysts in the pharmaceutical industry is their ability to impart enantioselectivity, which involves the selective synthesis of one enantiomer of a chiral product from achiral reagents.[2] It is very important to note that often only one of a drug's enantiomers is considered safe and effective.

1.1.1 Use of 1st-Row Transition Metals as Catalysts

Although most transition metal-catalyzed processes in the pharmaceutical industry involve the use of 2nd- or 3rd-row transition metals such as palladium, ruthenium, and iridium, there are important advantages to utilizing 1st-row transition metals as catalysts. Firstly, 1st-row transition metal catalysts are cheaper to use compared to 2nd and 3rd-row transition metal catalysts, making 1st-row transition metal catalysts more cost-effective. Moreover, 1st-row transition metals are more Earth-abundant than 2nd- or 3rd-row transition metals, meaning that the use of 1st-row transition metals are more environmentally friendly.[3] An additional advantage of employing 1st-row transition metal catalysts is their ability to undergo oxidation state changes by one unit, which can be useful in the catalysis of radical reactions. In contrast, 2nd- and 3rd-row transition metal catalysts more often undergo changes of oxidation state by two units.

The use of 1st-row transition metal catalysts has thus far shown promise and potential in the pharmaceutical industry. For example, Abbott Laboratories has shown copper(I) chloride (CuCl) to be an active catalyst in a C–N cross-coupling reaction involved as a key step in the kilogram-scale synthesis of an H_3 receptor antagonist used to treat attention deficit hyperactivity disorder (ADHD).[4] Additionally, the State Key

Laboratory of Drug Research in China has shown that the nickel complex $NiCl_2$(dppp) (where dppp = 1,3-bis(diphenylphosphino)propane) is a useful catalyst in a Kumada-Corriu coupling reaction that is considered a key step in the overall synthesis of atazanavir,[5] a drug used to treat HIV/AIDS that is on the World Health Organization's (WHO) List of Essential Medicines as of 2019.[6] The Chirik group, in collaboration with the pharmaceutical company Merck, has demonstrated the ability of the simple cobalt compound $CoCl_2 \cdot 6H_2O$ and the chiral phosphine ligand (Ph-BPE-*R*,*R*) to form an *in situ* catalyst that has shown to be enantioselective in the asymmetric hydrogenation of an enamide that yields the anticonvulsant levetiracetam in 98.2% ee (enantiomeric excess).[3,7] The iron complex $Fe(acac)_2$ (where acac = acetylacetonate) has been reported as an efficient stereoselective catalyst in a C–C cross-coupling reaction that is a key step in the synthesis of sitagliptin,[8] a medication used to treat type 2 diabetes. Lastly, the iron complex $Fe(CO)_3\{\eta^4\text{-}(CH_2)_4(SiMe_3)_2C_5O\}$ has proven to be an active catalyst in a nucleophilic allylic substitution reaction that yields the drug cinnarizine,[9,10] which is an antihistamine used to treat motion sickness.

1.2 Transition Metal Complexes in Medicine

In addition to the use of transition metal complexes as catalysts in the pharmaceutical industry, transition metal complexes have also shown the ability to act as pharmaceuticals themselves. Although most currently approved drugs are organic molecules,[11] bioinorganic chemists have been increasingly interested in the potential of transition metal complexes to act as drugs.[12] Unlike purely organic molecules, transition metal complexes have unique features that make them have a great deal of pharmaceutical potential, especially as anti-cancer therapeutics. These features include the ability of transition metal ions to be involved in biological redox reactions, the possibility of transition metals to display a wide range of coordination geometries and coordination numbers, the varied reactivity that transition metal compounds display toward organic substrates,[12] and the potential for transition metal complexes to demonstrate stereoisomerism at their metal centers.[13] Because of these unique features, transition metal-containing drugs can display mechanisms of action that are vastly different from organic molecules, ultimately leading to different types of transport pathways and novel drug targets. Therefore, drugs containing transition metals have the potential to overcome resistances to organic drugs developed by pathogens or cancer cells.[11,14]

1.2.1 Use of 1st-Row Transition Metals as Drugs

Most approved or promising transition metal-containing drugs contain 2nd- or 3rd-row transition metals, with perhaps the most important example being the platinum-containing anticancer drug cisplatin, *cis*-$Pt(NH_3)_2Cl_2$.[15] However, there has recently been an increasing interest in developing 1st-row transition metal-containing pharmaceuticals, due to their greater cost-effectiveness and Earth-abundance. Additionally, 1st-row transition metals are generally less toxic than 2nd- and 3rd-row transition metals, although there are some notable exceptions to this claim: some nickel compounds, the most infamous example being $Ni(CO)_4$, and many chromium(VI) compounds are toxic and carcinogenic, while many silver and gold compounds are considered fairly harmless.[16]

An example of a promising drug candidate that contains a 1st-row transition metal is the vanadium complex [bis(ethylmaltolato)oxovanadium(IV)] (BEOV). Orvig and coworkers have been able to show the potential of this complex in the treatment of diabetes, especially type 2,[11,17,18] by successfully completing a small phase II clinical trial in which fasting blood glucose and HbA_{1c} (glycated hemoglobin) levels were shown to be overall reduced in a range from 10% to 40% in 5 out of 7 type 2 diabetes patients.[18] Furthermore, hydroxycobalamin and cyanocobalamin, which are two forms of vitamin B_{12} (a vitamin that is essential in the formation of red blood cells, DNA synthesis, metabolism of cells, and nerve function[19]) and which both contain cobalt, are well known and widely used in medicine. More specifically, hydroxycobalamin, which is on the WHO List of Essential Medicines as of 2019,[6] is known for treating vitamin B_{12} deficiency[11] and cyanide poisoning,[20] whereas cyanocobalamin treats only vitamin B_{12} deficiency.[11] Another example of a cobalt-containing complex that has shown pharmaceutical potential is Doxovir, also known as CTC-96 or [bis(2-methylimidazole)[bis(acetylacetone)(ethylenediimine)]cobalt(III). Doxovir has shown promising antiviral activity by successfully completing phase II clinical trials for the treatment of the herpes simplex virus.[11,21] Moreover, doxovir has shown potential antiviral activity in the treatment of ophthalmic herpetic keratitis[22] and adenoviral conjunctivitis[23] (viral eye infections) by successfully completing phase I clinical trials.[11] The iron complex 7-chloro-*N*-(2-((dimethylamino)methyl)ferrocenyl)quinolin-4-amine, or ferroquine, has proven to be a promising organometallic drug candidate in the treatment of malaria.[11,24,25] Specifically, ferroquine has shown antimalarial activity at concentrations in the nanomolar range against both chloroquine-susceptible and chloroquine-resistant *Plasmodium falciparum*, which is the parasite that causes the deadliest form of malaria. (Note: chloroquine is a purely organic drug used to treat malaria.) Ferroquine as an antimalarial agent is currently in the process of undergoing phase II clinical trials.[25] Lastly, the iron-containing drug sodium nitroprusside, $Na_2[Fe(CN)_5NO]$, is already a widely used drug in the treatment of hypertension[11,26] and is on the WHO List of Essential Medicines as of 2019.[6] The medicinal use of sodium nitroprusside is discussed further in Section 1.4.2.

1.3 Motivation of Research Project

We were motivated to investigate the potential pharmaceutical applications of novel 1st-row transition metal complexes, in particular the medicinal potential of transition metal complexes containing both a 1st-row transition metal *and* unusual ligands that have not previously been widely studied. In this way, we could expand the knowledge of a class of complexes that could potentially be beneficial in the pharmaceutical industry. A class of rare ligands that piqued our interest is that of the diaryl azodioxides, *cis*-Ar(O)NN(O)Ar, which belong to the wider class of organic derivatives of nitric oxide (NO).

1.4 Nitric Oxide (NO)

1.4.1 NO in the Immune and Nervous Systems

Nitric oxide (NO) is a diatomic free radical with several roles in the human body. Firstly, NO has important roles in the immune and nervous systems. In the immune system, NO demonstrates antitumor, antimicrobial, and cytotoxic activity, which involves the generation of reactive oxygen species (ROS), which then lead to inactivation of enzymes and the modification of proteins, ultimately killing pathogens such as bacteria, fungi, and viruses, as well as tumor cells. In the nervous system, NO acts as a neurotransmitter by regulating the intake of nutrients, perception of pain, and blood flow to the brain.[27]

1.4.2 NO in Vasodilation

A particularly important physiological role of NO is its ability to induce vasodilation, a process that involves the widening of blood vessels, thus lowering blood pressure and increasing blood flow. Vasodilation occurs when NO activates the heme enzyme soluble guanylate cyclase (sGC), which is responsible for the catalytic transformation of guanosine triphosphate (GTP) to cyclic guanosine monophosphate (cGMP),[28,29] and the formation of cGMP as a secondary messenger molecule signals the smooth muscle in blood vessels to relax, which leads to a decrease in blood pressure. Without NO, sGC would be inactive and the formation of cGMP would not occur. The role of NO as a vasodilator was discovered by Robert Furchgott, Louis Ignarro, and Ferid Murad, who shared the Nobel Prize in Physiology or Medicine in 1998 for this discovery.[28]

The role of NO in vasodilation has been widely exploited in medicine. The organic drugs amyl nitrite and nitroglycerin are examples of vasodilators that are known for treating angina in people who have coronary artery disease. Amyl nitrite and nitroglycerin release NO into the body when reacting with physiological thiols.[28] In addition to amyl nitrite and nitroglycerin, the iron-containing drug sodium nitroprusside, $Na_2[Fe(CN)_5NO]$, which was briefly mentioned in Section 1.2.1, also acts as an antihypertensive drug.[13,26,28] However, unlike amyl nitrite and nitroglycerin, sodium nitroprusside releases NO gradually into the body on its own.[28] Sodium nitroprusside can also be taken by surgical patients in order to reduce bleeding during surgery.[30] Importantly, sodium nitroprusside and nitroglycerin are on the WHO List of Essential Medicines as of 2019.[6] Another important vasodilator worth mentioning is sildenafil (Viagra). Unlike the other vasodilators mentioned thus far, sildenafil does not release NO into the body, either directly or indirectly. Rather, sildenafil acts as a vasodilator by inhibiting cGMP degradation and thus indirectly increasing the activity of the NO generated by the body.[31]

1.4.3 NO as a Ligand in Coordination Chemistry

The involvement of NO in vasodilation is due to the ability of NO to bind to transition metals as a ligand. In particular, NO binds to the heme iron center in sGC, which causes the histidine ligand in the axial position *trans* to NO to dissociate, hence leading to a change in the conformation of sGC. This altered conformation is what activates sGC to catalyze cGMP formation.[29,32] When NO is bound to transition metals, it is referred to as the nitrosyl ligand and can coordinate to transition metals in either a linear or bent fashion. When NO coordinates to a transition metal in the linear binding mode, it acts as a three-electron donor in its neutral form or as a two-electron donor in the ionic form NO^+ (isoelectronic with the well-known π-acceptor ligands CO and CN^-). On the other hand, when NO coordinates to a transition metal in the bent binding mode, it acts as a one-electron donor in its neutral form or as a two-electron donor in the ionic form NO^-.[32,33] These linear and bent binding modes of the nitrosyl ligand to a transition metal are depicted in Figure 1 ("M" represents a generic transition metal).

Importantly, NO is able to behave as a redox-active ligand in transition metal complexes, in that the conversion from the linear coordination mode to the bent coordination mode involves an increase in a metal's oxidation state by two and a decrease in its overall electron count by two, along with the opening of a binding site. In fact, some transition metal complexes containing the NO ligand in the linear geometry can exist in equilibrium with those containing the NO ligand in the bent geometry. This usually happens when the energy difference between the two binding modes is small and can be thought of as an electron-transfer process from the metal to the NO ligand. Figure 2 shows a cobalt complex with an NO ligand in the linear geometry in equilibrium with the same complex containing the NO ligand in the bent geometry. This redox-active behavior of NO has been employed in catalysis.[34]

Linear **Bent**

Figure 1: Linear and bent modes of coordination of NO ligand.

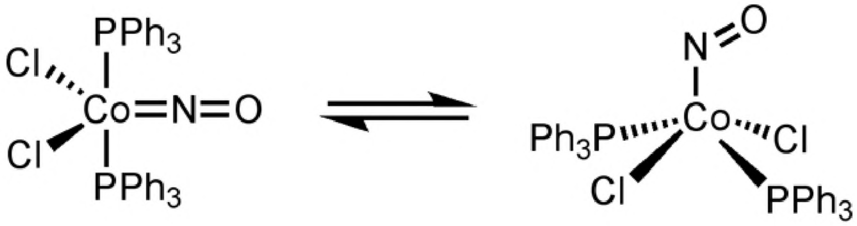

Co(I), 18e⁻ complex **Co(III), 16e⁻ complex**

Figure 2: Conversion from linear NO to bent NO in a transition metal complex.

1.5 *N,N'*-Azodioxides

Though the coordination chemistry of NO is well established, there is a comparative paucity of information regarding the coordination chemistry of organic derivatives of NO,[33,35] particularly the nitrosoarenes (ArNO). (When NO is a substituent in an organic molecule, it is referred to as the nitroso group.) Nitrosoarenes can undergo dimerization to form *cis*- and *trans*-*N,N'*-azodioxides as shown in Figure 3. Whether a nitrosoarene dimerizes or not depends on its aryl group. The aryl group of the nitrosoarene also dictates whether the dimer will be favored in the *cis* or the *trans* form. Monomeric nitrosoarenes are generally favored in the solution phase, whereas dimeric azodioxides are favored in the solid phase.[33,35]

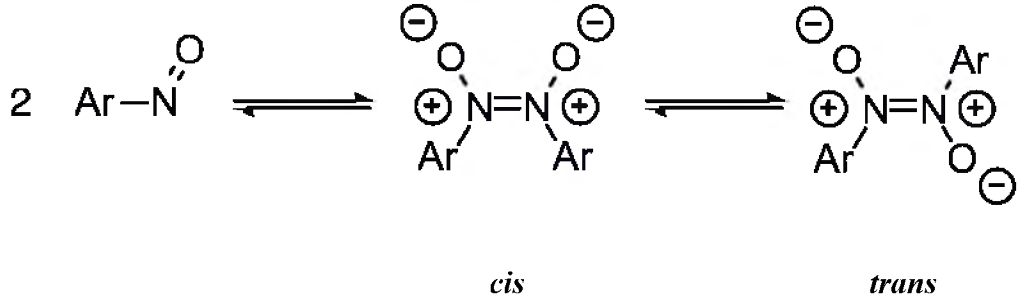

Figure 3: Dimerization of nitrosoarenes to dimeric *N,N′*-azodioxides.

Of the *cis*- and *trans*-*N,N′*-azodioxides that result from dimerization, the *cis* form is of particular interest because it can act as a bidentate (two points of attachment) chelating ligand, forming a five-membered ring with a metal center; such five-membered chelate rings are frequently especially stable because they have very low ring strain.[36] Figure 4 shows how a generic *cis*-*N,N′*-azodioxide coordinates to a generic metal (M). In general, metal complexes with chelating ligands like *cis*-*N,N′*-azodioxides are more stable than metal complexes with monodentate (one point of attachment) ligands like ArNO that bind to metals through O atoms. The greater stability of metal complexes possessing chelating ligands can be explained by the thermodynamic and kinetic chelate effects. Regarding thermodynamics, an increase in entropy occurs when chelating ligands replace similar monodentate ligands because the total number of molecules increases in such a reaction. The kinetic chelate effect refers to the fact that as soon as one of the donor atoms of a chelating ligand binds to a metal, it is likely the other donor atom(s) of the chelating ligand will rapidly bind to the metal due to their close proximity.[36]

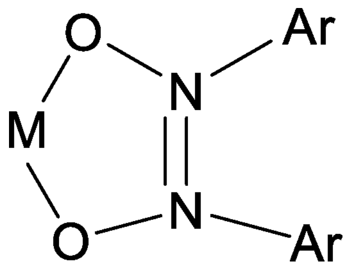

Figure 4: *cis*-*N*,*N'*-azodioxide coordinated to a metal.

More specifically, this project concentrates on the coordination chemistry of a prototypic ligand of the azodioxide group, *cis*-*N*,*N'*-diphenylazodioxide, Ph(O)NN(O)Ph, which is formed from the dimerization of nitrosobenzene (PhNO); notably, the *cis*-diastereomer of Ph(O)NN(O)Ph is favored in the solid state.[33,37] A plausible explanation for why Ph(O)NN(O)Ph is favored in the *cis* form is that this isomer's polar structure may lead to the formation of crystals that are more thermodynamically stable due to dipole-dipole attractions between neighboring molecules. In addition to *cis*-Ph(O)NN(O)Ph possessing chelating ability, its N–O and N–N bond lengths, which were obtained from its crystal structure,[37] correspond to significant π delocalization. This delocalization is depicted by the resonance structures in Figure 5 and can be viewed as analogous to that of the 1,3-butadiene dianion.

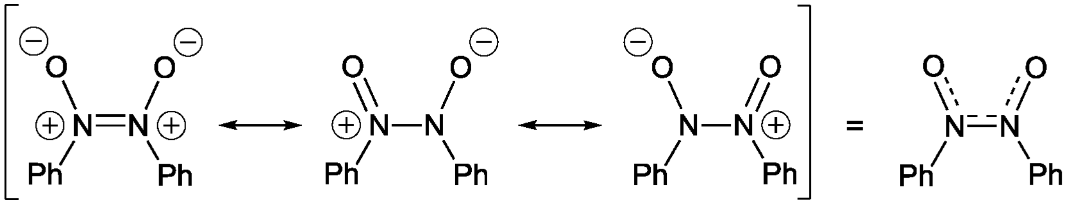

Figure 5: Resonance structures of *cis*-Ph(O)NN(O)Ph.

1.6 Azodioxide Complexes

Despite the stability of azodioxide complexes suggested by the presence of a chelating ligand with significant π delocalization, only five crystallographically characterized azodioxide metal complexes have thus far been reported in the literature. Additionally, spectroscopically characterized azodioxide complexes such as those of the form $MCl_4\{Ph(O)NN(O)Ph\}$ (M = Sn, Ti),[38] $[R_2Pb\{R(O)NN(O)R\}](NO_3)_2$ (R = Me, Et),[39] and $[Me_2Sn\{Me(O)NN(O)Me\}](NO_3)_2$[40] have been reported, although none of their crystal structures were determined. It is possible that azodioxide complexes are as rare as they are because PhNO tends to exist as a dimer in the solid phase but as a monomer in the solution phase, thus making solution-phase synthesis of complexes of the dimer more difficult.[33,37]

1.6.1 Structurally Characterized Azodioxide Complexes Prior to Our Work

Of the five structurally characterized azodioxide complexes reported in the literature, three of these complexes were reported prior to our work. One of these complexes is the scandium(III), d^0 (no valence *d* electrons) complex[41] $Sc(OTf)_3(H_2O)_2\{Ar(O)NN(O)Ar\}$ (Ar = $2\text{-}MeOC_6H_4$ and OTf = OSO_2CF_3), whose structure is shown in Figure 6. This scandium azodioxide complex has shown reactivity by undergoing a reaction with 1,3-cyclohexadiene to yield a hetero-Diels-Alder adduct with $(2\text{-}MeOC_6H_4)NO$, which is the monomeric form of its corresponding dimeric azodioxide ligand. A second azodioxide complex that was reported prior to our work is the calcium(II) (main group metal) complex salt[42] $[Ca\{Ph(O)NN(O)Ph\}(H_2O)_2(THF)_3]I_2$, whose structure is shown in Figure 7. To the best of our knowledge, the reactivity of this calcium azodioxide complex has not been investigated. The last azodioxide complex to mention that was reported prior to our work is the salt of an iron(II), d^6 complex cation with iron(III) complex anions[43] $[Fe\{Ph(O)NN(O)Ph\}_3](FeCl_4)_2$, which has been shown to be a competent catalyst for allylic amination/C–C double-bond transposition reactions of alkenes with hydroxylamines.[44]

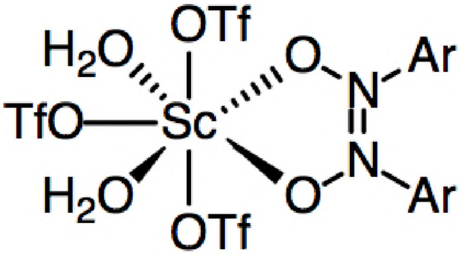

Figure 6: Structure of $Sc(OTf)_3(H_2O)_2$ {Ar(O)NN(O)Ar}.

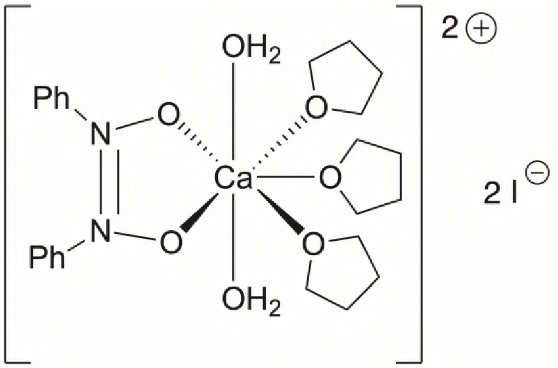

Figure 7: Structure of [Ca{Ph(O)NN(O)Ph}$(H_2O)_2(THF)_3]I_2$.

The transition metal complex salt [Fe{Ph(O)NN(O)Ph}$_3$]$(FeCl_4)_2$ was of particular interest to our group because, prior to our work, it was the only crystallographically characterized, non-d^0 azodioxide transition metal complex salt reported in the literature. The synthesis of [Fe{Ph(O)NN(O)Ph}$_3$]$(FeCl_4)_2$ was conducted by Nicholas and coworkers[43] and is shown in Figure 8a. It is evident that the reaction depicted in Figure 8a is not balanced, as this reaction yields a mixture of byproducts in addition to the complex salt. Given the fact that the complex salt contains an Fe(II) complex cation and an Fe(III) complex anion, it is very likely that PhNO or its dimeric form acts as an oxidizing agent, oxidizing some Fe(II) in $FeCl_2$ to Fe(III). This is supported by the GC-MS detection of the reduced organic products azoxybenzene, Ph(O)NNPh, and azobenzene, PhNNPh, in the reaction mixture. Moreover, while conducting the synthesis of [Fe{Ph(O)NN(O)Ph}$_3$](FeCl$_4$)$_2$, Nicholas' group also observed a rust-brown precipitate, which is likely iron(III) oxide (Fe_2O_3).[43] A proposed balanced reaction equation for the synthesis of [Fe{Ph(O)NN(O)Ph}$_3$](FeCl$_4$)$_2$ in which PhNO or its dimer is undergoing only partial deoxygenation is depicted in Figure 8b. (A similar reaction equation could be written for the complete deoxygenation of PhNO or its dimer to form azobenzene.) Furthermore, the six-coordinate Fe(II) complex cation shown in Figures 8a and 8b displays a trigonal prismatic coordination geometry (much less common than an octahedral geometry for six-coordinate metal complexes) and has N–O and N–N bond lengths that are similar to those in *cis*-Ph(O)NN(O)Ph and that suggest that substantial π delocalization is preserved upon coordination.[43]

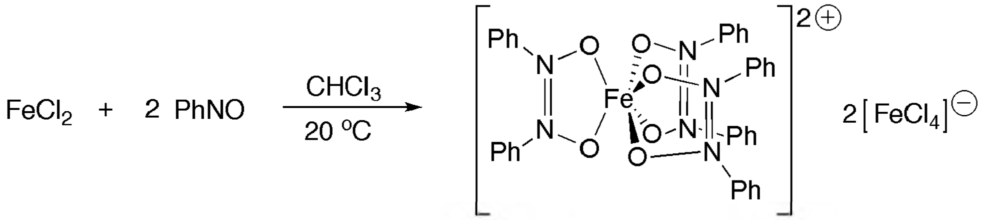

Figure 8a: Synthesis of [Fe{Ph(O)NN(O)Ph}$_3$](FeCl$_4$)$_2$.

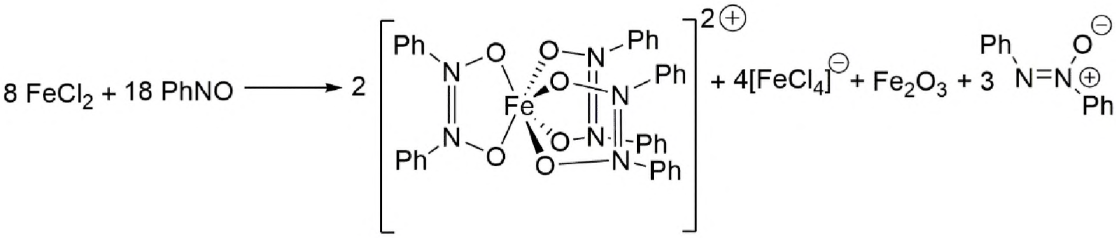

Figure 8b: Proposed balanced reaction equation for the synthesis of [Fe{Ph(O)NN(O)Ph}$_3$](FeCl$_4$)$_2$.

1.6.2 Homoleptic Cobalt(II) Azodioxide Complex in the Boyd Group

In addition to the three azodioxide complexes that have been structurally characterized prior to our group's work, I (as an undergraduate student) assisted a former graduate student in the Boyd research group, Dr. Lakshmi Balaraman (Ph.D. May 2019), on the preparation of the novel, homoleptic (only one type of ligand) cobalt(II) azodioxide complex $[Co\{Ph(O)NN(O)Ph\}_4](PF_6)_2$, which was the first azodioxide complex crystallographically characterized by our group. The synthesis and characterization of $[Co\{Ph(O)NN(O)Ph\}_4](PF_6)_2$ has been published in *ACS Omega*.[45] The synthesis of $[Co\{Ph(O)NN(O)Ph\}_4](PF_6)_2$ is shown in Figure 9.

It is important to note that $[Co\{Ph(O)NN(O)Ph\}_4]^{2+}$ has an unusually high coordination number of eight with a distorted tetragonal coordination geometry. Most Co(II) complexes are either tetrahedral or octahedral.[46] There are only a few examples in the literature of eight-coordinate monometallic Co(II) complexes: $[(Ph_4As)_2[Co(NO_3)_4]$, in which $[Co(NO_3)_4]^{2-}$ is an eight-coordinate dodecahedral complex anion; $[CoL_2](ClO_4)_2$ (L = 2,11-diaza[3.3.](2,6)pyridinophane), which is another example of a Co(II) eight-coordinate dodecahedral species; and the crown ether complex cations $[Co(12\text{-crown-}4)_2]^{2+}$ and $[Co(benzo\text{-}12\text{-crown-}4)_2]^{2+}$, which are eight-coordinate with a square antiprismatic coordination geometry.[47]

Furthermore, like the N–O and N–N bond lengths in free (uncoordinated) *cis*-Ph(O)NN(O)Ph and in $[Fe\{Ph(O)NN(O)Ph\}_3](FeCl_4)_2$, those in $[Co\{Ph(O)NN(O)Ph\}_4](PF_6)_2$ are indicative of π delocalization.[45]

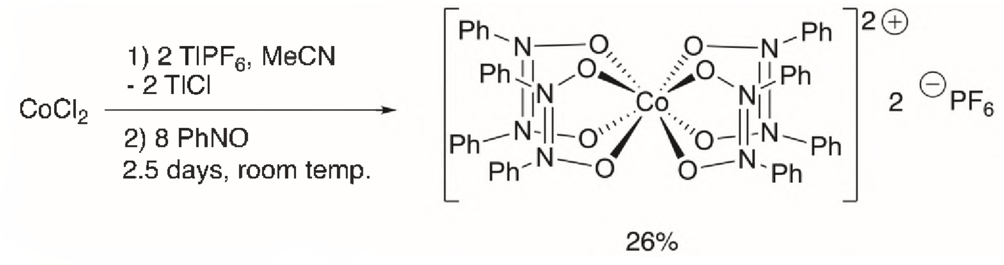

Figure 9: Synthesis of [Co{Ph(O)NN(O)Ph}$_4$](PF$_6$)$_2$.

CHAPTER II

REDOX-ACTIVE LIGANDS

2.1 Introduction

Ligands with substantial π delocalization are potentially redox active. A redox-active ligand is one for which more than one assignment of charge is plausible. Therefore, there is ambiguity in assigning the oxidation state of a metal center in complexes bearing these types of ligands, as it depends on the charge assigned to the redox-active ligand(s).[48] Transition metal complexes containing redox-active ligands are widely employed in the catalysis of organic reactions.[49]

2.2 2,2′-Bipyridyl (bpy)

An example of a well-known class of redox-active ligands is that of the aromatic diimines, which are bidentate chelating ligands. An especially important aromatic diimine is 2,2′-bipyridyl (bpy). Many complexes containing this ligand are known to be photochemically active, with an electronic excited state accessible through metal-to-ligand charge transfer (MLCT).[50] This type of charge transfer involves electron transfer to a primarily ligand-based molecular orbital (MO) from a primarily metal *d* orbital-based MO. Generally, MLCT is observed in transition metal complexes containing ligands with empty π antibonding (π*) orbitals that are fairly low in energy.[51] Aromatic diimine ligands such as bpy possess such low-lying, empty π* orbitals. In addition to a ligand possessing low-lying π* orbitals, the transition metal in a complex must have a sufficiently low oxidation number for MLCT to occur. The low oxidation number of the metal would make the energy gap between the metal *d* orbitals and the empty low-lying π* ligand orbital small enough for MLCT to take place.[51] Figure 10 shows an example of a ruthenium(II) complex with three bpy ligands, $Ru(bpy)_3^{2+}$, undergoing MLCT. When this complex absorbs photons of visible light with energy *hv*, Ru(II) is oxidized to Ru(III), whereas one of the neutral bpy ligands is reduced to a radical monoanion ($bpy^{\cdot -}$).[50] In other words, the excited state of this complex can be represented as $(Ru^{3+})(bpy)_2(bpy^{\cdot -})$, as opposed to the ground state of $(Ru^{2+})(bpy)_3$. Since $Ru(bpy)_3^{2+}$ can be easily excited, it can act as a photosensitizer, and since the lifetime of its excited state is long (on the order of microseconds),[51] that excited state is able to mediate chemical reactions.[50] An important application of $Ru(bpy)_3^{2+}$, as well as related ruthenium complexes with bpy derivatives as ligands, is their use in water oxidation systems.[52] Furthermore, the Yoon group has demonstrated the use of salts of $Ru(bpy)_3^{2+}$ and related cations as active photocatalysts for [2+2] cycloaddition reactions.[53]

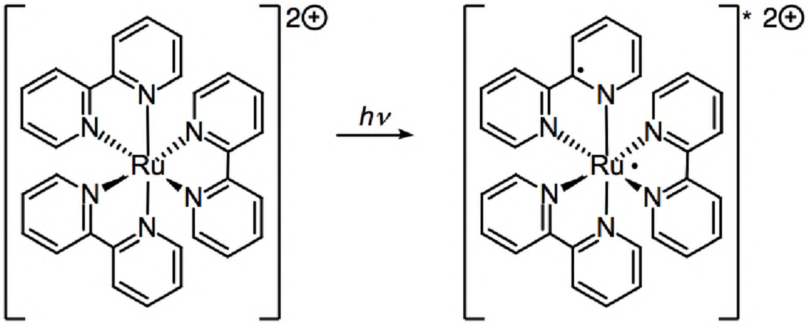

Figure 10: $Ru(bpy)_3^{2+}$ undergoing photoinduced MLCT.

2.3 3,5-Di-*tert*-butylcatecholate (3,5-DBCat^{2-})

In addition to the aromatic diimine bpy, the dianion 3,5-di-*tert*-butylcatecholate (3,5-DBCat^{2-}) is also a known redox-active ligand.[54] Upon one-electron oxidation of this ligand, the radical monoanion 3,5-di-*tert*-butylsemiquinone (3,5-DBSQ^{-}) is formed. If a second one-electron oxidation were to occur, the neutral 3,5-di-*tert*-butyl-*ortho*-benzoquinone would form. These redox states are shown in Figure 11.

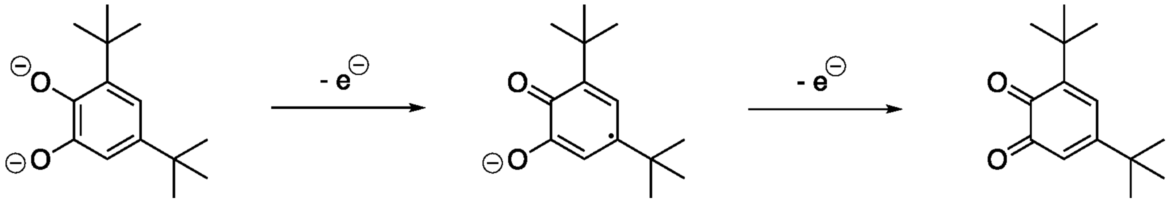

3,5-DBCat^{2-} **3,5-DBSQ^{-}**

Figure 11: Redox states of 3,5-DBCat.

Solution-phase spectroscopic analysis and magnetic measurements indicated an equilibrium between the cobalt(III) complex Co^{III}(3,5-DBCat)(3,5-DBSQ)(bpy), prepared by Pierpont and coworkers, and its electroisomer (valence tautomer) Co^{II}(3,5-DBSQ)$_2$(bpy), which is a cobalt(II) complex, as shown in Figure 12.[54] This electroisomerization equilibrium is a result of ligand-to-metal charge transfer (LMCT). Unlike MLCT, LMCT involves electron transfer to a primarily metal-based MO from a primarily ligand-based MO. Frequently, LMCT is observed in transition metal complexes that contain a transition metal with a high oxidation number, *e.g.* Mn(VII) in MnO_4^-, and ligands that have additional lone pairs of electrons.[51] However, the Pierpont group's transition metal complex Co^{III}(3,5-DBCat)(3,5-DBSQ)(bpy) was demonstrated to undergo LMCT even though Co is only in the +3 oxidation state, which is not exceedingly high for Co, as the most common oxidation states for Co in its compounds are +2 and +3.[55]

Therefore, this result from the Pierpont group shows that a higher-than-usual oxidation state for a transition metal is not always required for LMCT to occur.[54] Moreover, for LMCT to occur, the nonbonding electrons on the ligands should be fairly high in energy, while the empty metal *d* orbitals should be fairly low in energy.[51] Referring again to the electroisomerization equilibrium depicted in Figure 12, the 3,5-DBCat^{2-} ligand in the Co^{III}(3,5-DBCat)(3,5-DBSQ)(bpy) complex transfers an electron to the Co(III) center, hence undergoing LMCT. In this process, 3,5-DBCat^{2-} is oxidized to 3,5-DBSQ^{-}, whereas Co(III) is reduced to Co(II), yielding the product Co^{II}(3,5-DBSQ)$_2$(bpy).[54] One may think of this electroisomer product as a thermally accessible, low-lying electronic excited state that is favored at high temperatures. In contrast, UV-visible spectroscopy involves a molecule being excited via the absorption of light to an electronic excited state that is much higher in energy (as is commonly observed in the photochemistry of bpy complexes) than those states that can be significantly populated by heating.[56] With the complex Co^{III}(3,5-DBCat)(3,5-DBSQ)(bpy), the Pierpont group had the rare opportunity of investigating electron transfer between a metal and ligands under the conditions of thermal equilibrium.[54]

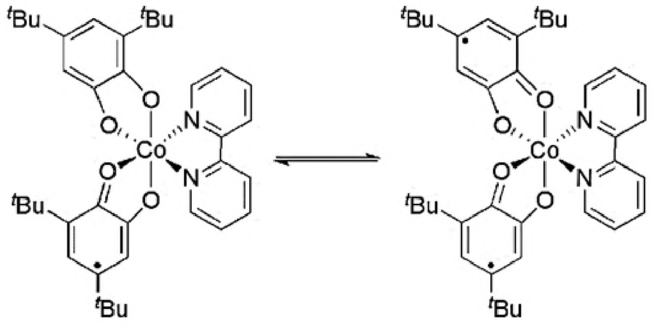

Co^{III}(3,5-DBCat)(3,5-DBSQ)(bpy)   **Co^{II}(3,5-DBSQ)$_2$(bpy)**

Figure 12: Electroisomerization equilibrium in a Co catecholate/semiquinone complex.

2.4 2,4-Di-*tert*-butyl-6-*tert*-butylamidophenolate (ap^{2-})

The last important redox-active ligand to be discussed here is 2,4-di-*tert*-butyl-6-*tert*-butylamidophenolate (ap^{2-}). The Heyduk group has shown this ligand to be useful in reactions of transition metal complexes that entail changing a ligand's oxidation state rather than changing a metal's oxidation state. More specifically, the Heyduk group has demonstrated the use of the ap^{2-} ligand to allow for zirconium(IV), d^0 complexes to undergo reactions similar to oxidative addition and reductive elimination, but in which the Zr metal center remains in the +4 oxidation state during the reactions.[57,58] Technically, an oxidative addition reaction is observed when a molecule of the form X–Y adds to a transition metal center in order to form two new bonds of the form M–X and M–Y, with the X–Y bond being cleaved in the process. As a result, the metal's oxidation number, the total electron count at the metal, and the coordination number increase by two. Therefore, for an oxidative addition to occur, the metal ion must have a *d* electron configuration of at least d^2. Reductive elimination reactions are the reverse of oxidative addition reactions that involve the coupling of two ligands and the elimination of its coupling product from the metal center.[59] One might think that an oxidative addition to a Zr(IV) metal center in its complexes is impossible, considering Zr in the +4 oxidation state has a d^0 electron configuration. However, the Heyduk group was able to show that oxidative addition-like and reductive elimination-like reactions can occur with Zr(IV), d^0 complexes through the cooperative redox reactivity of the redox-active ligand ap^{2-} and the Zr(IV), d^0 metal. Figures 13a and 13b depict a Zr(IV), d^0 complex undergoing an oxidative addition-like reaction with Cl_2 or $PhICl_2$ in which the ap^{2-} ligands are oxidized to iminosemiquinone (isq^-) and another Zr(IV), d^0 complex undergoing a reductive elimination-like reaction involving the generation of a biaryl product in which the isq$^-$ ligands are reduced back to ap^{2-}. During the course of these reactions, the oxidation state of Zr remains +4 while the ligands act as electron sources or sinks. Importantly, the Heyduk group was able to demonstrate new mechanistic pathways for transition metal complexes containing a Group 4 transition metal that could mediate reactions involving bond formation.[57,58]

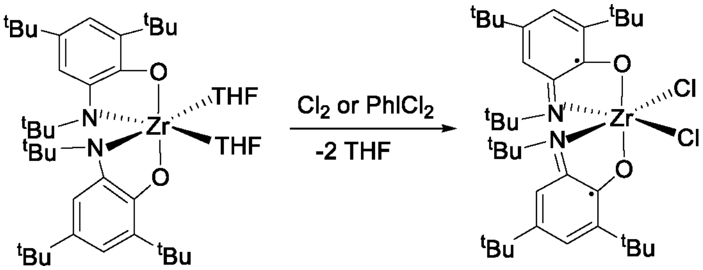

Figure 13a: Ligand-based oxidative addition-like reaction of a Zr(IV), d^0 complex.

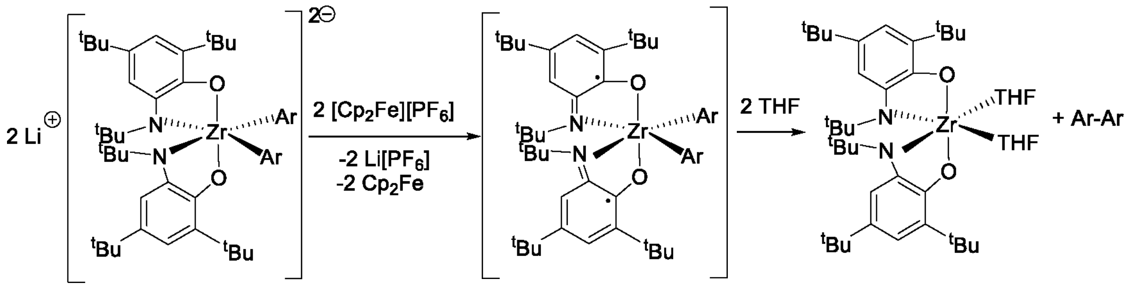

Figure 13b: Ligand-based reductive elimination-like reaction of a Zr(IV), d^0 complex.

2.5 Redox Activity Potential of Azodioxides

Since *cis*-Ph(O)NN(O)Ph shows considerable π delocalization, it has the potential to behave as a redox-active ligand. As shown in Figure 14, a neutral azodioxide ligand (**1**) could potentially be subjected to a one-electron reduction to form a radical monoanion (**2**), followed by another one-electron reduction to a closed-shell dianion (**3**). On the other hand, the neutral azodioxide (**1**) could also potentially be subjected to a one-electron oxidation to form a radical monocation (**4**), followed by another one-electron oxidation to a closed-shell dication (**5**). A metal center M in an azodioxide complex with an oxidation state *n* (when considering the azodioxide ligand as **1**) could more accurately be represented as having an oxidation state of *n* + 1, *n* + 2, *n* - 1, or *n* - 2, if the azodioxide ligand is acting as **2**, **3**, **4**, or **5**, respectively.

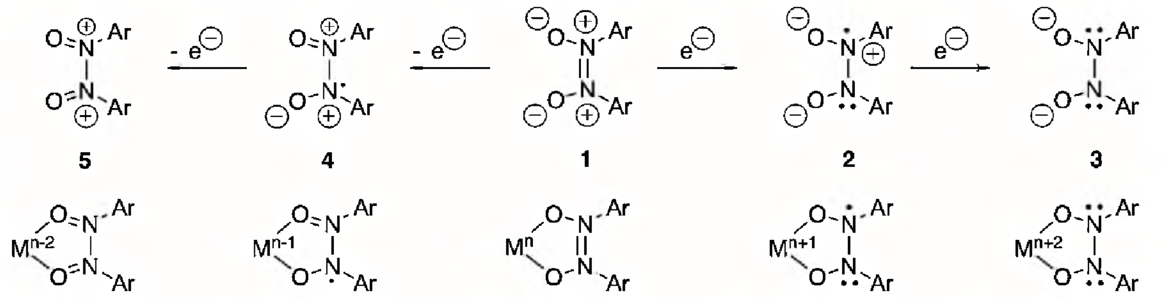

Figure 14: Possible redox states of azodioxides in their free and coordinated forms.

However, prior to our work, redox activity studies had not been conducted on azodioxide metal complexes. When the Nicholas group studied the complex salt [Fe{Ph(O)NN(O)Ph}$_3$](FeCl$_4$)$_2$, the presence of FeCl$_4^-$ anions become problematic when it comes to measuring the electronic properties and redox activity of the compound.[60] This is because FeCl$_4^-$ is a highly paramagnetic anion, with five unpaired electrons. As a result, the presence of this anion would make magnetic and spectroscopic measurements of the complex salt difficult to interpret. Specifically, since FeCl$_4^-$ has five unpaired electrons, it has a large magnetic susceptibility, meaning it could overshadow the magnetic susceptibility signal resulting from the unpaired electrons in the complex cation [Fe{Ph(O)NN(O)Ph}$_3$]$^{2+}$. Also, regarding spectroscopic analysis, FeCl$_4^-$ would show absorption peaks in UV-visible spectroscopy, although the peaks would not be too intense since the anion's transitions are spin-forbidden, in which the molar extinction coefficients (ε) for the absorption at each wavelength would be quite small.[51] For example, a visible spectrum of the salt NH$_4$FeCl$_4$ in diethyl ether has three maximum absorption peaks at 534, 619, and 688 nm with molar extinction coefficients of 1.4, 0.52, and 0.72 $M^{-1} \cdot cm^{-1}$, respectively. These weak absorption bands are known to be characteristic for the $FeCl_4^-$ anion.[61] Furthermore, a UV spectrum of the salt $NaFeCl_4$ in the gaseous state has three maximum absorption bands at 240, 310, and 360 nm with molar extinction coefficients of 4.2×10^{-3}, 2.7×10^{-3}, and 2.5×10^{-3} $M^{-1} \cdot cm^{-1}$, respectively. These weak absorption peaks are also known to be characteristic for the $FeCl_4^-$ anion.[62] Thus, for redox activity studies on azodioxide complexes to be performed, complex salts containing cationic azodioxide complexes with diamagnetic, redox-stable, and noncoordinating (or at least weakly coordinating) anions had to be synthesized.

CHAPTER III

SYNTHESIS AND CHARACTERIZATION OF A MIXED-LIGAND COBALT(II) BIPYRIDYL/DIPHENYLAZODIOXIDE COMPLEX SALT

3.1 Rationale

Since a former graduate student in my research group (Dr. Lakshmi Balaraman) studied 1st-row transition metal azodioxide complexes that are homoleptic (and, as I have previously mentioned, I had the privilege of working on some of this chemistry as an undergraduate), the first goal of this project was to synthesize and characterize a 1st-row transition metal azodioxide complex that is heteroleptic (a complex with at least two different types of ligands). In particular, our interest was to synthesize at least one complex that contains both azodioxide and another ligand with known redox activity, since complexes like these had not been reported in the literature prior to our work. The specific heteroleptic complexes of interest are those with azodioxide and bpy ligands. (See Chapter II, Section 2.2 for the details on the redox activity of bpy.)

For the synthesis of bpy/azodioxide complexes, it was desired to prepare their cationic heteroleptic complexes with counteranions that are diamagnetic, redox-stable, and non-coordinating or weakly coordinating (to prevent strong interactions between the cation and anion), if we wished to conduct redox activity studies. An example of such a counteranion is hexafluorophosphate (PF_6^-). Since this counteranion's structure is symmetrical, it is able to distribute the -1 charge equally among the six F atoms, making PF_6^- weakly coordinating. Also, the highly electronegative F atoms in PF_6^- decrease the overall Lewis basicity of PF_6^-. Unfortunately, it was noted by Nicholas' group that attempts to prepare salts of his cation $[Fe\{Ph(O)NN(O)Ph\}_3]^{2+}$ with BF_4^- or BPh_4^- as counteranions were unsuccessful.[63] Furthermore, we hypothesized that the presence of chloride (Cl^-) in the reaction mixture in Nicholas' group's preparation of $[Fe\{Ph(O)NN(O)Ph\}_3](FeCl_4)_2$ led to the oxidation of some Fe(II) to Fe(III). Since Cl^- is a π-donor ligand (a ligand containing at least one additional lone pair of electrons in a donor atom's *p* orbitals that is able to donate the electrons to a metal's empty π-symmetry *d* orbitals[64]) that can stabilize metals in higher oxidation states, soluble Cl^- could favor the formation of the problematic $FeCl_4^-$ anion. When broadening this type of synthesis to other transition metals, production of similar MCl_x^{y-} anions could remain an issue. Therefore, a synthetic strategy removing soluble Cl^- from the reaction mixture before PhNO is added was implemented.

Since my former lab-mate, Dr. Lakshmi Balaraman, had success in preparing a homoleptic cobalt(II) azodioxide complex cation with PF_6^- counteranions, I decided to attempt the synthesis of a cationic, heteroleptic bpy/azodioxide complex with cobalt as the metal center and PF_6^- counteranions.

3.2 Synthetic Strategy

The cobalt(II) species $Co(bpy)Cl_2$ was used as a synthon in the synthesis of a cobalt bpy/azodioxide complex. This synthon was prepared following a procedure reported by Iqbal and coworkers,[65] albeit with minor modifications.[66] The synthesis of $Co(bpy)Cl_2$ is depicted in Figure 15. The details of this preparation are explained in Section 3.4.2 of this chapter.

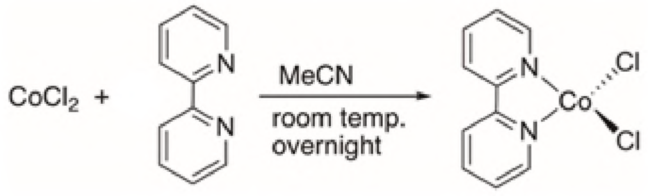

Figure 15: Synthesis of Co(bpy)Cl_2.

The first step in the synthesis of a cobalt bpy/azodioxide complex involved treating a suspension of Co(bpy)Cl_2 in acetonitrile (MeCN) with a solution of 2 equivalents of $TlPF_6$ (thallium hexafluorophosphate) in MeCN to remove Cl^- as insoluble TlCl and form a solution of a proposed reaction intermediate of the form $[Co(bpy)(NCMe)_n]^{2+}$, where n is likely equal to 2 or 4.[66] Although thallium compounds are toxic, $TlPF_6$ was used to remove Cl^- as TlCl, rather than the safer $AgPF_6$ (silver hexafluorophosphate) being used to precipitate AgCl, because Tl^+, unlike Ag^+, is not a strong oxidizing agent, and we wished to avoid any possible oxidation of Co(II) to Co(III). Also, it is worth mentioning that MeCN is known for being a good coordinating solvent. A good coordinating solvent like MeCN was necessary for our specific synthesis in order to allow for Cl^- removal by TlCl precipitation. Generally, it is more favorable to remove Cl^- from the reaction mixture if it will lead to the formation of a solvated complex ion such as $[Co(bpy)(NCMe)_n]^{2+}$, where n = 2 or 4, as opposed to poorly solvated ions in a more weakly coordinating solvent.[67] After stirring the reaction mixture long enough to ensure that the precipitation of TlCl was complete in the first step of the synthesis, 6 equivalents (an excess) of PhNO (nitrosobenzene) in MeCN were added to the reaction mixture containing the proposed

$[Co(bpy)(NCMe)_n]^{2+}$ intermediate. This reaction resulted in the formation of a cobalt bpy/azodioxide complex salt of the form $[Co(bpy)\{Ph(O)NN(O)Ph\}_2](PF_6)_2$. The synthesis of $[Co(bpy)\{Ph(O)NN(O)Ph\}_2](PF_6)_2$ is depicted in Figure 16 and has been published in *ACS Omega*.[66] Once the reaction was complete, TlCl was removed by filtration from the reaction mixture, followed by the removal of MeCN solvent from the filtrate *in vacuo*. Recrystallization from a mixture of dichloromethane (DCM) and diethyl ether (Et_2O) yielded garnet-red crystals of $[Co(bpy)\{Ph(O)NN(O)Ph\}_2](PF_6)_2$.[66]

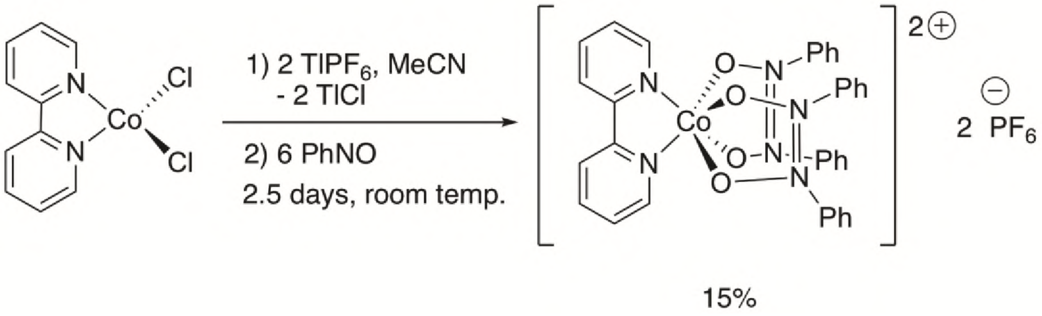

Figure 16: Synthesis of $[Co(bpy)\{Ph(O)NN(O)Ph\}_2](PF_6)_2$.

3.3 Characterization of $[Co(bpy)\{Ph(O)NN(O)Ph\}_2](PF_6)_2$

3.3.1 Single-Crystal X-Ray Diffraction

Single-crystal X-ray diffraction, generally the "gold standard" of characterization techniques in inorganic chemistry, was performed by Prof. Wiley Youngs' former Ph.D. student Dr. Michael Stromyer at the University of Akron in order to determine the structure of our cobalt bpy/azodioxide complex salt reaction product. This characterization allowed for the determination not only of the product's topology, but also its bond lengths and bond angles. Its crystal structure as a thermal ellipsoid plot[66] is presented in Figure 17.

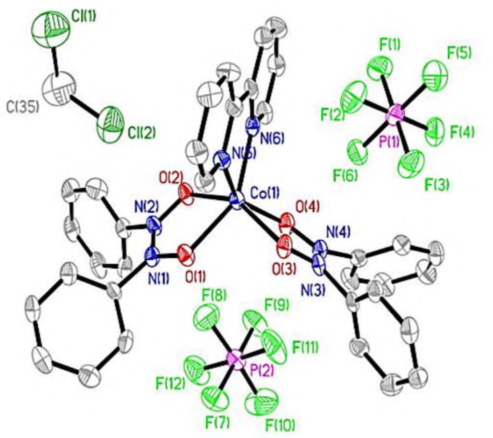

Figure 17: Thermal ellipsoid plot of $[Co(bpy)\{Ph(O)NN(O)Ph\}_2](PF_6)_2$. The recrystallization solvent CH_2Cl_2 is present in the crystal lattice.

It is important to note that the six-coordinate complex cation $[Co(bpy)\{Ph(O)NN(O)Ph\}_2]^{2+}$ has a trigonal prismatic coordination geometry. Most six-coordinate transition metal complexes display octahedral, rather than trigonal prismatic geometry. A trigonal prismatic geometry is usually less common than an octahedral geometry for two reasons: each ligand in a transition metal complex with a trigonal prismatic geometry is in an eclipsed conformation in relation to another ligand, resulting in more ligand-ligand repulsion[68] than that in an octahedral geometry, and trigonal prismatic complexes, in many cases, have smaller ligand field stabilization energies[68] (this energy is the difference between the *d*-electron energy of a complex and that of a free atom/ion[69]) than those of octahedral complexes, meaning trigonal prismatic complexes are usually more reactive or less stable than the comparable octahedral complexes. Therefore, the formation of trigonal prismatic complexes usually requires ligand-ligand interactions that are favorable. An important example of a class of ligands in which the ligand-ligand interactions are favorable is the dithiolenes ($R_2C_2S_2$), which are bidentate chelating ligands that contain S donor atoms.[70] More specifically, dithiolene ligands in transition metal complexes have been proposed to experience inter-ligand S–S interactions. These S–S interactions, which are considered direct and weak, are proposed to make the trigonal prismatic geometry that exists in dithiolene complexes stable.[71,72] Other trigonal prismatic complexes require the implementation of small σ-donating ligands (*e.g.* CH_3^-) and d^0 metal ions so that π-bonding effects are not present and steric effects are minimized.[70] An example of such a complex is the highly reactive organometallic species hexamethyltungsten(VI), $W(CH_3)_6$.[73]

Furthermore, trigonal prismatic Co(II) complexes are particularly unusual, as most Co(II) complexes are either tetrahedral or octahedral.[74] Most crystallographically characterized Co(II) complexes with trigonal prismatic geometry possess rigid, complicated hexadentate ligands that are known as clathrochelates[75] or pseudoclathrochelates.[68,76] These types of ligands possess six coordinating atoms each that are arranged to encapsulate metal ions, resulting in the formation of trigonal prismatic "cage" complexes where the geometry of the ligand's donor atoms enforces the trigonal prismatic coordination geometry.[68,75,76] Another example of a structurally characterized Co(II) trigonal prismatic complex that contains a hexadentate ligand is [Co(hpy)]Br_2, where hpy = tris([2,2′-bipyridin]-6-yl)methanol, but unlike the other clathrochelate and pseudoclathrochelate examples that have been cited, this complex contains a redox-active ligand with a π system that is extended.[77] Prior to our work, however, only two monometallic, trigonal prismatic Co(II) complexes containing only bidentate ligands had been crystallographically characterized: Co(NO_2phen)(3,6-DBSQ)$_2$ (NO_2phen = 5-nitro-1,10-phenanthroline and 3,6-DBSQ$^-$ = 3,6-di-*tert*-butylsemiquinone) and Co(dafl)(3,6-DBSQ)$_2$ (dafl = 4,5-diaza-fluoren-9-one).[78]

More importantly, not only does our complex cation $[Co(bpy)\{Ph(O)NN(O)Ph\}_2]^{2+}$ possess a trigonal prismatic coordination geometry, but the complex cation $[Fe\{Ph(O)NN(O)Ph\}_3]^{2+}$, from Nicholas' group, also possesses this geometry. (Refer back to Figures 8a and 8b in Chapter I, Section 1.6.1) A plausible hypothesis for why a trigonal prismatic geometry is observed in both complex cations is that the azodioxide ligand *cis*-Ph(O)NN(O)Ph is isolobal with dithiolene dianions ($R_2C_2S_2^{2-}$). The term "isolobal," devised by the great theoretical chemist Roald Hoffmann, is used to describe molecules, ions, or fragments of molecules which have similar energy, symmetry, and electron occupation of their frontier orbitals. In other words, isolobal fragments suggest the possibility of similarities in bonding between fragments that might otherwise seem unrelated. As an example, two fragments that are considered isolobal are CH_3 (the methyl radical) and $Mn(CO)_5$ (an organometallic fragment with a d^7 electron count) since each has one electron occupying its highest energy hybrid frontier orbital, and each must form one bond to achieve a closed shell on its central atom (an octet of electrons on C and 18 electrons on Mn).[79] Transition metal dithiolene complexes, which have the form $M(R_2C_2S_2)_3$ (in which "M" is an early transition metal and in which the complex can be neutral, cationic, or anionic) often possess a trigonal prismatic coordination geometry.[72,80] Moreover, dithiolene has different redox states and may be considered as $R_2C_2S_2^{2-}$ (a closed-shell dianion), $R_2C_2S_2^{-}$ (a radical monoanion), or $R_2C_2S_2$ (a neutral, closed-shell species). Similarly, as it was previously mentioned in Chapter II, Section 2.5, the neutral azodioxide ligand Ph(O)NN(O)Ph may be considered as $[Ph(O)NN(O)Ph]^{+}$ (a radical monocation) or $[Ph(O)NN(O)Ph]^{2+}$ (a closed-shell dication).[66] Importantly, as it was mentioned earlier, inter-ligand S–S interactions are favorable in dithiolenes,[70] so in this aspect, the observation of a trigonal prismatic coordination geometry in the transition metal tris(dithiolene) complexes, $M(R_2C_2S_2)_3$, is not surprising. Additionally, chelating ligands with a small bite angle (ligand-metal-ligand angle) formed can result in a distortion from an octahedral geometry to a trigonal prismatic geometry.[70]

As shown in Table I, the average N–N and N–O bond lengths in $[Co(bpy)\{Ph(O)NN(O)Ph\}_2](PF_6)_2$ are similar to those in uncoordinated *cis*-Ph(O)NN(O)Ph and in the azodioxide complexes[63,66] $[Fe\{Ph(O)NN(O)Ph\}_3](FeCl_4)_2$ and $[Co\{Ph(O)NN(O)Ph\}_4](PF_6)_2$, as well as in the non-$d^0$ azodioxide complexes[81,82] $Sc(OTf)_3(H_2O)_2\{Ar(O)NN(O)Ar\}$ and $[Ca\{Ph(O)NN(O)Ph\}(H_2O)_2(THF)_3]I_2$.[66] The near-invariance of these bond lengths suggests the azodioxide ligand Ph(O)NN(O)Ph may not be either a strong π-acceptor or a strong π-donor ligand, so coordination to a metal does not significantly deplete the population of a π-bonding MO or increase the population of a π-antibonding one. In contrast, the average Co–O bond lengths in $[Co(bpy)\{Ph(O)NN(O)Ph\}_2](PF_6)_2$ are much shorter than those in $[Co\{Ph(O)NN(O)Ph\}_4](PF_6)_2$ and the average Sc–O and Ca–O bond lengths[81,82] in $Sc(OTf)_3(H_2O)_2\{Ar(O)NN(O)Ar\}$ and $[Ca\{Ph(O)NN(O)Ph\}(H_2O)_2(THF)_3]I_2$, respectively.[66] Interestingly, the average Co–O bond lengths in $[Co(bpy)\{Ph(O)NN(O)Ph\}_2](PF_6)_2$ are similar to the Fe–O bond lengths in $[Fe\{Ph(O)NN(O)Ph\}_3](FeCl_4)_2$. This result is intriguing in light of the fact that the Co metal center in $[Co(bpy)\{Ph(O)NN(O)Ph\}_2](PF_6)_2$ has an oxidation state of +2 with a d^7 electron count, whereas the Fe in $[Fe\{Ph(O)NN(O)Ph\}_3](FeCl_4)_2$ has an oxidation state of +2 with a d^6 electron count. Therefore, the X-ray crystallography data suggest that M–O (M = Fe, Co) bond lengths in azodioxide complexes might show a stronger dependence on coordination number, which is perhaps due to steric effects from the ligands, than on the *d*-electron count and identity of the metal.[66] However, the $[Ca\{Ph(O)NN(O)Ph\}(H_2O)_2(THF)_3]I_2$ complex has a coordination number of 7, as does the Sc(III) azodioxide complex,[81,82] but it has average Ca–O bond lengths greater than the average Co–O bond lengths in $[Co\{Ph(O)NN(O)Ph\}_4](PF_6)_2$, which has a coordination number of 8. In fact, the Ca(II) azodioxide complex has the longest M–O bond length out of all five of the structurally characterized azodioxide complexes. It is possible that there is a strong ion-dipole interaction between *cis*-Ph(O)NN(O)Ph and Ca, an alkaline earth metal, that contributes to the nature of their bonding, which causes the Ca–O bond lengths in the Ca(II) azodioxide complex to be longer than M–O bond lengths in the other four azodioxide complexes since the M–O bonds in the other complexes have greater covalent bonding character because in these cases, *cis*-Ph(O)NN(O)Ph is able to bond to transition metals containing valence *d* orbitals. Nevertheless, in order to determine if the strong dependency of M–O bond lengths on metal coordination number is a general trend, more azodioxide metal complexes must be synthesized and crystallographically characterized. Additionally, it is important to point out that $[Co\{Ph(O)NN(O)Ph\}_4](PF_6)_2$ is the only known azodioxide complex in which the chelate rings are in a “puckered” (envelope) conformation, causing the Co metal center to lie outside the plane. The other azodioxide complexes, on the other hand, have planar chelate rings.[66]

Compound	Average N-N bond length (Å)	Average N-O bond length (Å)	Average M-O bond length (Å)	Chelate rings
cis-Ph(O)NN(O)Ph	1.32	1.27	--	--
[Co(bpy){Ph(O)NN(O)Ph}$_2$](PF$_6$)$_2$	1.31	1.28	2.10	planar
[Fe{Ph(O)NN(O)Ph}$_3$](FeCl$_4$)$_2$	1.29	1.28	2.12	planar
[Co{Ph(O)NN(O)Ph}$_4$](PF$_6$)$_2$	1.31	1.28	2.24	puckered
Sc(OTf)$_3$(H$_2$O)$_2${Ar(O)NN(O)Ar}	1.29	1.28	2.21	planar
[Ca{Ph(O)NN(O)Ph}(H$_2$O)$_2$(THF)$_3$]I$_2$	1.30	1.27	2.42	planar

*OTf = OSO$_2$CF$_3$, Ar = 2-MeOC$_6$H$_4$

Table I: Important structural parameters for *cis*-Ph(O)NN(O)Ph and its corresponding Fe and Co complexes.[66]

With a crystal structure obtained for [Co(bpy){Ph(O)NN(O)Ph}$_2$](PF$_6$)$_2$, it is especially important to note that this complex salt is the first structurally characterized heteroleptic complex containing azodioxide and a known redox-active ligand.[66] By publishing the synthesis and characterization of [Co(bpy){Ph(O)NN(O)Ph}$_2$](PF$_6$)$_2$, we were able to add more azodioxide metal complexes to the very few reported in the literature and further develop the coordination chemistry of azodioxides. However, since a single crystal (one that was used for single-crystal X-ray diffraction) may not constitute the bulk of a material or product,[83] other characterization techniques were applied in order to establish the identity of our new complex salt.

3.3.2 Elemental Analysis (CHN Analysis)

After obtaining a crystal structure of [Co(bpy){Ph(O)NN(O)Ph}$_2$](PF$_6$)$_2$, elemental analysis was performed on our compound by Galbraith Laboratories, Inc (Knoxville, TN) in order to determine the compound's purity. More specifically, the carbon, hydrogen, and nitrogen (CHN) content of our compound was determined *via* sample combustion.

The experimentally determined percentages of C, H, and N for $[Co(bpy)\{Ph(O)NN(O)Ph\}_2](PF_6)_2$ were 38.81%, 2.65%, and 10.29%, respectively. The theoretical (expected) percentages of C, H, and N for our compound are 43.75%, 3.02%, and 9.00%, respectively.[66] It is important to note that the carbon content of our compound is ~5% lower than expected, whereas its nitrogen content is ~1.3% higher than expected. The experimentally determined lower percentage of carbon is likely due to the presence of thallium-containing impurities since we used $TlPF_6$ as part of our synthetic scheme for $[Co(bpy)\{Ph(O)NN(O)Ph\}_2](PF_6)_2$. Importantly, the high molar mass of thallium (204.37 g/mol) could have possibly caused the determination of a lower percentage of carbon in our compound, as a small per-mole impurity of a thallium compound corresponds to a larger mass percent impurity. Moreover, the specific impurity containing lower carbon content that is likely present in our bulk $[Co(bpy)\{Ph(O)NN(O)Ph\}_2](PF_6)_2$ product is the reaction intermediate $[Co(bpy)(NCMe)_n]^{2+}$, where n = 2 or 4.[66] The presence of this reaction intermediate is probable because MeCN coordinates strongly to the metal center, which makes it difficult to displace by the azodioxide ligand in the second step of our synthetic scheme for $[Co(bpy)\{Ph(O)NN(O)Ph\}_2](PF_6)_2$. Meanwhile, the higher percentage of nitrogen that was experimentally determined for our compound is likely due to a small PhNO impurity, which is probable because excess PhNO was used in the synthesis of $[Co(bpy)\{Ph(O)NN(O)Ph\}_2](PF_6)_2$.[66]

3.3.3 UV-Visible Spectroscopy

UV-visible spectroscopy was performed on $[Co(bpy)\{Ph(O)NN(O)Ph\}_2](PF_6)_2$

in order to determine the types of electronic transitions it experiences, so that we could gain information about its electronic structure. When taking UV-visible absorption spectra of [Co(bpy){Ph(O)NN(O)Ph}$_2$](PF$_6$)$_2$ in MeCN, the spectra had revealed two peaks with maximum absorbances at wavelengths (λ_{max}) of 246 nm and 304 nm.[66] (See Figure 18a.) With this information, we were able to calculate molar absorptivity (ε) values for each λ_{max} using the Beer-Lambert law of $A = \varepsilon Lc$, where A = absorbance, L = path length of cuvette, c = concentration of analyte. The molar absorptivity represents the absorption strength of a compound at a particular wavelength.[84] For our Beer-Lambert law study, we were able to observe the expected linear relationship between absorbance and concentration when we worked with low concentrations of [Co(bpy){Ph(O)NN(O)Ph}$_2$](PF$_6$)$_2$ in the 10^{-5} M range.

The experimental molar absorptivities at 246 nm and 304 nm were 1.38×10^4 $M^{-1} \cdot cm^{-1}$ and 2.26×10^4 $M^{-1} \cdot cm^{-1}$, respectively. The absorption at 246 nm is likely due to a ligand-centered $\pi \rightarrow \pi^*$ transition at the bpy ligand in [Co(bpy){Ph(O)NN(O)Ph}$_2$](PF$_6$)$_2$.[66] The $\pi \rightarrow \pi^*$ transition is usually intense, with ε values ranging from 5,000-100,000 $M^{-1} \cdot cm^{-1}$.[85] These transitions are commonly observed in the UV region (200-400 nm) of a UV-visible spectrum. Moreover, this type of electronic transition involves orbitals with high overlap, making the probability of the transition large.[86] This assignment of a $\pi \rightarrow \pi^*$ transition at 246 nm is based on the fact that a UV-visible spectrum of uncoordinated bpy in MeCN showed a maximum absorbance peak at λ_{max} = 237 nm ($\varepsilon = 2.78 \times 10^4$ $M^{-1} \cdot cm^{-1}$). An experimental UV-visible spectrum of bpy is shown in Figure 18b. On the other hand, the absorption at 304 nm is likely due to a charge transfer (*e.g.* metal-to-ligand (MLCT), ligand-to-metal (LMCT) between *cis*-Ph(O)NN(O)Ph and Co, since the UV-visible spectra of [Co{Ph(O)NN(O)Ph}$_4$](PF$_6$)$_2$ show a maximum absorption peak at almost the same wavelength, λ_{max} = 305 nm (ε = 4.62 × 10^4 $M^{-1}\cdot cm^{-1}$).[66] An experimental UV-visible spectrum of the homoleptic Co(II) azodioxide complex $[Co\{Ph(O)NN(O)Ph\}_4](PF_6)_2$ is depicted in Figure 18c. Charge transfer transitions are typically strong, with ε values ranging from 1,000 to 50,000 $M^{-1}\cdot cm^{-1}$. These transitions are also fully "allowed" by the spectroscopic selection rules.[87]

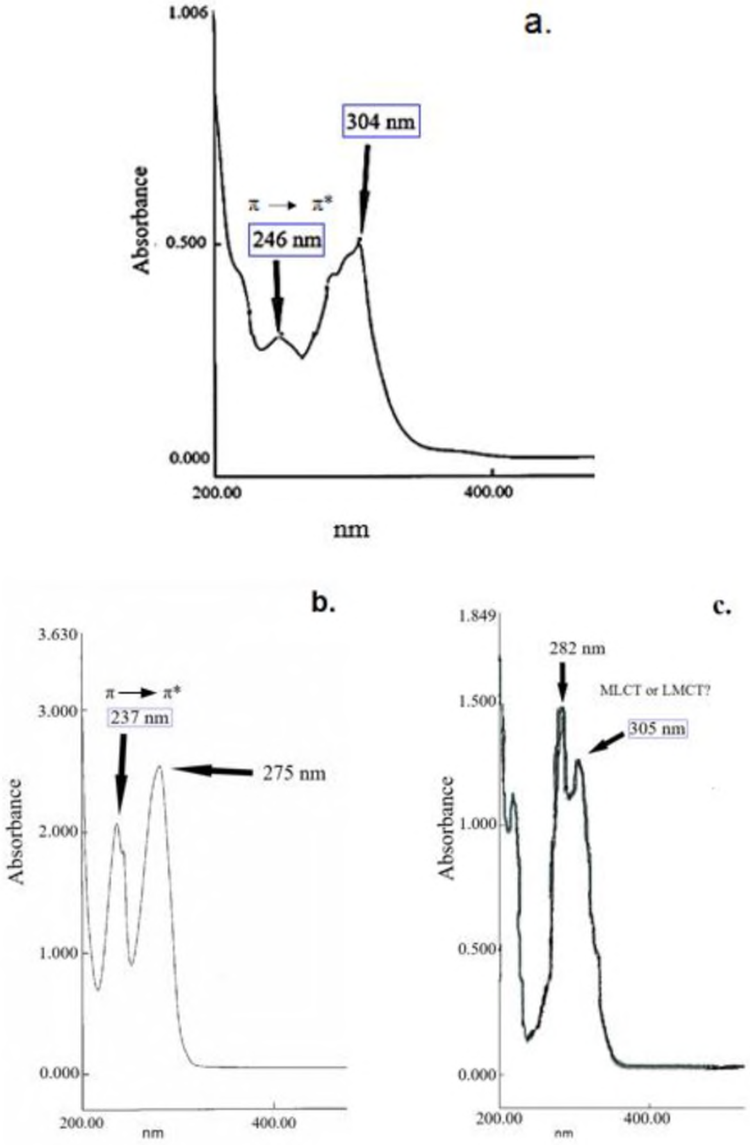

Figure 18: Experimental UV-visible spectra of solutions of (a) $[Co(bpy)\{Ph(O)NN(O)Ph\}_2](PF_6)_2$ in MeCN (b) bpy in MeCN (c) $[Co\{Ph(O)NN(O)Ph\}_4](PF_6)_2$ in MeCN.

3.3.4 IR Spectroscopy

Solid-phase infrared (IR) spectroscopy in attenuated total reflectance (ATR) mode was conducted on $[Co(bpy)\{Ph(O)NN(O)Ph\}_2](PF_6)_2$ in order to confirm the presence of particular functional groups. The ATR mode was chosen for IR analysis because when our air-sensitive compound is in the solid phase, as opposed to the solution phase, O_2 cannot readily diffuse into it.

The experimental IR spectrum of $[Co(bpy)\{Ph(O)NN(O)Ph\}_2](PF_6)_2$, shown in Figure 19a, appears to have three broad peaks in the N–O stretching region: 1370 cm^{-1}, 1444 cm^{-1}, and 1478 cm^{-1}.[66,88] In fact, the IR spectra of homoleptic $[Co\{Ph(O)NN(O)Ph\}_4](PF_6)_2$ and uncoordinated *cis*-Ph(O)NN(O)Ph also each display three intense N–O stretches from 1370-1390 cm^{-1} and 1458-1485 cm^{-1}. The experimental IR spectrum of *cis*-Ph(O)NN(O)Ph that was taken in ATR mode is shown in Figure 19b. The weak IR peak at 1577 cm^{-1} in Figure 19a is possibly a C=N stretch, due to its presence in the bpy ligand.[66] Although the C=N stretching region ranges from 1640 – 1690 cm^{-1},[89] it is possible that the observed frequency is lower because the C–N bonds in bpy have a bond order between 1 and 2 due to π delocalization in the aromatic rings. The experimental IR spectrum of bpy that was taken in ATR mode is shown in Figure 19c. Lastly, two important IR stretches to note in the IR spectrum of $[Co(bpy)\{Ph(O)NN(O)Ph\}_2](PF_6)_2$ (Figure 19a) are the broad stretches at 3534 cm^{-1} and 3606 cm^{-1}. These peaks are located at unusually high energies within the N–H and O–H functional group region. However, neither N–H nor O–H moieties are present in $[Co(bpy)\{Ph(O)NN(O)Ph\}_2](PF_6)_2$. It is possible that these peaks arise from charge transfer (*e.g.* MLCT, LMCT) between *cis*-Ph(O)NN(O)Ph and Co.[66]

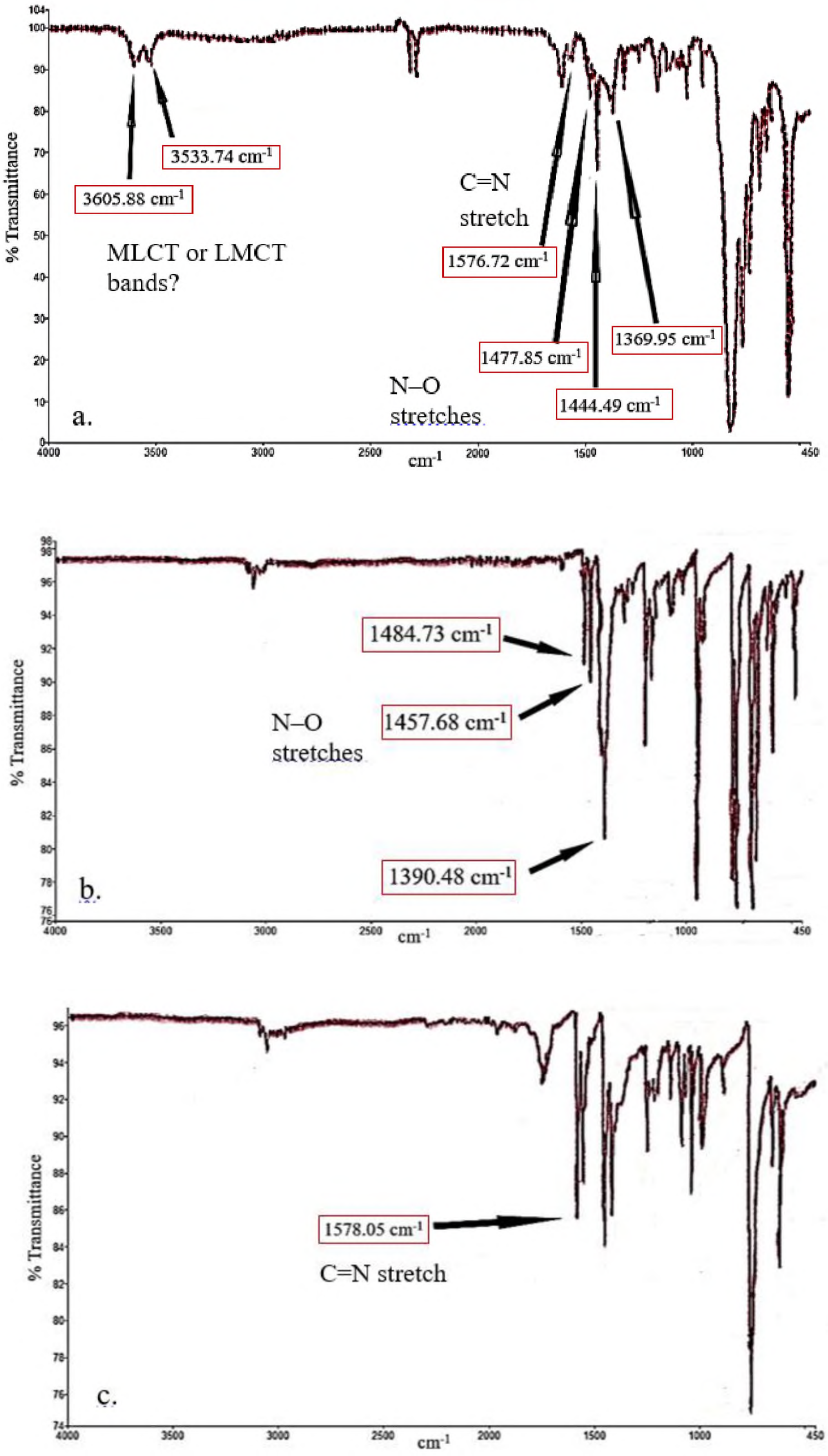

Figure 19: Experimental solid-phase IR spectra of (a) [Co(bpy){Ph(O)NN(O)Ph}$_2$](PF$_6$)$_2$ (b) *cis*-Ph(O)NN(O)Ph (c) bpy.

3.3.5 Magnetic Susceptibility

The magnetic susceptibility (χ) of $[Co(bpy)\{Ph(O)NN(O)Ph\}_2](PF_6)_2$ was measured in order to determine its number of unpaired electrons and confirm the oxidation state of cobalt so that we could gain further information on the complex's electronic state. Magnetic susceptibility measures a substance's ability to be either attracted to or repelled by a magnetic field.[90] Using the measured magnetic susceptibility (χ) and Bain and Berry's[90] Pascal constants to correct for diamagnetism (which results due to the presence of paired core electrons and paired electrons in covalent bonds), we were able to calculate a solid-state effective magnetic moment (μ_{eff}) of 4.74 Bohr magnetons (μ_B, where 1 $\mu_B = 9.274 \times 10^{-24}$ J/T) at 22°C for our complex.[66] The μ_{eff} value is the measure of a complex's paramagnetism, with greater μ_{eff} values corresponding to a more paramagnetic species.[91]

The experimentally determined magnetic moment of 4.74 μ_B is within the range of magnetic moments (4.1-5.2 μ_B) seen for high-spin Co(II) complexes, which possess three unpaired electrons.[92] Often, when a 1st-row transition metal atom or ion is part of a complex, its *d* electrons interact with their nonspherical environment, often causing the orbital angular momentum to be quenched. This would mean that for some 1st-row transition metal complexes with unpaired electrons, a spin-only magnetic moment could be calculated since only the spin angular momentum would remain.[91] However, high-spin Co(II) complexes, which have a d^7 electron configuration, have experimental magnetic moments that deviate significantly from their theoretical spin-only magnetic moment, which is only 3.87 μ_B. For example, the trigonal prismatic high-spin Co(II) complex salt $[Co(PccBF)](BF_4)$, where $PccBF^-$ is the hexadentate clathrochelate fluoroborotris(2-carboxaldoximo-6-pyridyl)phosphine, has a magnetic moment of 4.91 μ_B.[93] This large deviation from spin-only magnetic moments is because high-spin $3d^7$ complexes have a substantial orbital angular momentum contribution to their measured magnetic moments. This orbital angular momentum is present in these complexes because they have at least one unfilled (or half-filled) orbital with an energy that is similar to the orbitals that are filled by unpaired electrons and are of the appropriate symmetry. When a magnetic field is applied, this leads to the circulation of electrons around the metal with the use of these low-lying orbitals, therefore resulting in the orbital angular momentum contribution to magnetic moment.[91] Thus, our calculated μ_{eff} value of 4.74 μ_B for $[Co(bpy)\{Ph(O)NN(O)Ph\}_2](PF_6)_2$ corresponds to a Co(II) metal center with three unpaired electrons, with a significant orbital angular momentum contribution to the magnetic moment.[66]

3.3.6 EPR Spectroscopy

Electron paramagnetic resonance (EPR) spectroscopy is a characterization technique that can be applied to paramagnetic transition metal complexes, that is, complexes with at least one unpaired electron. In contrast to NMR spectroscopy, which involves the interaction of electromagnetic radiation (EMR) with nuclei possessing nonzero spin, EPR involves the interaction of EMR with the unpaired electrons in a transition metal complex or even in an organic radical. Moreover, in EPR, the EMR frequency is typically in the microwave region and is usually kept constant while the magnetic field strength is varied. In NMR, the magnetic field strength is kept constant while the frequency is varied.[94] It is important to mention that before we conducted EPR studies, we attempted to acquire ^1H NMR spectra of our paramagnetic $[Co(bpy)\{Ph(O)NN(O)Ph\}_2](PF_6)_2$. However, our NMR spectra did not show any peaks of this compound; instead, small amounts of the impurity PhNO were detected, which was confirmed by spiking experiments.[66]

EPR spectroscopic measurements were conducted on our complex salt [Co(bpy){Ph(O)NN(O)Ph}$_2$](PF$_6$)$_2$ in order to gain further information about its electronic state, in addition to what we had determined using UV-visible spectroscopy and magnetic susceptibility. Transition metal complexes with more than one unpaired electron can have very fast relaxation times at room temperature, which makes their EPR signals too broad to detect.[95] In fact, we first attempted to acquire a room-temperature EPR spectrum of our complex from the instrument in Dr. Sudha Chakrapani's group at the Case Western Reserve University School of Medicine, but the EPR signal was broad enough to be barely visible over the baseline noise. Therefore, low-temperature EPR studies at 4.5 K were conducted on our complex, in which liquid helium was used to cool it so that the relaxation would not be as efficient.

The low-temperature EPR spectrum of our complex was taken at Miami University, in collaboration with Dr. Robert McCarrick and Prof. David Tierney. The EPR spectrum of [Co(bpy){Ph(O)NN(O)Ph}$_2$](PF$_6$)$_2$ as a plot of the first derivative of signal intensity $d(\text{signal})/dB$ vs. magnetic field strength (B) in units of Gauss (G) is presented in Figure 20. Importantly, this EPR spectrum shows that $d(\text{signal})/dB = 0$ at around a magnetic field strength of 1670 G, which converted to Tesla (T) would be 0.167 T. Using this value of 0.167 T, we were able to calculate the g-factor,[95] which is a numerical value that is a distinguishing feature of molecules with unpaired electrons. The g-factor for [Co(bpy){Ph(O)NN(O)Ph}$_2$](PF$_6$)$_2$ was calculated using the formula $hv = g\mu_B B$. Here, hv is the energy of a photon (of EMR) with the frequency (v) being equal to the microwave frequency used for our EPR studies (9.629 GHz), μ_B is a constant equal to 9.274×10^{-24}

J/T, and B for this signal is 0.167 T. Our calculated g-factor was approximately equal to 4.12. This g-factor of 4.12 indicates that the unpaired electrons (radical character) are primarily centered on the Co metal ion in $[Co(bpy)\{Ph(O)NN(O)Ph\}_2](PF_6)_2$. If the unpaired electrons were mainly centered on main-group atoms such as O or N atoms in our complex, then the g-factor would be extremely close to that of a free electron (for which $g = 2.0023$), in the range of 1.99-2.01.[95] Furthermore, many transition metal ions as part of complexes, especially those with more than one unpaired electron, have g-factors that are significantly different from 2.0023 because their orbital angular momentum is partially or completely quenched.[96] Additionally, the two most common oxidation states for cobalt are +2 and +3, with most Co(II) complexes being high-spin (three unpaired electrons) and most Co(III) complexes being low-spin (no unpaired electrons, hence no EPR signal).[74] Therefore, our EPR results offer further confirmation that the Co center in $[Co(bpy)\{Ph(O)NN(O)Ph\}_2](PF_6)_2$ is in the +2 oxidation state with three unpaired electrons (high-spin). Another important feature to note in the EPR spectrum of $[Co(bpy)\{Ph(O)NN(O)Ph\}_2](PF_6)_2$ (Figure 18) is the splitting around the 1670 G signal. This splitting is likely caused by a hyperfine coupling[95] in which the unpaired electrons are interacting with its ^{59}Co nucleus (the isotope with 100% natural abundance), which has a spin of 7/2, making it magnetic. Finally, there can be seen in the acquired EPR spectrum a small signal around B = 11900 G. This signal very likely corresponds to a small O_2 impurity, since the EPR sample was prepared in a glove bag at Miami University, which does not have as anaerobic of an environment as our glovebox, and O_2 is itself a triplet diradical in its ground state.[97]

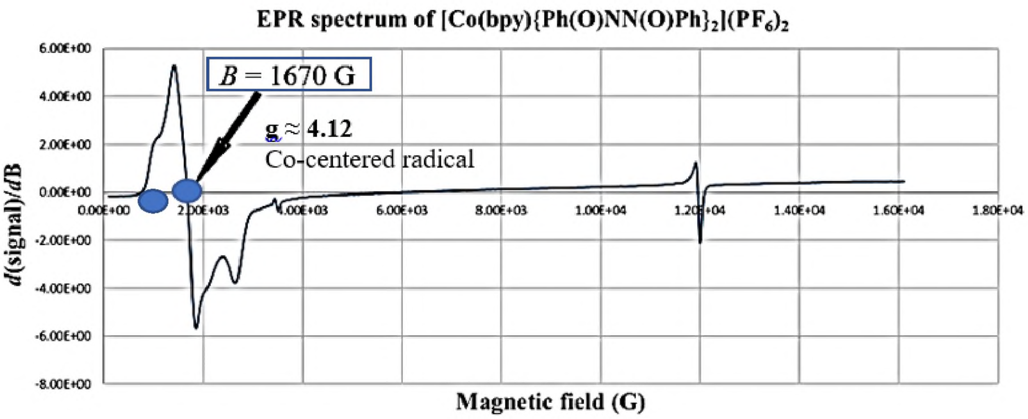

Figure 20: EPR spectrum of [Co(bpy){Ph(O)NN(O)Ph}$_2$](PF$_6$)$_2$.

3.4 Experimental Methods

3.4.1 General Experimental Considerations

Elemental Analysis was carried out at Galbraith Laboratories, Inc in Knoxville, TN. A Shimadzu UV-2600 spectrometer was used to acquire UV-visible spectra of solutions of [Co(bpy){Ph(O)NN(O)Ph}$_2$](PF$_6$)$_2$ in MeCN in gastight cuvettes, which have a 1.2 cm path length. A PerkinElmer Spectrum 2 spectrometer was used to acquire IR spectra of [Co(bpy){Ph(O)NN(O)Ph}$_2$](PF$_6$)$_2$ as a neat solid in ATR mode. A Sherwood Scientific MK 1 magnetic susceptibility balance was used to obtain the magnetic susceptibility measurement. A Bruker Avance III 400 MHz spectrometer was used to obtain NMR spectra.[66] The EPR spectrum of a solution of [Co(bpy){Ph(O)NN(O)Ph}$_2$](PF$_6$)$_2$ in MeCN and DCM, that was prepared in a glovebag, was obtained at 4.5 K at Miami University using a Bruker X-band EPR spectrometer with a microwave frequency of 9.629 GHz. Solvents used for synthesis and characterization were sparged with nitrogen to remove O$_2$ and dried through an activated alumina column in an MBraun MB-SPS solvent purification system. Reagents that were used in the syntheses of Co(bpy)Cl$_2$ and

[Co(bpy){Ph(O)NN(O)Ph}$_2$](PF$_6$)$_2$ were purchased from Sigma-Aldrich, Fisher, Strem, and TCI.[66]

3.4.2 Single-Crystal X-Ray Diffraction Experiment

A garnet-red crystal of [Co(bpy){Ph(O)NN(O)Ph}$_2$](PF$_6$)$_2$ was coated in paratone oil and then mounted on a CryoLoop. This CryoLoop was then placed on a goniometer under a nitrogen stream. The data set for the crystal structure was obtained on a Bruker Kappa APEX II Duo CCD system that was supplied with an Mo ImuS source and a Cu ImuS micro-focus source provided with QUAZAR optics (λ = 1.54178 Å). Using reflections from three different orientations, the unit cell of the crystal structure was determined. APEX II software packages were used to collect the data set, the APEX II software suite was used to process the data set, and SAINT was used to integrate the data set. Using multi-scan SADABS, an empirical absorption correction as well as other corrections were applied to the data set. Using the Bruker SHELXTL package, structure solution, refinement, and modelling were performed. The crystal structure of [Co(bpy){Ph(O)NN(O)Ph}$_2$](PF$_6$)$_2$ was determined by the full-matrix least-squares refinement of F^2 and the selection of appropriate atoms from the difference map. Hydrogen atoms were calculated and U_{iso}(H) values were fixed based on a riding model.[66]

Crystal data for [Co(bpy){Ph(O)NN(O)Ph}$_2$](PF$_6$)$_2$(CH$_2$Cl$_2$): $C_{35}H_{30}Cl_2CoF_{12}N_6O_4P_2$, M = 1018.42 g/mol, monoclinic unit cell, a = 28.0797(9) Å, b = 13.4393(4) Å, c = 25.3112(8) Å, α = 90°, β = 103.746(2)°, γ = 90°, V = 9278.2(5) Å^3, T = 100(2) K, space group C2/c, Z = 8,57343 reflections measured, 9419 independent reflections (R_{int} = 0.0725). The final $R1$ values were 0.0775 ($I > 2\sigma(I)$). The final $wR(F2)$ values were 0.2463 ($I > 2\sigma(I)$). The final $R1$ values were 0.1171 (all data). The final $wR(F2)$

values were 0.2832 (all data). Using PLATON SQUEEZE, two disordered CH_2Cl_2 molecules were removed.[66]

3.4.3 Synthesis of Co(bpy)Cl$_2$

The synthesis of the Co(II) synthon Co(bpy)Cl_2 was followed from a procedure reported by Iqbal and coworkers,[65] albeit with minor modifications. A solution of 1.57 g (9.92 mmol) bpy in 30 mL MeCN was treated with 1.28 g (9.86 mmol) solid anhydrous $CoCl_2$. This reaction was carried out in an MBraun air- and moisture-free nitrogen glovebox for 24 hours at room temperature and resulted in the formation of a light blue precipitate. Once the reaction was complete, MeCN solvent was removed *in vacuo* and the light blue powder was washed with Et_2O and dried under vacuum in order to yield 0.74 g (26%) of the light blue Co(bpy)Cl_2.[66]

3.4.4 Synthesis of [Co(bpy){Ph(O)NN(O)Ph}$_2$](PF$_6$)$_2$

0.517 g (1.79 mmol) of the light blue-colored Co(II) synthon Co(bpy)Cl_2 was suspended in 50 mL MeCN. A solution of 1.31 g (3.75 mmol) $TlPF_6$ in 10 mL MeCN was added to the Co(bpy)Cl_2 suspension, which resulted in the formation of TlCl as a white precipitate, along with a color change of the solution from blue to a peach color. After waiting for 30 minutes, 1.15 g (10.7 mmol) PhNO in 25 mL MeCN was added to the reaction mixture, turning the mixture a deep green. The reaction was carried out in an MBraun air- and moisture-free nitrogen glovebox for 2.5 days at room temperature. Due to the deep green color of PhNO, no further color changes were observed throughout the reaction. Once the reaction was complete, the white solid TlCl was removed from the reaction mixture by filtration through a medium glass-fritted funnel, followed by the removal of MeCN solvent from the filtrate *in vacuo* in order to yield the crude

$[Co(bpy)\{Ph(O)NN(O)Ph\}_2](PF_6)_2$ product. Recrystallization of the product was then performed by the following two steps: first the crude product was dissolved in minimal DCM and kept in the glovebox freezer (-30°C) for 24-48 hours so that any unreacted PhNO dimer could precipitate; the vials were then filled about halfway with the supernatant, and Et_2O was layered atop the supernatant. The vials were then kept in the glovebox freezer for 72 hours to yield garnet-red crystals of $[Co(bpy)\{Ph(O)NN(O)Ph\}_2](PF_6)_2$. The overall product yield was 0.25 g (0.27 mmol, 15%).[66]

CHAPTER IV

REDOX ACTIVITY STUDIES OF THE COBALT(II) BIPYRIDYL/DIPHENYLAZODIOXIDE COMPLEX SALT USING ELECTROCHEMICAL METHODS

4.1 Rationale

Once the synthesis and initial characterization of the complex salt $[Co(bpy)\{Ph(O)NN(O)Ph\}_2](PF_6)_2$ was completed, the next focus of this project was to continue the characterization of this compound by investigating the potential redox activity of its azodioxide ligands. As discussed in Chapter II, Section 2.5, we hypothesized that azodioxides may be able to display redox activity, based on their significant π delocalization. This hypothesis is supported by the fact that Ph(O)NN(O)Ph has N–O and N–N bond lengths that correspond to substantial π delocalization, both as a free molecule[98] and as a ligand[99] in complexes. In addition, evidence of redox activity has been reported in free nitrosoarenes, ArNO (the monomers of diarylazodioxides),[100,101] as well as in complexes in which ArNO is considered a neutral ligand,[102] a radical monoanion ($ArNO^{\bullet -}$),[102,103] or a closed-shell dianion ($ArNO^{2-}$).[102,104] In this respect, ArNO species are electronically somewhat similar to O_2.[100] However, prior to our work, the redox activity of azodioxide complexes had not been studied. It is important to note that, since our newly prepared heteroleptic complex contains a non-azodioxide ligand, bpy, which has long been known to be redox-active itself,[105] we believed that it was quite likely that this novel complex would display some ligand-based redox activity due to bpy, even if the azodioxide ligands did not contribute to this property.

We decided to investigate the redox activity of the $[Co(bpy)\{Ph(O)NN(O)Ph\}_2](PF_6)_2$ complex salt using electrochemical techniques, in particular, cyclic voltammetry (CV) and UV-visible spectroelectrochemistry. Electrochemical techniques are very useful in the study of electron-transfer reactions, by measuring the ability of an applied potential to induce oxidation or reduction (redox) reactions in the compounds studied. CV, in which the applied electrode potential is varied over time and the resulting current is measured, is particularly useful in the characterization of redox processes of molecular species. In fact, CV has become a widely used electrochemical method for conducting initial electrochemical studies of new systems[106] (in our case, azodioxide complexes). Moreover, the related method of UV-visible spectroelectrochemistry has the capability of identifying redox processes along with the corresponding species (such as reactive intermediates or products) at each step in a redox reaction.[107] UV-visible spectroelectrochemistry can thus be utilized to further understand redox processes that were initially examined by CV. Importantly, the use of both CV and UV-visible spectroelectrochemical methods can help indicate whether the redox activity in novel transition metal complexes is primarily metal-based or ligand-based.

4.2 Background on Electrochemical Studies for Nitrosoarenes and its Complexes

As redox activity studies of ArNO and their complexes have been reported, we were interested in obtaining from the literature background information on investigations of the redox activity of ArNO that employed electrochemical methods, since this information was potentially useful as a comparison to our electrochemical studies of $[Co(bpy)\{Ph(O)NN(O)Ph\}_2](PF_6)_2$, which contains the ArNO-related ligand diphenylazodioxide, Ph(O)NN(O)Ph. In particular, some research groups have reported extensive electrochemical data on free ArNO molecules as well as on ArNO complexes.

Lessard and coworkers performed CV studies in the potential window of -1.00 to -2.60 V *vs.* $Ag/AgNO_3$ (0.05 M) of PhNO, azoxybenzene (Ph(O)NNPh), and azobenzene (PhNNPh) in organic solvents. The CV studies of PhNO showed one reversible redox couple, $PhNO/[PhNO]^{\bullet -}$, with a cathodic peak at -1.39 V *vs.* $Ag/AgNO_3$ (0.05 M) and an anodic peak at -1.32 V; an irreversible cathodic peak at -2.29 V corresponding to the one-electron reduction of $[PhNO]^{\bullet -}$ to $[PhNO]^{2-}$; and a second reversible redox couple, $Ph(O)NNPh/[Ph(O)NNPh]^{\bullet -}$, with a cathodic peak at -1.84 V and an anodic peak at -1.77 V. The Ph(O)NNPh species is proposed to be formed *in situ* from a reaction of $[PhNO]^{\bullet -}$ with residual water that also involves the elimination of OH^-. The CV studies for Ph(O)NNPh showed one reversible redox couple, $Ph(O)NNPh/[Ph(O)NNPh]^{\bullet -}$, with a cathodic peak at -1.84 V *vs.* $Ag/AgNO_3$ and an anodic peak at -1.75 V, which is in agreement with the reversible redox couple $Ph(O)NNPh/[Ph(O)NNPh]^{\bullet -}$ at -1.84 V/-1.77 V in the CV studies of PhNO; an irreversible cathodic peak at -2.24 V that corresponded to $[Ph(O)NNPh]^{\bullet -}$ being reduced to $[PhNNPh]^{\bullet -}$, the azobenzene radical monoanion, which forms as a result of a multistep reaction process involving disproportionation, protonation, and two–electron-transfer steps; and a second irreversible cathodic peak at -2.35 V that corresponded to the one-electron reduction of $[PhNNPh]^{\bullet -}$ to $[PhNNPh]^{2-}$. The CV studies for PhNNPh showed one reversible redox couple, $PhNNPh/[PhNNPh]^{\bullet -}$, with a cathodic peak at -1.81 V *vs.* Ag/AgNO$_3$ and an anodic peak at -1.74 V, and an irreversible cathodic peak at -2.35 V corresponding to the one-electron reduction of [PhNNPh]$^{\bullet-}$ to [PhNNPh]$^{2-}$, which is in agreement with the irreversible cathodic peak observed at -2.35 V in CV studies of Ph(O)NNPh.[108] The results of the CV studies conducted by the Lessard group are in close agreement with earlier reported CV studies for PhNO,[109-111] Ph(O)NNPh,[109,110,112,113] and PhNNPh.[109,112,114]

Ottenwaelder and coworkers conducted CV studies on free ArNO molecules *p*-RC$_6$H$_4$NO, where R = H, Cl, Br, NMe$_2$, or NO$_2$. One reversible redox couple, ArNO/[ArNO]$^{\bullet-}$, with a half-wave potential ($E_{1/2}$) ranging from -1.69 to -0.93 V *vs.* ferrocenium/ferrocene (Fc$^+$/Fc), was detected in the CV of all the free ArNO molecules studied, where -1.69 V (the most negative $E_{1/2}$) corresponded to the molecule with R = NMe$_2$, which is the most electron-donating substituent of those studied, and -0.93 V (the least negative $E_{1/2}$) corresponded to the molecule with R = NO$_2$, which is the most electron-withdrawing substituent. A second reversible redox couple, Ar(O)NNAr/[Ar(O)NNAr]$^{\bullet-}$, with an $E_{1/2}$ ranging from -1.86 to -1.33 V *vs.* Fc$^+$/Fc was also detected in the CV studies of all the free ArNO molecules except R = NMe$_2$, where the most negative $E_{1/2}$ corresponded to PhNO (R = H) and the least negative $E_{1/2}$ corresponded to the molecule with the most electron-withdrawing substituent (R = NO$_2$).[115] The redox potentials are clearly dependent on the *para* substituent.

In addition to performing CV studies on certain free ArNO, Ottenwaelder and coworkers performed extensive CV studies on Cu complexes containing the studied ArNO species as ligands, as well as the ancillary neutral ligand TMPD (*N,N,N',N'*- tetramethyl-1,3-propanediamine) and the counteranion F$_3$CSO$_3^-$ (triflate). It is important to note that

Cu is in the +1 oxidation state in its complex with TMPD, [Cu(TMPD)(MeCN)](F_3CSO_3), before it reacts with ArNO to form Cu/ArNO adducts. In the Cu/ArNO complex with R = NMe_2, Cu remains in the +1 oxidation state and the ArNO is considered a neutral ligand. However, in the Cu/ArNO complexes with R = H, Cl, or Br, Cu is oxidized to the +2 oxidation state and ArNO is reduced to the radical monoanion $ArNO^{\bullet-}$. Additionally, the Cu/ArNO complex with R = NO_2 is a dinuclear species, [$TMPDCu^{II}(\mu\text{-}\eta^2{:}\eta^2\text{-}PhNO^{2-})(\mu\text{-}F_3CSO_3)Cu^{II}TMPD$]($F_3CSO_3$), in which both Cu ions are in the +2 oxidation state and ArNO is reduced to a dianion $[ArNO]^{2-}$. In the CV studies of the Cu/ArNO complexes, one irreversible cathodic peak was detected for all the complexes studied with $E_{1/2}$ values ranging from -1.05 to -0.72 V *vs.* Fc^+/Fc, where the most negative $E_{1/2}$ (-1.05 V) corresponded to R = NMe_2 and the least negative $E_{1/2}$ (-0.72 V) corresponded to R = NO_2. In the $E_{1/2}$ range of -1.75 to -1.17 V *vs.* Fc^+/Fc, a quasireversible redox couple was detected for all the Cu/ArNO complexes except for that containing PhNO, (when R = H, a second irreversible cathodic peak was determined instead) where the most negative $E_{1/2}$ corresponded to R = NMe_2 and the least negative $E_{1/2}$ corresponded to R = NO_2. Ottenwaelder's group proposed that this quasireversibility is a result of the dissociation of ArNO from Cu, since the $E_{1/2}$ values are very similar to the ones they obtained for the second reversible redox couple in the CV of free ArNO. Lastly, in the $E_{1/2}$ range of -0.36 to -0.11 V *vs.* Fc^+/Fc, a quasireversible redox couple was detected for all the Cu/ArNO complexes, where once again the most negative $E_{1/2}$ corresponded to R = NMe_2 and the least negative $E_{1/2}$ corresponded to R = NO_2.[115] Just as in the CV of free ArNO, the redox potentials in the CV of Cu/ArNO complexes are dependent on the *para* substituent of ArNO, with redox processes occurring at more negative potentials when the *para* substituent is an electron-donating group and at less negative potentials when the *para* substituent is an electron-withdrawing group.

4.3 Background on Electrochemical Studies for Cobalt Aromatic Diimine Complexes

Numerous studies of ruthenium complexes with redox-active aromatic diimine ligands have been reported (see Chapter II, Section 2.2 for details on the redox activity of bpy), but there have been comparatively fewer reports on the studies of cobalt complexes with similar types of redox-active ligands. However, some studies have reported interesting electrochemical data on cobalt complexes of bpy, 2,2′:6′,2″-terpyridine (tpy), 1,10-phenanthroline (phen), and derivatives of these ligands that are useful points of reference to our electrochemical studies.

CV studies of the complexes $Co(bpy)_3^{2+}$ and $Co(tpy)_2^{2+}$ (as well as of similar complexes containing substituted analogs of the bpy and tpy ligands) were performed by Conradie and coworkers. These studies showed three reversible redox couples for each complex. Based on density functional theory (DFT) calculations, one redox couple was assigned as Co(III)/Co(II), which is a Co-based redox process, in the $E_{1/2}$ range of -0.266 to -0.081 V *vs.* Fc^+/Fc, where $E_{1/2}$ becomes less negative as the substituent on bpy or tpy becomes less electron-donating; a second redox couple was assigned as Co(II)/Co(I), indicating another Co-based redox process, in the $E_{1/2}$ range of -1.673 to -1.189 V *vs.* Fc^+/Fc, where $E_{1/2}$ becomes less negative as the substituent on bpy or tpy becomes less electron-donating; and a third redox couple was assigned as $Co(I)/Co(I)(L^{\bullet-})$, indicating a ligand-based redox process in which a Co(I) complex undergoes a reduction such that one of the initially neutral bpy or tpy ligands ("L") is reduced to a radical anion, but the +1 oxidation state of Co remains the same, in the $E_{1/2}$ range of -2.141 to -2.032 V *vs.* Fc^+/Fc, where, again, $E_{1/2}$ becomes less negative as the substituent on bpy or tpy becomes less electron-donating.[116,117] Conradie's group also conducted CV studies of $Co(phen)_3^{2+}$ and similar complexes bearing substituted phenanthroline ligands. In these cases, the authors were able to identify an analogous set of three reversible redox couples, although the reduction of $Co(5\text{-nitro-phen})_3^{2+}$ indicated irreversible behavior. DFT calculations indicated that the irreversibility was due to ligand-based reduction.[116,118]

Fontecave and coworkers performed CV studies on eight $Co(tpy)_2^{2+}$ complexes with varying substituents on the tpy ligands. Based on DFT calculations, the authors were able to assign one redox couple for each complex as Co(II)/Co(I), indicating a Co-based redox process. This redox couple was also assigned as being reversible for all eight complexes studied. On the other hand, a second redox couple, which appeared at more negative potentials than the other redox couple, was assigned as either reversible or irreversible depending on the ligand. Based on DFT calculations, the second redox couple was assigned by the authors as a ligand-based redox process in which a Co(I) complex undergoes a reduction such that one of the substituted tpy ligands is reduced to a radical anion but the +1 oxidation state of Co remains the same.[116,119] As with the CV studies conducted by Conradie and coworkers,[117] these authors were also able to propose that ligand-based redox processes tend to occur at more negative potentials than those for Co-based redox processes.

Other CV studies were conducted by MacFarlane and coworkers on $Co(bpy)_3^{2+}$ in various organic solvents and ionic liquids.[116,120] Like Conradie's group,[117] the authors were able to assign the Co(III)/Co(II) redox couple as being reversible. The second redox couple Co(II)/Co(I), in contrast to that studied by Conradie and coworkers,[117] was assigned by these authors as being irreversible. The Co(II)/Co(I) redox couple identified by MacFarlane and coworkers appeared at more negative potentials than their Co(III)/Co(II) redox couple. The authors hypothesized that the irreversibility of the Co(II)/Co(I) redox couple is due to irreversible dissociation of the bpy ligand from the short-lived Co(I) species $Co(bpy)_3^+$. To test this hypothesis, these authors conducted a CV experiment on $Co(bpy)_3^{2+}$ in the presence of excess bpy. Their hypothesis was supported by the observation under these conditions of a reversible Co(II)/Co(I) redox couple.[116,120]

4.4 Results and Discussion

Our redox activity studies of the $[Co(bpy)\{Ph(O)NN(O)Ph\}_2](PF_6)_2$ complex salt, in addition to the homoleptic $[Co\{Ph(O)NN(O)Ph\}_4](PF_6)_2$ complex salt, using CV and UV-visible spectroelectrochemistry were performed in collaboration with Dr. Jerry Mundell and Prof. Mekki Bayachou of Cleveland State University, and have been published in *Inorganica Chimica Acta*.[116]

A CV measurement[116] of $[Co(bpy)\{Ph(O)NN(O)Ph\}_2](PF_6)_2$ that was taken in the cathodic direction (the potential swept negatively) at a sweep rate of v = 100 mV/s is depicted in Figure 21. This CV shows two redox couples, where the first redox couple is indicated as 1C/1A, the second redox couple indicated as 2C/2A, "C" standing for the cathodic peak and "A" standing for the anodic peak. The first redox couple 1C/1A has a peak potential separation ΔE_p (the difference between the cathodic peak potential and its corresponding anodic peak potential[106]) of 40 mV and a half-wave potential $E_{1/2}$ (the halfway potential between a cathodic peak and its corresponding anodic peak[106]) of -560 mV. The second redox couple 2C/2A was calculated as having ΔE_p = 116 mV and $E_{1/2}$ = -1018 mV. The peak dip that is shown in Figure 21 around -1.000 V is likely either a preequilibrium or an impurity. In addition, the CV in Figure 21 shows a signal at a more negative potential (-2.500 V). This signal is proposed to be due to a reduction of the solvent DMF and/or a reduction of our supporting electrolyte ^{n}Bu$_4$NPF$_6$ occurring at the Pt working electrode, since this signal was also observed when performing electrochemical cleanings of the Pt working electrode in a blank ^{n}Bu$_4$NPF$_6$ solution.[116]

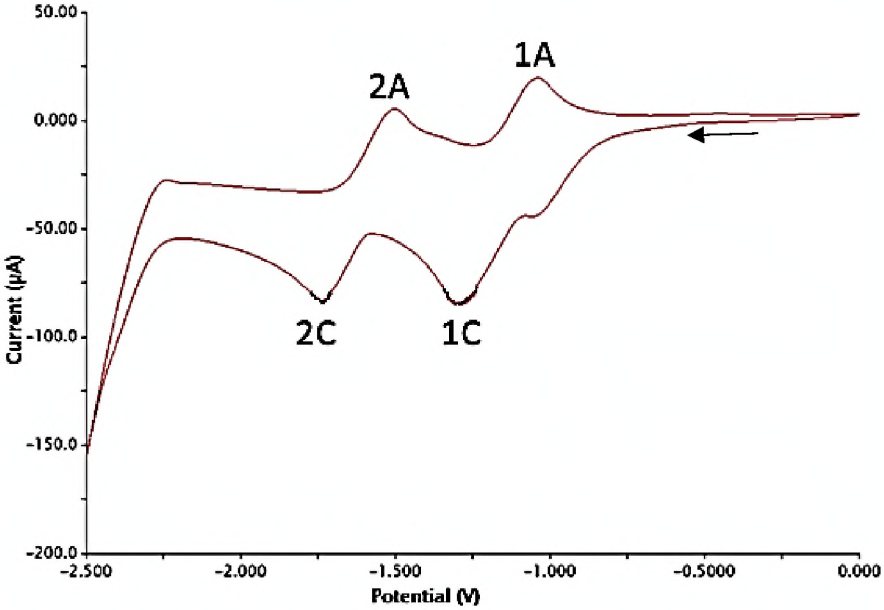

Figure 21: CV of [Co(bpy){Ph(O)NN(O)Ph}$_2$](PF$_6$)$_2$ at v = 100 mV/s with potential swept in negative (cathodic) direction.

CV data for [Co(bpy){Ph(O)NN(O)Ph}$_2$](PF$_6$)$_2$ were obtained at sweep rates ranging from 100 to 500 mV/s. Cathodic and anodic peak currents ($i_{p,c}$ and $i_{p,a}$ respectively) were plotted vs. $v^{1/2}$ for both redox couples, and the shape of these plots was compared to that predicted by the Randles-Sevcik equation, $i_p = 0.4463(F^3/RT)^{1/2}n^{3/2}AD^{1/2}C^*v^{1/2}$, where F is Faraday's constant, n is the number of electrons transferred in the redox process, A is the area of the working electrode's surface, D is the analyte's diffusion coefficient, and C^* is the analyte's concentration in the bulk solution. This equation predicts that a plot of i_p vs. $v^{1/2}$ will be linear, and such linearity was indeed observed in the plots, with the exception of the outlier point at 200 mV/s for the first redox couple.[116] The linear plots indicated diffusion control of the analyte $[\mathrm{Co(bpy)\{Ph(O)NN(O)Ph\}_2}]^{2+}$ in electrolyte solution, although with a nonzero intercept that is proposed to be due to a portion of current arising from non-redox processes.[121] The plots for both redox couples[116] are shown in Figure 22. For each redox couple, ΔE_p increased gradually as v increased, which is more noticeable for the first redox couple. Average ΔE_p as well as $E_{1/2}$ values were calculated, along with their standard deviations, over all v studied (except for the outlier at 200 mV/s for the first redox couple)[116] and are presented in Table II.

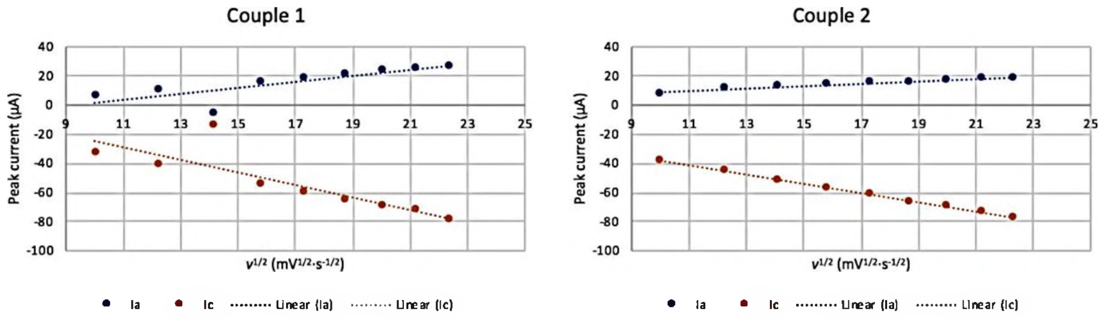

Figure 22: Randles-Sevcik plots for both redox couples.

Redox couple	1	2
Average ΔE_p (mV)	68 ± 22	135 ± 12
Average $E_{1/2}$ (mV)	-567 ± 4	-1016 ± 2

Table II: Average ΔE_p and $E_{1/2}$ values for both redox couples.

The two redox couples observed in our CVs of $[\mathrm{Co(bpy)\{Ph(O)NN(O)Ph\}_2}](\mathrm{PF_6})_2$ are proposed to correspond to quasireversible electron-transfer reactions, falling between being fully reversible and fully irreversible. Both redox couples had average peak potential separations (ΔE_p) that were significantly greater than 58 mV, which is the value expected for fully reversible redox couples at ambient temperature.[122,123] As mentioned previously, for both redox couples, ΔE_p increased gradually as v increased, another behavior that is predicted for quasireversible couples.[122,124] Importantly, quasireversibility behavior was also determined for the two redox couples observed in the CVs of the homoleptic $[Co\{Ph(O)NN(O)Ph\}_4](PF_6)_2$ complex salt.[116] A plausible reason why quasireversibility is observed in the heteroleptic $[Co(bpy)\{Ph(O)NN(O)Ph\}_2](PF_6)_2$ complex salt would be the dissociation of Ph(O)NN(O)Ph or bpy ligands upon reduction,[116] which are similar to CV results for $Co(bpy)_3^{2+}$ that were obtained by MacFarlane and coworkers.[120] However, it is unlikely that this ligand dissociation is fully irreversible because there was no evidence of linearity between peak potential and the logarithm of v.[123,125] We propose that the first redox couple observed for $[Co(bpy)\{Ph(O)NN(O)Ph\}_2](PF_6)_2$ corresponds to a Co-based reduction of Co(II) to Co(I), based on recent DFT calculations of Co(II) complexes containing polypyridyl and phenanthroline ligands that were performed by Conradie and coworkers,[117,118] whereas the second redox couple is proposed as corresponding to a ligand-based reduction on either the Ph(O)NN(O)Ph or the bpy ligand with the Co metal center in the +1 oxidation state.[116] MacFarlane's group showed that the Co(II)/Co(I) redox couples with bpy ligand dissociation appeared at more negative potentials (-1210 to -1400 mV)[120] than those observed in our CVs of $[Co(bpy)\{Ph(O)NN(O)Ph\}_2](PF_6)_2$ and even in the CVs of $[Co\{Ph(O)NN(O)Ph\}_4](PF_6)_2$.[116] This suggests that the dissociation of Ph(O)NN(O)Ph is more likely than the dissociation of bpy. Furthermore, Conradie and coworkers[117,118] and Fontecave and coworkers[119] were also able to observe the Co(II)/Co(I) redox couples for their Co complexes containing aromatic diimine ligands occurring at more negative potentials than those observed for $[Co(bpy)\{Ph(O)NN(O)Ph\}_2](PF_6)_2$ and $[Co\{Ph(O)NN(O)Ph\}_4](PF_6)_2$. The strong electron-withdrawing nature of azodioxides is proposed to make the reduction of our complex more thermodynamically favorable, and thus occurring at less negative electrode potentials, than that of complexes containing aromatic diimine ligands alone.[116]

In order to further understand the redox behavior of $[Co(bpy)\{Ph(O)NN(O)Ph\}_2](PF_6)_2$, UV-visible spectroelectrochemical studies were performed. Absorbance spectra[116] at various potentials were taken for $[Co(bpy)\{Ph(O)NN(O)Ph\}_2](PF_6)_2$. Figure 23 shows the overlaid absorbance spectra. As it can be seen in Figure 23, there is an absorbance peak at 305 nm before performing electrolysis. However, when performing electrolytic reduction at a potential of -2071.6 mV, the peak at 305 nm disappears and a new absorbance peak at 284 nm appears. Following electrolysis, the reoxidation process shows the peak at 284 nm disappearing slowly with the absorbance peak at 305 nm reappearing, albeit with less intensity than the initial 305 nm absorbance peak. Since the initial absorbance spectrum was partially, but not fully, recovered upon reoxidation, this is indicative of quasireversible redox behavior, consistent with that observed in the CV studies of $[Co(bpy)\{Ph(O)NN(O)Ph\}_2](PF_6)_2$. In addition, we propose that the ligand-based redox activity that was proposed in the second redox couple from the CV studies yields the absorbance peak at 284 nm, though some decomposition seemed to occur in this doubly reduced species, which is why the recovery of our complex is incomplete upon reoxidation.[116] Based on these results, we propose that the ligand-based redox activity corresponds to a reduction in the Ph(O)NN(O)Ph ligand as opposed to the bpy ligand. This conclusion is based on spectroelectrochemical studies of the ruthenium complex $Ru(bpy)_3^{2+}$ conducted by Heath and coworkers: their results suggest that the doubly reduced form of that complex is $[(Ru^{2+})(bpy)(bpy^-)_2]$, with a $\pi \rightarrow$

π^* transition of the unreduced bpy ligand responsible for the absorbance peak at 296 nm.[126] This wavelength is reasonably close to the peak observed at 284 nm for our doubly reduced species, and we thus propose it is due to absorbance by an unreduced bpy ligand. Additionally, UV-visible spectroelectrochemical studies of the homoleptic complex $[\mathrm{Co}\{\mathrm{Ph(O)NN(O)Ph}\}_4](\mathrm{PF}_6)_2$, which were performed under very similar experimental conditions as $[\mathrm{Co(bpy)}\{\mathrm{Ph(O)NN(O)Ph}\}_2](\mathrm{PF}_6)_2$, had shown its electrolysis being mostly reversible, suggesting that $[\mathrm{Co}\{\mathrm{Ph(O)NN(O)Ph}\}_4](\mathrm{PF}_6)_2$ undergoes the same type of process as $[\mathrm{Co(bpy)}\{\mathrm{Ph(O)NN(O)Ph}\}_2](\mathrm{PF}_6)_2$. Therefore, if ligand-based reduction is occurring, it is likely that the Ph(O)NN(O)Ph ligand is being reduced in both complexes, since the homoleptic species $[\mathrm{Co}\{\mathrm{Ph(O)NN(O)Ph}\}_4](\mathrm{PF}_6)_2$ does not contain a bpy ligand that could also be reduced.[116]

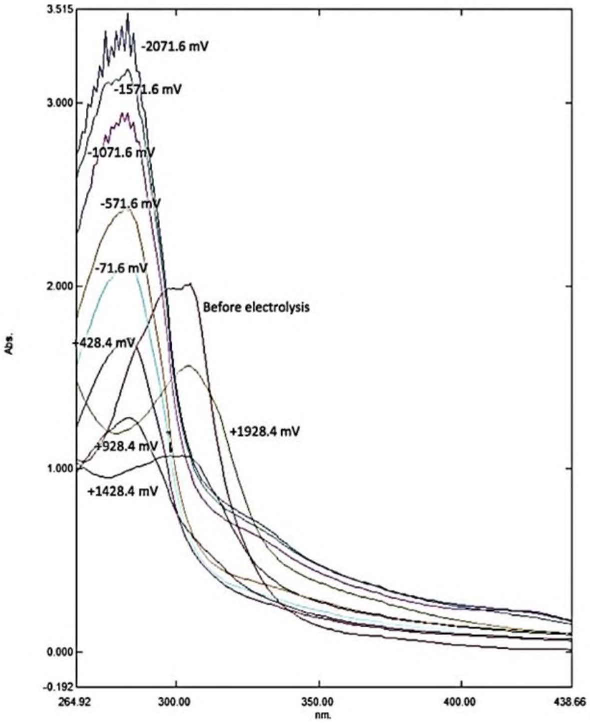

Figure 23: Spectroelectrochemical studies of $[\mathrm{Co(bpy)}\{\mathrm{Ph(O)NN(O)Ph}\}_2](\mathrm{PF}_6)_2$ in which absorbance spectra were taken at various potentials.

4.5 Experimental Methods

Electrochemical studies of our novel complex salt $[Co(bpy)\{Ph(O)NN(O)Ph\}_2](PF_6)_2$ were conducted using a WaveNow potentiostat from Pine Instrument Company.[116] For the CV studies, the working electrode, the electrode where the electrochemical event of interest takes place,[106] was a platinum disk,[116] the counter electrode, which is responsible for completing the electrical circuit with the working electrode,[106] used was a platinum wire,[116] and the reference electrode, which is commonly used as a point of reference against which other electrode potentials can be measured,[106] used was technically a silver (Ag) pseudoreference electrode.[116] In most cases, Ag^+/Ag reference electrodes, in which Ag^+ is present in aqueous solution, are utilized in systems with organic solvents. Unfortunately, when working with these types of electrodes, there is the possibility of this aqueous solution leaking into the solution containing the analyte.[106] Since we wished to perform these experiments under anhydrous conditions, we instead employed a silver pseudoreference electrode in addition to an internal standard.[106] Ferrocene, $(\eta^5\text{-}C_5H_5)_2Fe$ (abbreviated Fc), was used as our internal standard with the ferrocenium/ferrocene (Fc^+/Fc) redox couple as the reference potential due to its convenience, reproducibility, and allowability for a comparison of reduction potentials.[127] For UV-visible spectroelectrochemistry studies, a platinum honeycomb electrode from Pine Instrument Company was used as the working electrode and absorbance spectra were obtained from a Shimadzu UV-2600 spectrometer. All potentials in this study are reported in relation to the ferrocenium/ferrocene (Fc^+/Fc) redox couple as internal standard. The solvent that was employed in our electrochemical studies was dimethylformamide (DMF).[116] Not only were our complex and supporting electrolyte both highly soluble in DMF, but this solvent was shown to be stable toward redox processes in the potential windows we worked with. Even though $[Co(bpy)\{Ph(O)NN(O)Ph\}_2](PF_6)_2$ was synthesized in acetonitrile (MeCN), we opted not to use this solvent in our electrochemical studies because there was evidence of MeCN reduction at the more negative potential windows that were scanned. Importantly, DMF was degassed by sparging with nitrogen gas to remove O_2. The presence of O_2 in an electrochemical experiment can result in the formation of the oxygen radical anion $O_2^{\bullet -}$ (superoxide) from the reversible, one-electron reduction of O_2.[106] Therefore, O_2 can affect an analyte's response in an electrochemical study. DMF was also dried over activated 4 Å molecular sieves. Lastly, the supporting electrolyte used in our electrochemical studies was 0.1 M $^nBu_4NPF_6$.[116] Organic solvents, even highly polar ones like DMF, have a lower conductivity than water. Therefore, to increase the conductivity of the DMF solutions of our complex, the use of a supporting electrolyte was necessary. The salt $^nBu_4NPF_6$ is considered a good supporting electrolyte not only for the noncoordinating behavior of its PF_6^- anion, but also because it is highly soluble and stable in polar organic solvents like DMF.[106]

CHAPTER V

THE COBALT(II) BIPYRIDYL/DIPHENYLAZODIOXIDE COMPLEX SALT AS A CATALYST IN ALLYLIC AMINATION REACTIONS

5.1 Rationale

An important application of transition metal complexes containing redox-active ligands is in the catalysis of organic reactions.[128] We were interested to see if $[Co(bpy)\{Ph(O)NN(O)Ph\}_2](PF_6)_2$ possessed novel reactivity due to its unusual trigonal prismatic coordination geometry and the evidence of redox activity[129] in its azodioxide ligands. Specifically, we were interested in the investigation of $[Co(bpy)\{Ph(O)NN(O)Ph\}_2](PF_6)_2$ as a potential catalyst in allylic amination reactions, which involve the synthesis of allylic amines, since these reactions are of major utility. Allylic amines can act as advanced reaction intermediates in reactions such as asymmetric isomerization[130] and ring-closing metathesis[131].[132] Additionally, allylic amines can serve as starting materials in the syntheses of alkaloids,[133] carbohydrates and their derivatives,[134] and α- and β-amino acids.[135] Additionally, natural products containing allylic amine moieties are known.[136,137] The structure of allylamine, the simplest allylic amine, is shown in Figure 24.

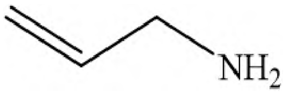

allylamine

Figure 24: Structure of allylamine.

In particular, as was previously mentioned in Chapter I, Section 1.1, transition metal complexes can be useful catalysts in the pharmaceutical industry, and allylic amination is itself important in the pharmaceutical industry since there are drugs that contain allylic amine moieties.[137] Examples of such pharmaceuticals are cinnarizine,[138] an antihistamine used to primarily treat motion sickness; terbinafine,[139] an antifungal used to treat ringworm and athlete's foot (which is on the WHO List of Essential Medicines as of 2019);[140] lisuride,[141] a drug used to treat Parkinson's disease and migraines; and vigabatrin,[142] a drug used to treat seizure disorders in infants. The two types of allylic amination reactions that are especially important for applications, including pharmaceutical applications, are the direct allylic amination of alkenes, which may also involve carbon-carbon (C–C) double-bond transposition, and nucleophilic allylic substitution.[136]

5.2 Types of Allylic Amination

5.2.1 Direct Allylic Amination/C–C Double-Bond Transposition

This type of allylic amination involves the breaking of a C–H bond, and also involves the movement of a C–C double bond from its original position in the original alkene substrate. Because of the bond strength of the C–H bond to be broken, the direct allylic amination of alkenes can be challenging to accomplish. This type of allylic amination is of interest because it has been shown to be useful in the synthesis of polyfunctional amines.[136] Importantly, the direct allylic amination of alkenes has been shown to be regioselective[143-147] (one isomer of all the possible isomers produced is the major product of the reaction[148]), in which the N atom of the amine substrate adds to the less substituted carbon of the original alkene carbons.[149] No additional products derived from the alkene are usually observed in these reactions.[143-147] A general reaction scheme for direct allylic amination/C–C double-bond transposition reactions is shown in Figure 25.[136]

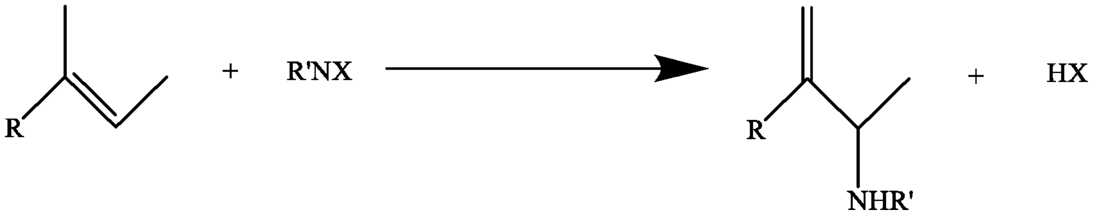

***R and R' represent alkyl or aryl groups**
***X represents an electronegative group**

Figure 25: General reaction scheme for direct allylic amination/C–C double-bond transposition reactions.

Most importantly, the direct allylic amination of alkenes has been shown to be catalyzed by the azodioxide complex salt $[Fe\{Ph(O)NN(O)Ph\}_3](FeCl_4)_2$ prepared by Nicholas' group (refer to Figures 8a and 8b in Chapter I, Section 1.6).[146,150,151] Nicholas' group proposed that the complex cation $[Fe\{Ph(O)NN(O)Ph\}_3]^{2+}$ was formed *in situ* when $FeCl_2$ or $FeCl_3$ was used as a precatalyst.[152] The isolated complex salt $[Fe\{Ph(O)NN(O)Ph\}_3](FeCl_4)_2$ was itself shown to be a competent catalyst for the particular reaction depicted in Figure 26,[150] where the reaction involved a 10 mol% catalyst loading of $[Fe\{Ph(O)NN(O)Ph\}_3](FeCl_4)_2$, a reaction temperature ranging from 70-100°C, and a reaction solvent of 1,4-dioxane.[146]

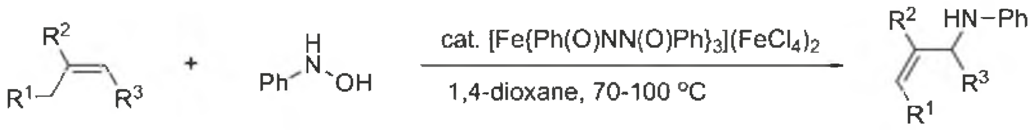

Figure 26: Allylic amination/C–C double-bond transposition catalyzed by [Fe{Ph(O)NN(O)Ph}$_3$](FeCl$_4$)$_2$.

The Nicholas group proposed a partial catalytic cycle[150] shown in Figure 27 for the reaction of Figure 26. The first step in the cycle is the dechelation of an azodioxide ligand from the catalyst [Fe{Ph(O)NN(O)Ph}$_3$](FeCl$_4$)$_2$, forming a five-coordinate reaction intermediate. After dechelation takes place, an alkene coordinates to the intermediate, yielding a π-complex adduct. The allyl hydroxylamine intermediate then forms as a result of the migration of the PhNO unit in the adduct to the alkene. During this step, a nitroso-ene reaction (a form of the Alder ene reaction in which the enophile is a nitroso compound[151,153]) takes place between an azodioxide ligand with an uncoordinated oxygen atom and the η^2-coordinated alkene (meaning two C atoms of an alkene ligand are bonded to the metal center),[154] indicating that this catalysis operates through an "on-metal" mechanism.[136,146,150,151] An on-metal mechanism is one in which PhNO (or its azodioxide dimer) remains coordinated to the metal while reacting with the alkene substrate, whereas an "off-metal" mechanism is one in which free (uncoordinated) PhNO is formed as an intermediate and acts as the main aminating agent during the catalysis.[136,151] The allyl hydroxylamine that was formed is then deoxygenated by an Fe(II) species, resulting in the formation of the allylic amine and an oxidized bimetallic Fe(III) species. The catalyst can then be regenerated by the reduction of the bimetallic Fe(III) species by phenylhydroxylamine (PhNHOH). It is important to note, however, that Nicholas' group observed the byproducts azoxybenzene, Ph(O)NNPh, and azobenzene, PhNNPh, both of which are deoxygenation products of PhNO or azodioxide, when they conducted a GC-MS analysis of their reaction mixture.[146,150,151] These deoxygenation reactions compete with the desired allylic amination reaction, and it has been reported that suppression of such side reactions is challenging, resulting in a decrease in the allylic amine yield.[136] Fortunately, the catalyst [Fe{Ph(O)NN(O)Ph}$_3$](FeCl$_4$)$_2$ was shown to improve the allylic amine yield and reduce the amounts of deoxygenation byproducts produced compared to a molybdenum(VI) dioxo complex[143] that Nicholas' group earlier investigated as a catalyst for this type of reaction,[136] indicating that either the presence of Fe(II) rather than Mo(VI), the azodioxide ligand in the catalyst [Fe{Ph(O)NN(O)Ph}$_3$](FeCl$_4$)$_2$, or both makes this catalyst more effective.

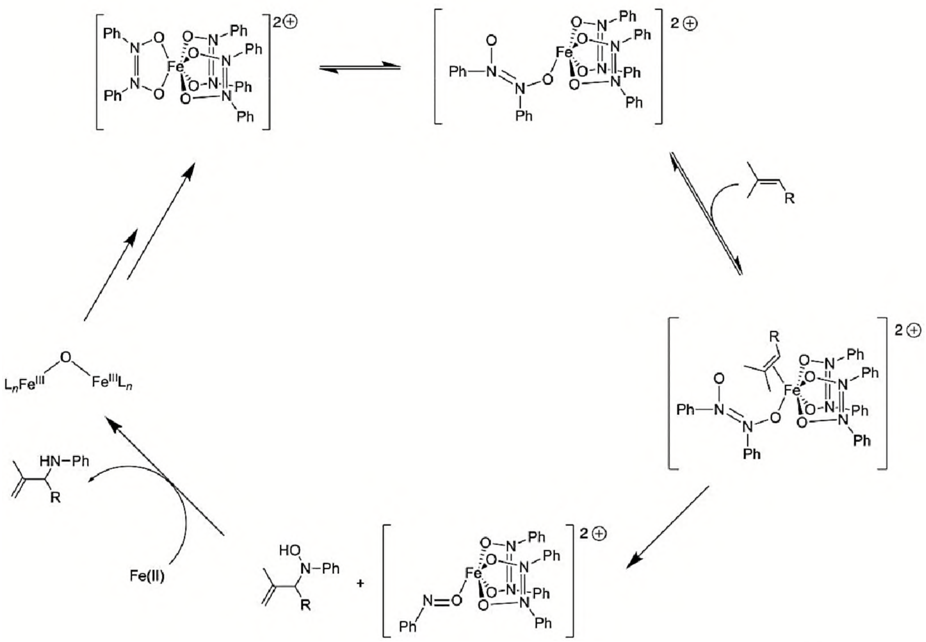

Figure 27: Partial catalytic cycle for the direct allylic amination of an alkene using [Fe{Ph(O)NN(O)Ph}$_3$](FeCl$_4$)$_2$ as a catalyst.

5.2.2 Nucleophilic Allylic Substitution

Nucleophilic allylic substitution is one of the most simple and direct types of allylic amination.[136] These reactions have shown great efficiency and flexibility.[155] Most nucleophilic allylic substitution reactions involve the use of a substrate that contains a good leaving group. Since allylic alcohols contain a poor leaving group, they were initially not used as substrates. A transition metal catalyst is usually required to activate such substrates.[156] Recently, however, there has been a growing interest in the use of allylic alcohols as substrates for nucleophilic allylic substitutions due to their ready availability[136] and their ability to reduce byproduct formation, since nucleophilic allylic substitution on an allylic alcohol will yield H_2O as the other stoichiometric product, constituting a greener and more sustainable process.[155,156] A general reaction scheme for nucleophilic allylic substitution reactions is depicted in Figure 28.[136]

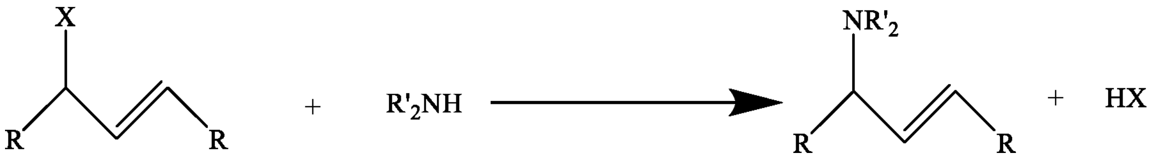

***R and R'$_2$ represent alkyl or aryl groups**
***X represents an electronegative group**

Figure 28: General reaction scheme for nucleophilic allylic substitution reactions.

Transition metal complexes have been shown to act as stereo-, regio-, and enantioselective catalysts for the nucleophilic allylic substitution of alcohols.[156] The most commonly used transition metal catalysts for the nucleophilic allylic substitution of allylic alcohols contain palladium or iridium,[155] which are 2nd- and 3rd-row transition metals, respectively. However, transition metal catalysts containing cheaper and more Earth-abundant 1st-row transition metals, especially iron and nickel, have been increasingly used.[157] In addition to the examples already mentioned, the iron complex $Fe(CO)_3\{\eta^4\text{-}(CH_2)_4(SiMe_3)_2C_5O\}$ has proven to be an active catalyst in the one-pot synthesis of the allylic amine drug cinnarizine,[138] whose synthesis involves the nucleophilic allylic substitution of the allylic alcohol cinnamyl alcohol with the amine 1-benzhydrylpiperazine.[158]

5.3 Results and Discussion

5.3.1 Direct Allylic Amination/C–C Double-Bond Transposition

Since Nicholas' group was able to show that an azodioxide complex can act as an active catalyst in direct allylic amination/C–C double-bond transposition reactions, we were interested in studying the reactivity of our newly synthesized heteroleptic azodioxide complex by assessing its catalytic ability in these types of reactions.

The effective catalysis of the direct allylic amination of 2-methyl-2-pentene and 2-methyl-2-hexene with PhNHOH by $[Co(bpy)\{Ph(O)NN(O)Ph\}_2](PF_6)_2$ has been demonstrated and published in *Results in Chemistry*.[151] We decided to study trisubstituted, unsymmetrical alkenes as substrates because Nicholas' group showed that such substrates gave the best allylic amine yields and regioselectivity when their catalyst was used.[146] The catalytic scheme[151] is demonstrated in Figure 29. When R = H, the catalytic turnover number is 4.0 with an isolated yield of the allylic amine product of 40%, whereas when R = CH_3, the catalytic turnover number becomes 1.4 with an isolated yield of only 14%. Other reaction conditions were attempted (different solvents, reaction times, reaction temperatures), but the conditions depicted in Figure 29 gave the best results. It is important to note that the allylic amine products are racemic mixtures of their *R* and *S* enantiomers since this catalysis is not enantioselective but regioselective. Importantly, the catalysis of the direct allylic amination of alkenes in which homoleptic complex salt $[Co\{Ph(O)NN(O)Ph\}_4](PF_6)_2$ was the catalyst gave very similar results.

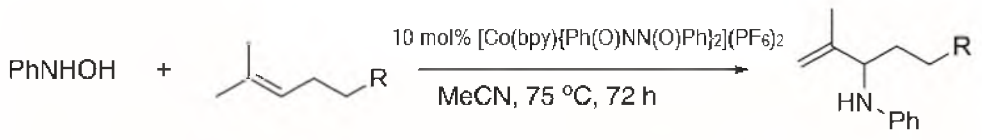

R	Isolated yield (%)	Turnovers
H	40	4.0
CH_3	14	1.4

Figure 29: Direct allylic amination reactions catalyzed by $[Co(bpy)\{Ph(O)NN(O)Ph\}_2](PF_6)_2$.

The turnover number for a catalyst refers to the average number of catalytic cycles completed before the catalyst becomes degraded.[159] As it can be seen in Figure 29, the reported turnover numbers for our catalytic reactions are low, suggesting that this limited catalytic efficiency may be caused by a side reaction or reactions of the catalyst. It is very likely that the azodioxide ligand is undergoing deoxygenation during the reaction since GC-MS analysis of a diethyl ether extract of the reaction mixtures showed the presence of both Ph(O)NNPh (*m/z* 198) and PhNNPh (*m/z* 182). As was previously mentioned, Nicholas' group also detected the deoxygenation products Ph(O)NNPh and PhNNPh when using their complex salt $[Fe\{Ph(O)NN(O)Ph\}_3](FeCl_4)_2$ as a catalyst in the direct allylic amination of alkenes. [146,150,151] Nicholas' group reported a turnover number of 8.8 for the direct allylic amination of 2-methyl-2-pentene with PhNHOH, although they calculated this number based on a yield from their GC analysis as opposed to an isolated yield as we did.[146] However, they did not report a yield for the direct allylic amination of 2-methyl-2-hexene with PhNHOH. Our observation of these byproducts not only further confirms the difficulty in suppressing their formation, but suggests, on the basis of our lower turnover numbers, that their formation is possibly more significant in our reactions.[151]

We performed an important control experiment to investigate the mechanism of our catalytic reactions. In particular, we were interested to find out if this catalysis operated by an "off-metal[136]" or "on-metal[136]" mechanism. In order to distinguish between these two main mechanistic types, a Diels-Alder trapping experiment[151] was performed by treating 2,3-dimethyl-1,3-butadiene with our catalyst $[Co(bpy)\{Ph(O)NN(O)Ph\}_2](PF_6)_2$ under the solvent and temperature conditions used in our catalytic reactions. As opposed to an allylic amination product of 2,3-dimethyl-1,3-butadiene, GC-MS analysis of the reaction mixture revealed the formation of a Diels-Alder cycloadduct of PhNO and 2,3-dimethyl-1,3-butadiene (*m/z* 189). This cycloadduct formation suggests that an "off-metal" mechanism for the catalysis of the direct allylic amination of alkenes by $[Co(bpy)\{Ph(O)NN(O)Ph\}_2](PF_6)_2$ is likely operative, in which free PhNO, rather than a coordinated azodioxide, acts as the aminating agent. The Diels-Alder trapping experiment[151] is depicted in Figure 30. In contrast, when Nicholas' group performed the analogous Diels-Alder trapping experiment with $[Fe\{Ph(O)NN(O)Ph\}_3](FeCl_4)_2$, they observed the allylic amination product of 2,3-dimethyl-1,3-butadiene, not its cycloadduct with PhNO. This suggests that, in contrast to our catalytic reactions, the allylic amination of alkenes catalyzed by $[Fe\{Ph(O)NN(O)Ph\}_3](FeCl_4)_2$ proceeds by an "on-metal" mechanism in which free PhNO is not generated as an intermediate. [136,146,150,151]

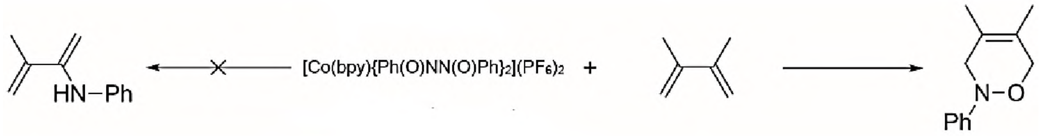

Figure 30: Diels-Alder trapping experiment with 2,3-dimethyl-1,3-butadiene.

With the “off-metal” mechanism being suggested by the trapping experiment described above, we were able to propose a partial catalytic cycle[151] for the catalysis of the direct allylic amination of alkenes by $[Co(bpy)\{Ph(O)NN(O)Ph\}_2](PF_6)_2$. This partial catalytic cycle[151] is shown in Figure 31. In this proposed cycle, uncoordinated PhNO, which forms from an azodioxide ligand dissociated from cobalt, reacts with an alkene substrate in a nitroso-ene reaction to yield a hydroxylamine. This hydroxylamine is then reduced to an allylic amine by Co(II), forming a bimetallic Co(III) complex with a bridging oxido ligand. In addition to the formation of the deoxygenation products Ph(O)NNPh and PhNNPh, another possible explanation for the low turnover number we observed for these reactions is an irreversible decomposition reaction of the bimetallic Co(III) complex (L_nCo^{III}–O–$Co^{III}L_n$) with water, leading to the formation of a Co(III) oxide or hydroxide, which are both thermodynamically stable. In the final step of our proposed partial catalytic cycle, PhNHOH is dehydrogenated by the bimetallic Co(III) complex in order to yield H_2O and regenerate PhNO and Co(II).

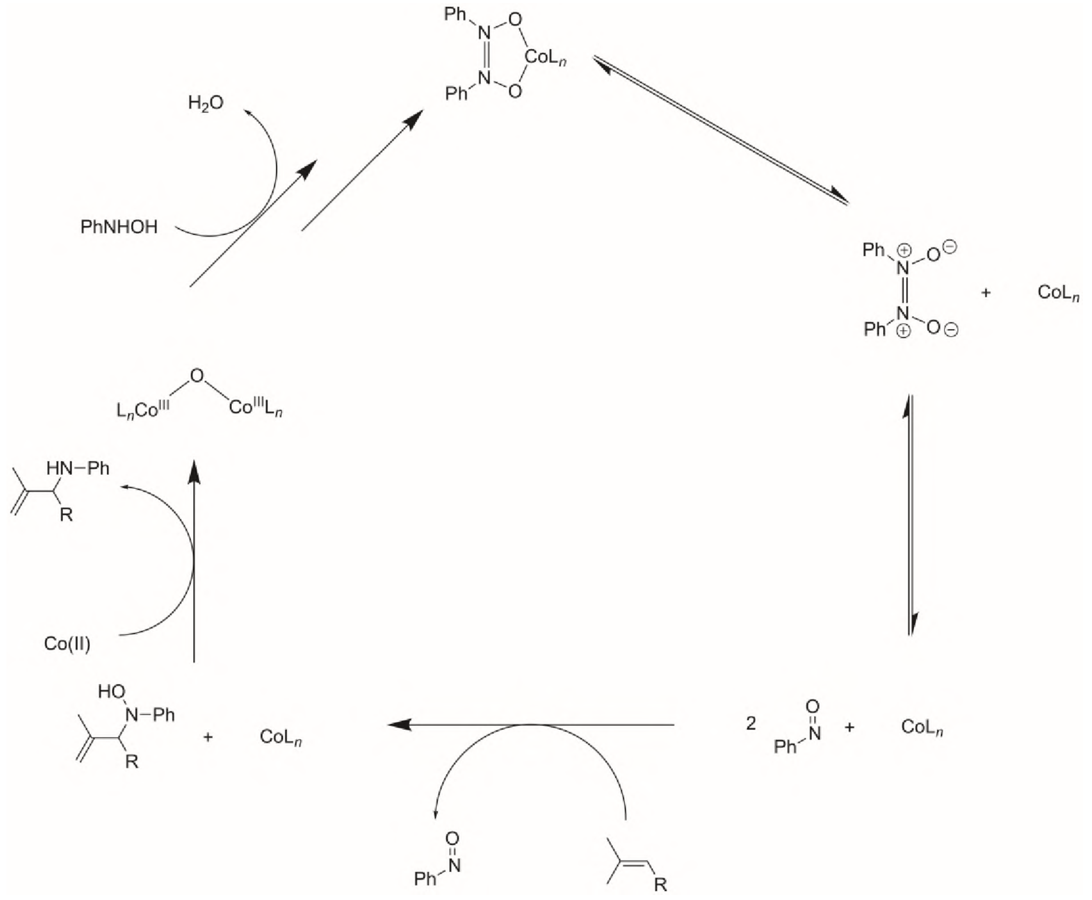

Figure 31: Proposed partial catalytic cycle for the direct allylic amination of alkenes by [Co(bpy){Ph(O)NN(O)Ph}$_2$](PF$_6$)$_2$.

Since a higher yield and turnover number resulted from the catalysis of the direct allylic amination of 2-methyl-2-pentene with PhNHOH, the characterization of its allylic amine reaction product $C_{12}H_{17}N$ will be discussed further. The allylic amine was characterized by GC-MS and ^{1}H NMR spectroscopy.

After removing nonvolatile cobalt-containing species from our reaction mixture *via* a silica gel pipette column, GC-MS analysis was performed on a diethyl ether extract of our crude reaction mixture to identify the organic products that were formed.[151] As was previously mentioned, in addition to the desired allylic amine product $C_{12}H_{17}N$ (*m/z* 175), the byproducts Ph(O)NNPh (*m/z* 198) and PhNNPh (*m/z* 182) were also identified. The *m/z* (mass-to-charge ratio) value reported for each product corresponds to its molecular ion peak (M^+). A molecular ion is formed when one electron from a molecule is removed using an ionization source such as electron ionization in a mass spectrometer and has the same molecular weight as the initial molecule.[160] Each reaction product peak in the gas chromatogram of the crude reaction mixture was identified by comparing each peak's corresponding experimental mass spectrum to that in a NIST library and by extracting ion chromatograms, where extracted ion chromatograms are plots of signal abundance versus retention time at selected *m/z* values.[161] The experimental mass spectrum of our allylic amine reaction product $C_{12}H_{17}N$ is depicted in Figure 32a, and the experimental mass spectra of the byproducts PhNNPh and Ph(O)NNPh are reported in Figures 32b and 32c, respectively. Most of the weak signals at *m/z* values greater than the molecular ion peaks in the mass spectra in Figure 32 possibly represent minor impurities from the GC column and/or mass spectrometer or noise. The experimental gas chromatogram of our crude reaction mixture with the allylic amine reaction product peak as well as the Ph(O)NNPh and PhNNPh byproduct peaks labeled is shown in Figure 33. Figure 33 shows that the retention time of the allylic amine was identified at 15.754 min and that the retention times of the byproducts PhNNPh and Ph(O)NNPh were identified at 5.217 min and 8.125 min, respectively. The unlabeled peaks in the gas chromatogram in Figure 33 are possibly minor impurities from the instrument, silicon-containing species from the GC column, or noise. Once we were able to identify the crude allylic amine reaction product by GC-MS, the next step was to separate and purify the allylic amine by preparative column chromatography before taking its ^1H NMR spectrum.[151]

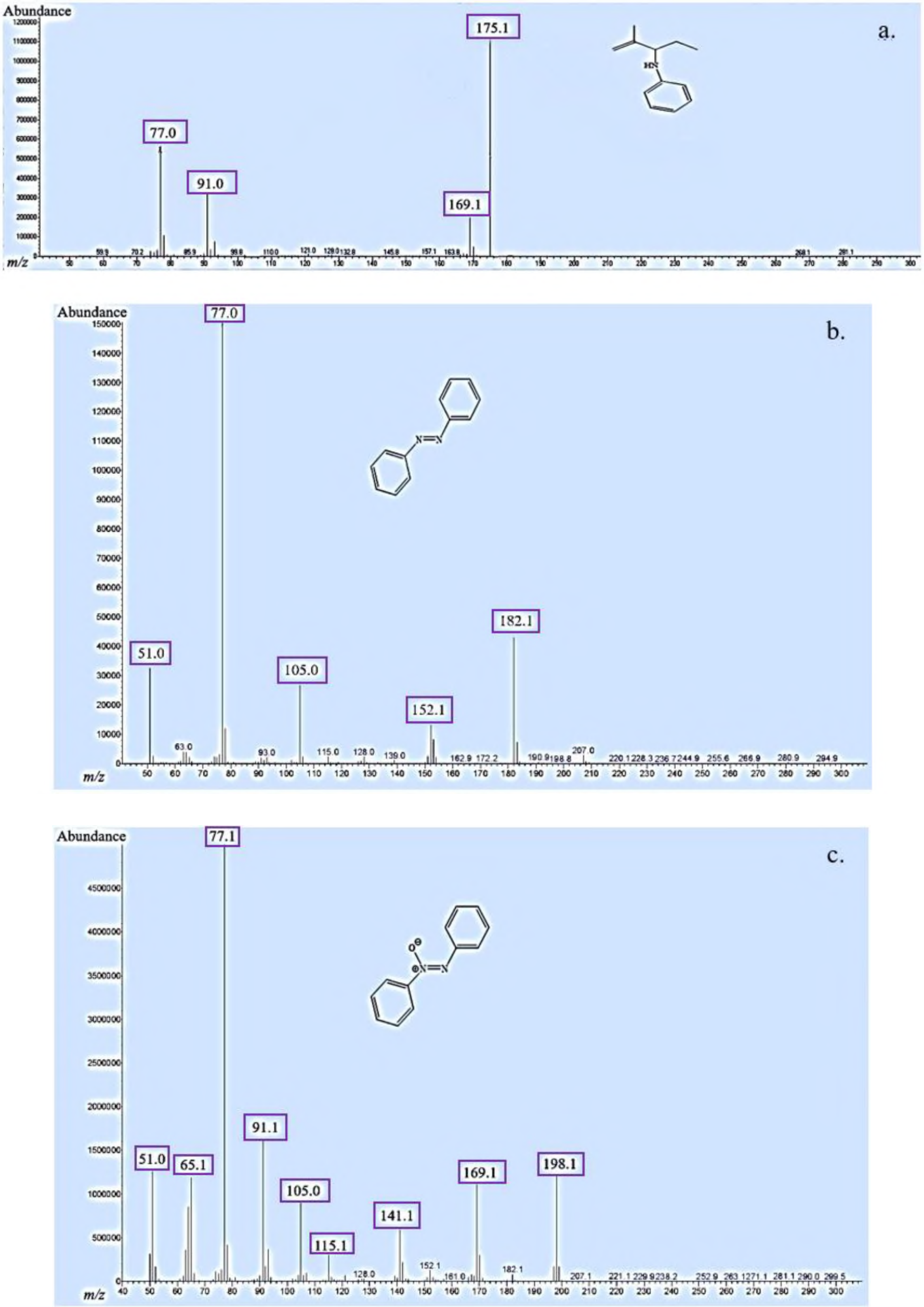

Figure 32: Experimental mass spectra of (a) allylic amine product (b) PhNNPh (c) Ph(O)NNPh.

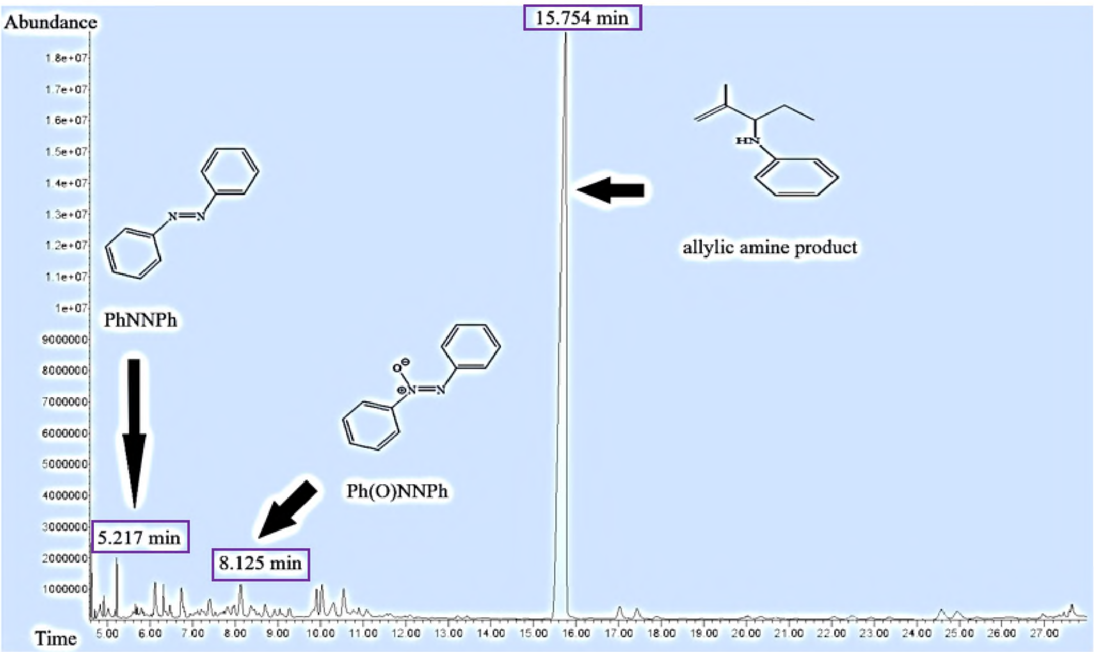

Figure 33: Experimental gas chromatogram of crude reaction mixture from the catalysis of the direct allylic amination of 2-methyl-2-pentene with PhNHOH.

The experimental ^{1}H NMR spectrum of our allylic amine reaction product $C_{12}H_{17}N$ is depicted in Figure 34c. Its spectrum is compared to the experimental ^{1}H NMR spectra of the starting materials 2-methyl-2-pentene (Figure 34a) and PhNHOH (Figure 34b). It can be seen in this comparison that our reaction product's spectrum mostly contains similar proton signals from both starting materials, indicating that a reaction product was made and is possibly an allylic amine.

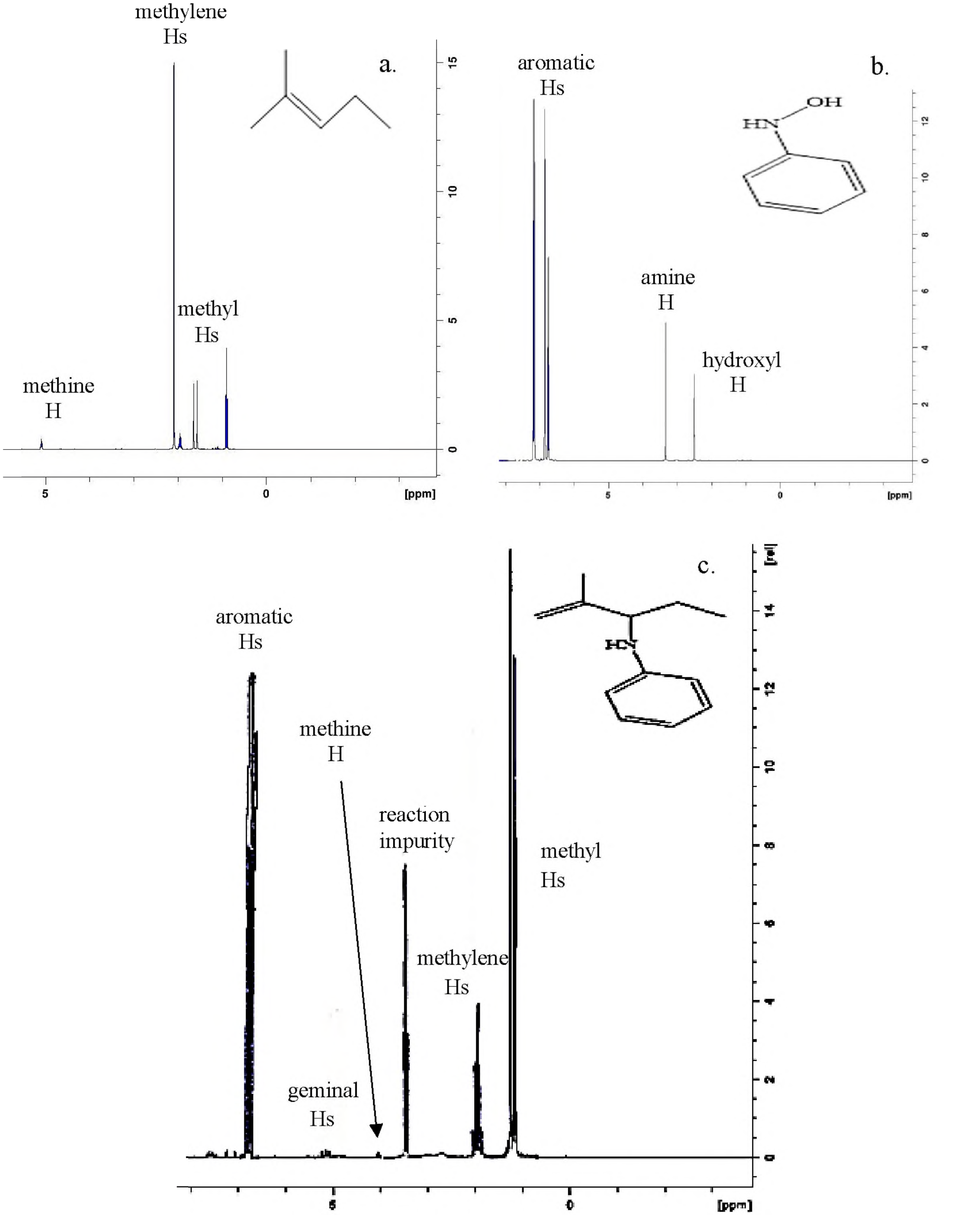

Figure 34: ^1H NMR spectra of (a) 2-methyl-2-pentene (b) PhNHOH (c) allylic amine reaction product.

Each of the proton signals in the ^{1}H NMR spectrum of the allylic amine product are worth discussing. For the explanation of the proton signals in the regions 1-6 ppm, I will refer to the protons in the allylic amine product's structure that give rise to them as being attached to carbon atoms that each have a certain number using the numerical scheme shown in Figure 35, except for the proton attached to the nitrogen atom. For the explanation of the aromatic proton signals in the 6-8 ppm range, I will refer to the aromatic protons as *ortho*, *meta*, or *para*. Furthermore, our experimental spectrum was compared to a literature spectrum[146] of the allylic amine product that was reported by Nicholas' group.

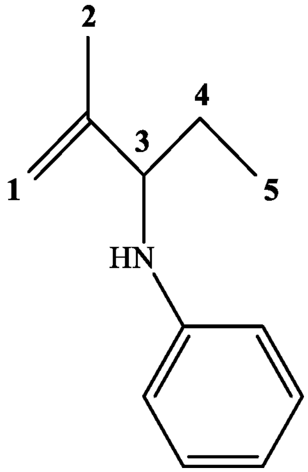

Figure 35: Numerical scheme of carbons in the allylic amine structure.

The proton signal around 1 ppm in the ^{1}H NMR spectrum of the allylic amine reaction product (Figure 34c) corresponds to the methyl protons that are attached to carbon 5. The splitting of this signal appears to be a triplet. Also, the integration of this peak was 2.9369, which rounded up to the nearest whole number is 3, indicating that 3 protons generate this signal. The 1 ppm region of the NMR spectrum of the allylic amine is shown in Figure 36. It is important to note that the expected splitting pattern for this signal is a doublet of doublets because the 2 protons that are attached to the neighboring carbon 4 are not of the same type. In other words, the 2 neighboring protons are in different chemical environments (chemically non-equivalent), with each proton producing its own signal with its own chemical shift in a ^{1}H NMR spectrum. With this being said, applying the $N + 1$ rule for each of the 2 neighboring, chemically non-equivalent protons, where "N" is the number of neighboring protons of a certain type, in order to determine the splitting pattern of the signal around 1 ppm, should have yielded a signal appearing as a doublet of doublets. (Since there are 2 neighboring, non-equivalent protons, the $N + 1$ rule needed to be applied twice, and since there is 1 proton of each of the 2 types in this scenario, the $N + 1$ rule yields the number 2 for each application of the rule, meaning the peak splitting is expected to be a doublet of doublets.) However, a triplet splitting pattern is observed in Figure 36 because the chemical environments of the 2 diastereotopic hydrogens on carbon 4 are very similar that these hydrogens' coupling constants with the hydrogens attached to carbon 5 are extremely close in value, and the diastereotopic hydrogens cannot be distinguished at the level of resolution provided by the 400-MHz NMR spectrometer we used. If the spectrum had been obtained on an NMR spectrometer with a very high frequency such as 1000 MHz, then the spectral resolution of the signals would be more resolved,[162] and the expected doublet of doublets signal would be observed around 1 ppm. Importantly, the literature spectrum with which we compared our NMR data also shows a signal with a triplet splitting pattern at 1.07 ppm (close to the 1 ppm value we observed) with an integration indicating that 3 protons give rise to this signal.[146]

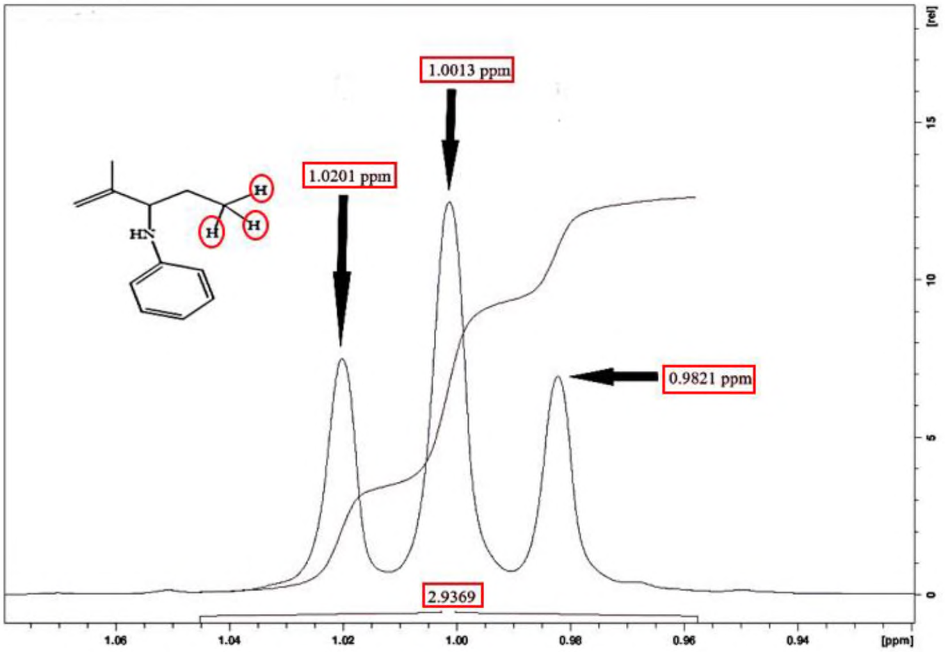

Figure 36: 1 ppm region of the ^{1}H NMR spectrum of allylic amine product.

The proton signal around 1.66 ppm in the ^{1}H NMR spectrum of the allylic amine reaction product (Figure 34c) corresponds to the methyl protons that are attached to carbon 2. The methyl protons on carbon 2 are more deshielded than the methyl protons on carbon 5 because these protons are attached to a carbon atom that is adjacent to an *sp*^{2}-hybridized carbon. In other words, the protons on carbon 2 are located closer to an *sp*^{2}-hybridized carbon atom than those on carbon 5. Since *sp*^{2}-hybridized carbon atoms are more electron-withdrawing than *sp*^{3}-hybridized carbon atoms, hydrogen atoms either directly attached to *sp*^{2}-hybridized carbon atoms or on nearby *sp*^{3}-hybridized carbon atoms are less shielded.[163] The signal at 1.66 ppm appears to be a singlet, with no splitting pattern. The absence of a splitting pattern is expected because these methyl hydrogens are not coupled to any hydrogens on adjacent carbon atoms. The integration of this peak was 2.8211, which when rounded to the nearest whole number is 3, indicating that 3 protons generate this signal. The 1.66 ppm region of the NMR spectrum of the allylic amine is depicted in Figure 37.

The literature spectrum also shows a singlet at around 1.77 ppm (close to the 1.66 ppm value we observed) with an integration indicating that 3 protons generate this signal.[146]

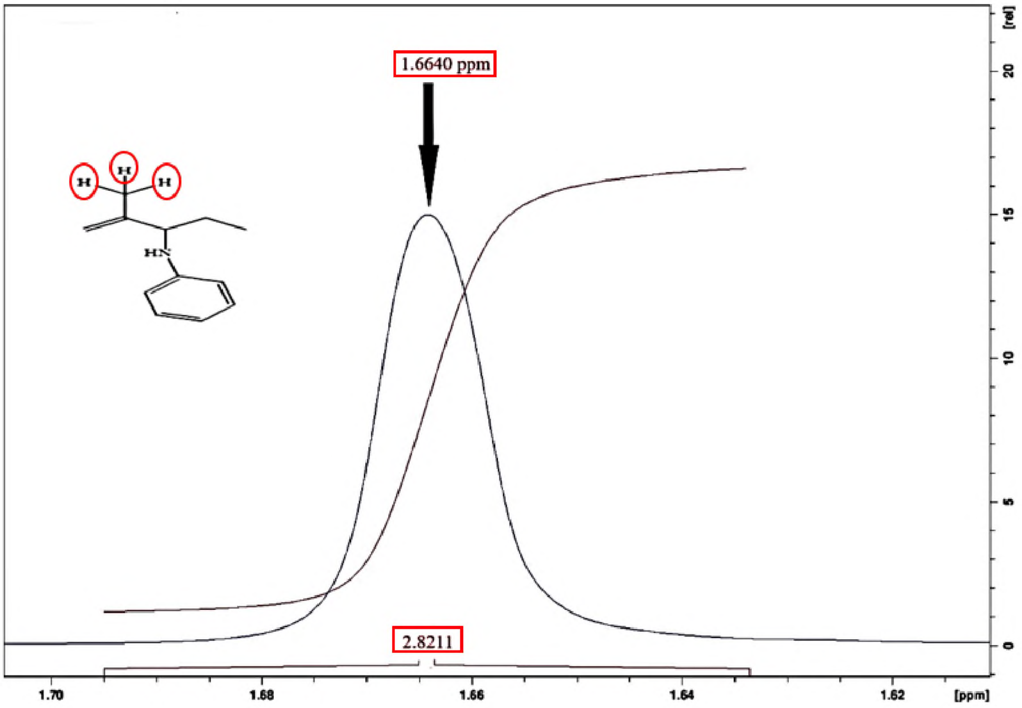

Figure 37: 1.66 ppm region of the ^{1}H NMR spectrum of allylic amine product.

The proton signal in the 2 ppm region of the ^{1}H NMR spectrum of the allylic amine reaction product (Figure 34c) corresponds to the 2 protons that are attached to carbon 4. The splitting of this signal appears to be a quintet. Also, the integration of this peak was 1.9532, which rounded to the nearest whole number is 2, indicating that 2 protons give rise to this signal. The 2 ppm region of the NMR spectrum of the allylic amine is shown in Figure 38. However, the 2 protons attached to carbon 4 are chemically non-equivalent, meaning that each proton should generate its own NMR signal at its own chemical shift. Specifically, these protons are known to be diastereotopic, because if the first proton and then the second proton are replaced by different atoms or groups of atoms, a pair of diastereomers will result.[164] (Diastereomers are types of stereoisomers that are not "mirror images" of each other.[165]) Additionally, the 2 protons attached to carbon 4 are attached to a carbon atom that is adjacent to a chiral carbon (carbon 3), and protons that are attached to a carbon adjacent to a chiral carbon (a carbon that is bonded to 4 different atoms or groups of atoms[166]) are usually diastereotopic.[164] Even though the protons on carbon 4 are chemically non-equivalent, the signal around 2 ppm in Figure 38 implies that the protons are chemically equivalent. When chemically non-equivalent protons show up on an NMR spectrum as being equivalent, this is known as accidental equivalence. Accidental equivalence can be observed when spectral resolution is limited, and thus insufficiently sensitive to distinguish diastereotopic protons as being chemically non-equivalent.[167] Moreover, the quintet splitting pattern that is observed in Figure 38 does not follow the $N + 1$ rule, which should yield a more complicated multiplet under conditions of sufficient spectral resolution, because our spectral resolution is limited.[162] Furthermore, for the protons attached to carbon 4, the literature spectrum reveals a multiplet in the chemical shift range 1.7-1.8 ppm (close to the 2 ppm value we observed) with an integration indicating that 2 protons give rise to this signal.[146] It seems that the 2H multiplet in the literature spectrum appears to be at a lower chemical shift than the 3H singlet at 1.77 ppm, whereas in our NMR data, the 2H multiplet appears at a higher chemical shift than the 3H singlet at 1.66 ppm. Perhaps this difference in chemical shift order between our data and the literature spectrum is concentration dependent.

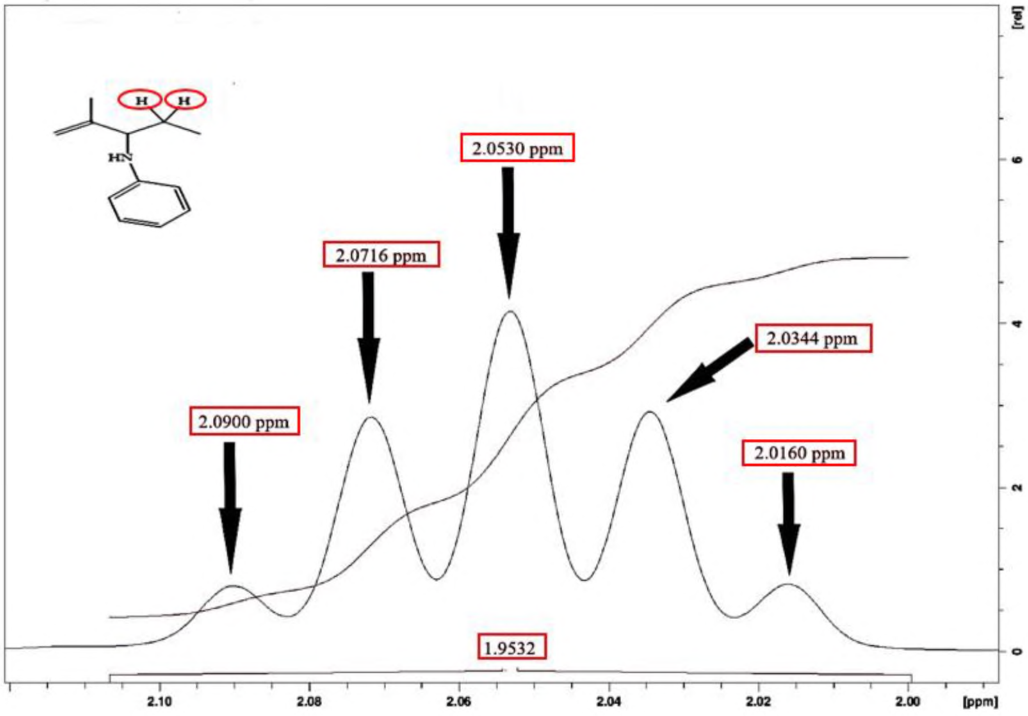

Figure 38: 2 ppm region of the ^{1}H NMR spectrum of allylic amine product.

The proton signal around 3.34 ppm in the ^{1}H NMR spectrum of the allylic amine reaction product (Figure 34c) likely corresponds to an impurity. It is important to note that the literature spectrum reported by Nicholas' group does not show a proton signal around 3.34 ppm. We know the 3.34 ppm signal is not due to residual chloroform NMR solvent since that residual solvent peak almost always appears as a singlet around 7.26 ppm.[168] Also, after comparing the 3.34 ppm signal to other solvents' NMR proton signals in the literature,[168] we do not believe the 3.34 ppm signal corresponds to a solvent impurity. Therefore, the only possible explanation for the observance of this signal is due to the presence of a reaction impurity. The splitting of the 3.34 ppm signal appears to be a triplet. However, the integration of this peak was 0.9800, which rounded to the nearest whole number is 1, indicating that 1 proton generates this signal. Interestingly, this 1H triplet around 3.34 ppm also appears in the ^{1}H NMR spectrum of the 2-methyl-2-pentene amination product that was produced in the allylic amination catalysis by the homoleptic complex salt [Co{Ph(O)NN(O)Ph}$_4$](PF$_6$)$_2$. The 3.34 ppm region of the NMR spectrum of the allylic amine is shown in Figure 39.

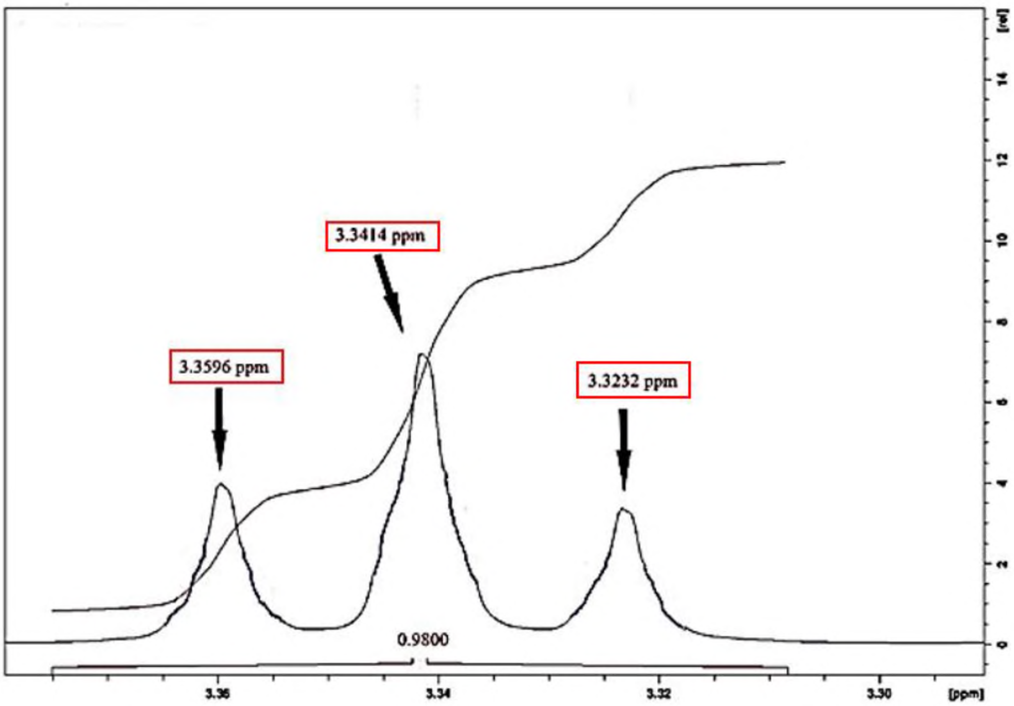

Figure 39: 3.34 ppm region of the NMR spectrum of the allylic amine.

The proton signal in the 4 ppm region of the ^{1}H NMR spectrum of the allylic amine reaction product (Figure 34c) corresponds to the proton attached to carbon 3. The splitting of this signal appears to be a triplet. Also, this peak was set as integrating to 1.0000, indicating that 1 proton gives rise to that signal. The 4 ppm region of the NMR spectrum of the allylic amine is shown in Figure 40. However, the expected splitting pattern from the $N + 1$ rule for this proton signal would be a doublet of doublets, since the 2 neighboring protons on carbon 4 are chemically non-equivalent. Again, because the spectral resolution was limited[162] and the NMR shows the 2 neighboring protons as being chemically equivalent, a triplet, as opposed to a doublet of doublets, is observed. For the proton attached to carbon 3, the literature spectrum reveals a triplet at around 3.77 ppm (close to the 4 ppm value we observed) with an integration indicating that 1 proton generates this signal.[146]

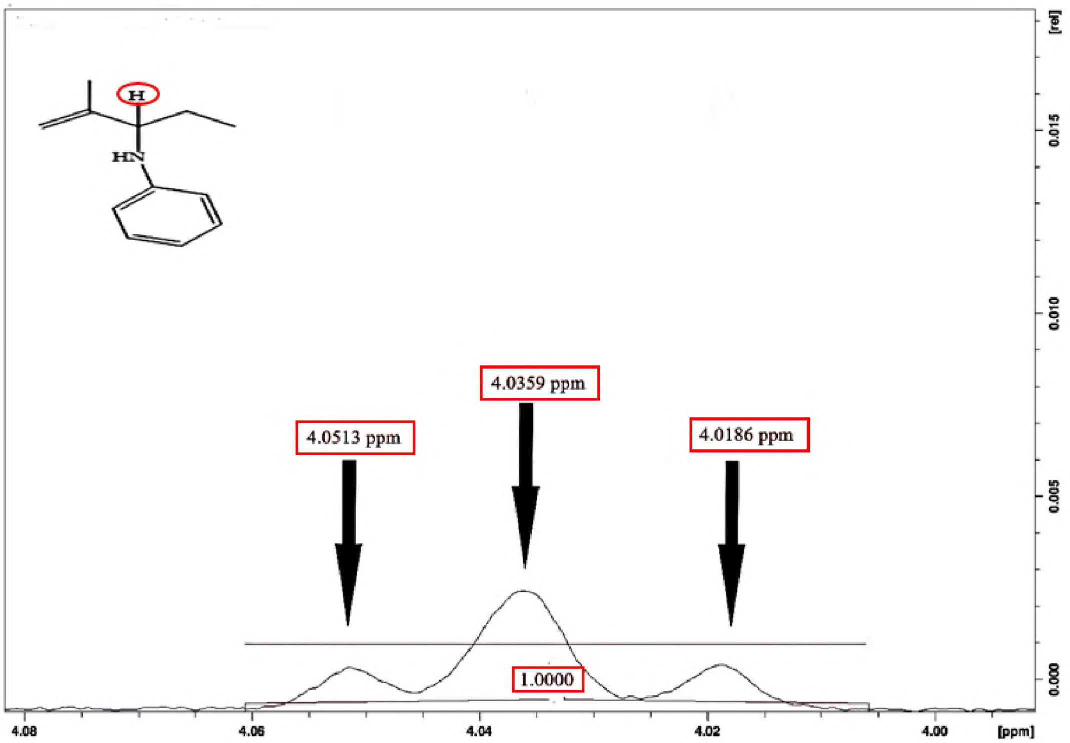

Figure 40: 4 ppm region of the ^{1}H NMR spectrum of the allylic amine.

The 2 proton signals around 5.18 and 5.31 ppm in the ^{1}H NMR spectrum of the allylic amine reaction product (Figure 34c) correspond to the 2 protons attached to carbon 1. Two different signals are observed in the 5 ppm region because the 2 protons on carbon 1 are chemically non-equivalent. These protons are known as geminal protons because they are chemically non-equivalent protons attached to the same carbon atom and interact with each other to cause splitting of each other's signal.[169] The proton signal around 5.18 ppm corresponds to the proton that appears closer to the methyl group that is attached to the carbon adjacent to carbon 1, whereas the signal around 5.31 ppm corresponds to the proton that appears closer to the amine group attached to carbon 3. The proton on carbon 1 that appears closer to the amine group in the allylic amine structure is more deshielded than the proton closer to the methyl group because the nitrogen atom in the amine is more electronegative than the carbon atom in the methyl group. The splitting of each signal appears to be a doublet, which is expected because each of the protons on carbon 1 splits the other to form doublets based on the $N + 1$ rule. Also, the integration of the 5.18 ppm and 5.31 ppm signals were 0.9895 and 1.0000, respectively, indicating that 1 proton generates each signal. The 5 ppm region of the NMR spectrum of the allylic amine is depicted in Figure 41. For the protons attached to carbon 1, the literature spectrum reveals two broad singlets around 5.03 ppm and 5.08 ppm (close to the 5.18 and 5.31 ppm values we observed) with an integration of each peak indicating that 1 proton generates each signal.[146] It is possible that broad singlets were observed in the NMR spectra taken by Nicholas' group because Nicholas' group used a 300-MHz NMR spectrometer,[146] which is a lower frequency than the 400-MHz spectrometer we used, which can lead to lower spectral resolution.

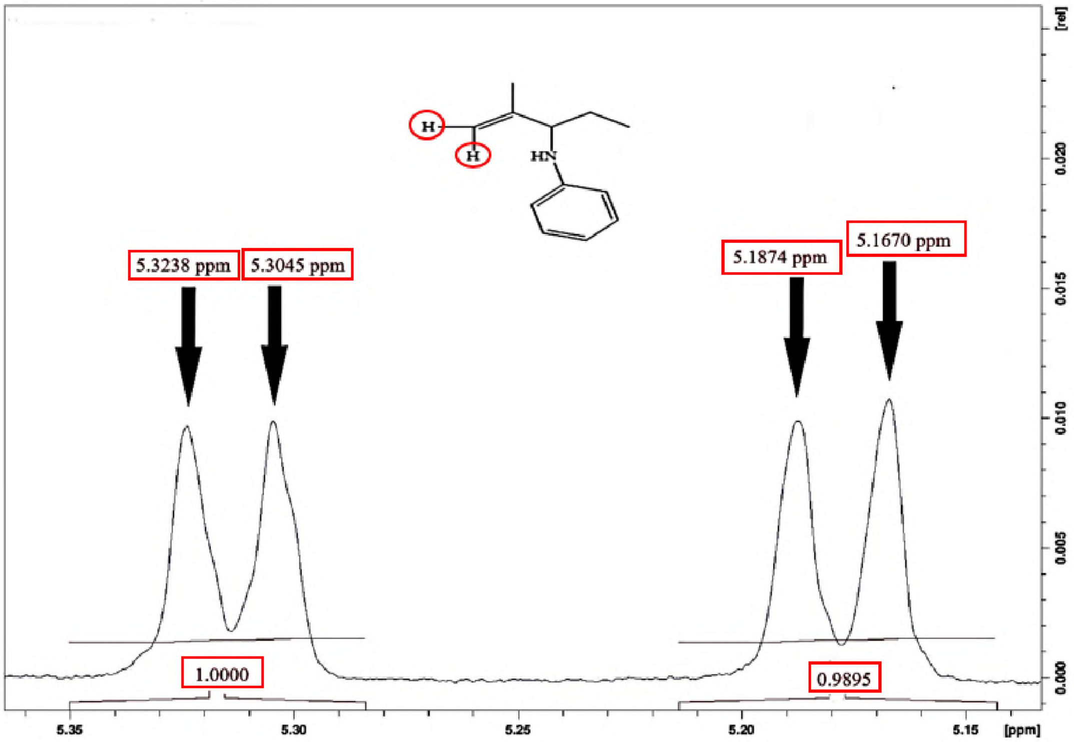

Figure 41: 5 ppm region of the ^{1}H NMR spectrum of the allylic amine.

The proton signals in the chemical shift range 6.85-7.58 ppm correspond to the aromatic protons on the phenyl group in the allylic amine structure. The signal around 6.85 ppm corresponds to the *ortho*-protons. This signal appears as a multiplet. Also, the integration of this peak was 1.9729, indicating that 2 protons generate this signal. The 6.85 ppm region of the NMR spectrum of the allylic amine is depicted in Figure 42a. The signal in the region 7.0-7.3 ppm corresponds to the *para*-proton. This signal appears as a multiplet. Also, the integration of this peak was 0.8591, indicating that 1 proton generates this signal. The 7.0-7.3 ppm region of the NMR spectrum of the allylic amine is depicted in Figure 42b. The signal around 7.5 ppm corresponds to the *meta*-protons. This signal appears as a multiplet. Also, the integration of this peak was 2.0000, indicating that 2 protons generate this signal. The 7.5 ppm region of the NMR spectrum of the allylic amine is depicted in Figure 42c. The literature spectrum reveals the aromatic proton signals being in the chemical shift range 6.6-7.4 ppm.[146]

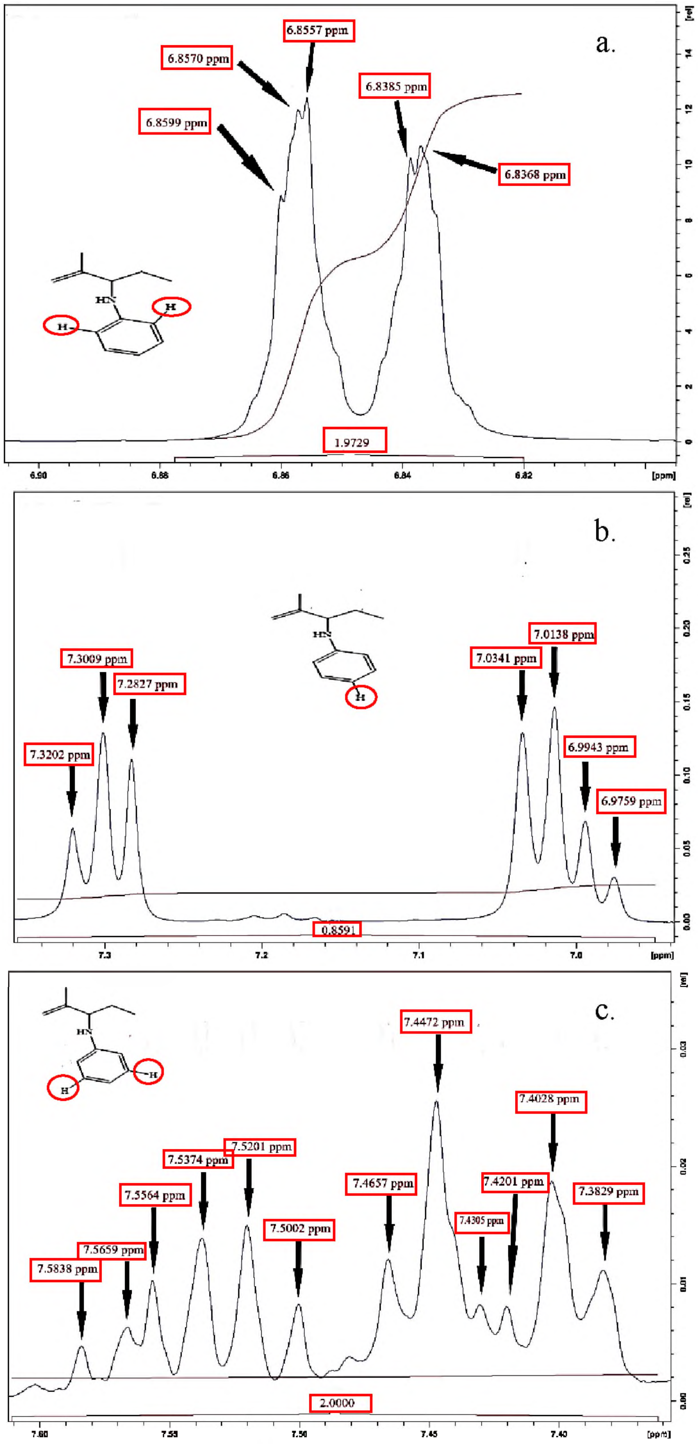

Figure 42: Aromatic proton regions of the ^{1}H NMR spectrum of the allylic amine showing (a) 6.85 region (b) 7.0-7.3 region (c) 7.5 region.

5.3.2 Nucleophilic Allylic Substitution

Once we were able to demonstrate that $[Co(bpy)\{Ph(O)NN(O)Ph\}_2](PF_6)_2$ acts as a competent catalyst in allylic amination/C–C double-bond transposition reactions, I then decided to investigate the catalytic ability of $[Co(bpy)\{Ph(O)NN(O)Ph\}_2](PF_6)_2$ in the synthesis of drugs containing allylic amine moieties, since catalysis in drug synthesis is one useful application of transition metal complexes in the medicinal field. Since 1st-row transition metal catalysts have been increasingly applied to allylic amination reactions,[157] and because I wanted to expand the catalytic applications of $[Co(bpy)\{Ph(O)NN(O)Ph\}_2](PF_6)_2$, I became interested in the possibility of conducting a one-pot, cobalt-catalyzed synthesis of an allylic amine drug involving an allylic amination mechanism, whether it be similar or different from the one previously described. A relevant study,[31] which was mentioned in Section 5.2.2, demonstrated that the iron complex $Fe(CO)_3\{\eta^4\text{-}(CH_2)_4(SiMe_3)_2C_5O\}$ served as a catalyst in the nucleophilic allylic substitution reaction of cinnamyl alcohol and 1-benzhydrylpiperazine to form the allylic amine drug cinnarizine.[138]

As a first approach, I wanted to see if by simply replacing the iron catalyst with the $[Co(bpy)\{Ph(O)NN(O)Ph\}_2](PF_6)_2$ complex salt that we prepared would also act as a catalyst in that same one-pot cinnarizine synthesis. Preliminary GC-MS results from my crude reaction mixtures have indicated the desired synthesis of cinnarizine $C_{26}H_{28}N_2$ (*m/z* 369), although the results also indicated the presence of the two substrates cinnamyl alcohol (*m/z* 134) and 1-benzhydrylpiperazine (*m/z* 251) in excess. The *m/z* value reported for each species corresponds to its molecular ion peak (M^+). The presence of excess substrates indicates that there is potential degradation in the catalyst after a certain time.

Each of the relevant peaks in the gas chromatogram of the crude reaction mixture was identified by comparing each peak's corresponding experimental mass spectrum to that in a NIST library and by extracting ion chromatograms. The experimental mass spectrum of cinnarizine $C_{26}H_{28}N_2$ is depicted in Figure 43. The weak signals at *m/z* values greater than the molecular ion peak at 369 in the mass spectrum in Figure 43 possibly represent minor impurities from the GC column and/or mass spectrometer or noise. The experimental gas chromatogram of our crude reaction mixture with the cinnarizine peak as well as the cinnamyl alcohol and 1-benzhydrylpiperazine peaks labeled is shown in Figure 44. Figure 44 shows that the retention time of cinnarizine was 25.279 min and that the retention times of cinnamyl alcohol and 1-benzhydrylpiperazine were 7.960 min and 15.031 min, respectively. The unlabeled peaks in the gas chromatogram in Figure 44 possibly represent minor impurities from the instrument, silicon-containing species from the GC column, or noise. Perhaps LC-MS/MS, as opposed to GC-MS, would have been a better choice for the initial characterization of cinnarizine, since cinnarizine has a boiling point that is too high to elute at the upper limit of the GC column oven at 280°C. However, our GC-MS system, unlike our LC-MS/MS system, is equipped with a NIST library of mass spectra, which was able to reveal to a 95% probability that the mass spectrum corresponding to the GC peak at 25.279 min in the GC chromatogram in Figure 44 was cinnarizine. The use of the NIST library, in addition to the extracted ion chromatograms, allowed us to identify the cinnarizine peak. The preliminary catalytic scheme for the catalysis of the nucleophilic allylic substitution of cinnamyl alcohol with 1-benzhydrylpiperazine (cinnarizine synthesis) with $[Co(bpy)\{Ph(O)NN(O)Ph\}_2](PF_6)_2$ as the catalyst is shown in Figure 45. Other reaction conditions were attempted for this catalysis, but the conditions shown in

Figure 45 gave the best preliminary results thus far. Work is still being done on the optimization of the reaction conditions in order to reduce the presence of excess substrates at the completion of the reaction. Unfortunately, attempts to separate and purify cinnarizine by preparative column chromatography have been unsuccessful thus far, and therefore NMR spectra have not yet been acquired to confirm the catalytic synthesis of cinnarizine and a turnover number and isolated yield have not yet been determined. Hence, it cannot be reported with certainty that cinnarizine was synthesized. Attempts at column chromatography are ongoing. The GC-MS results in Figures 43 and 44 do, however, show some initial promise in the potential application of [Co(bpy){Ph(O)NN(O)Ph}$_2$](PF$_6$)$_2$ as a catalyst in the synthesis of allylic amine drugs.

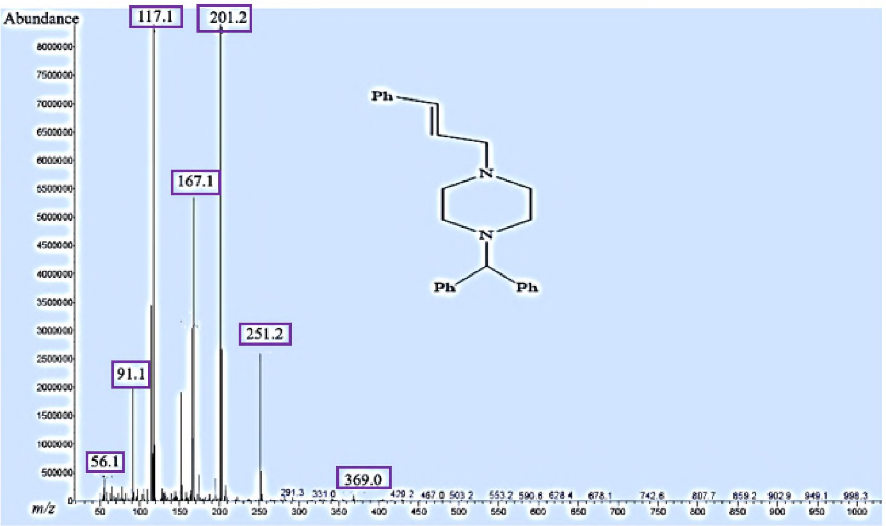

Figure 43: Experimental mass spectrum of cinnarizine.

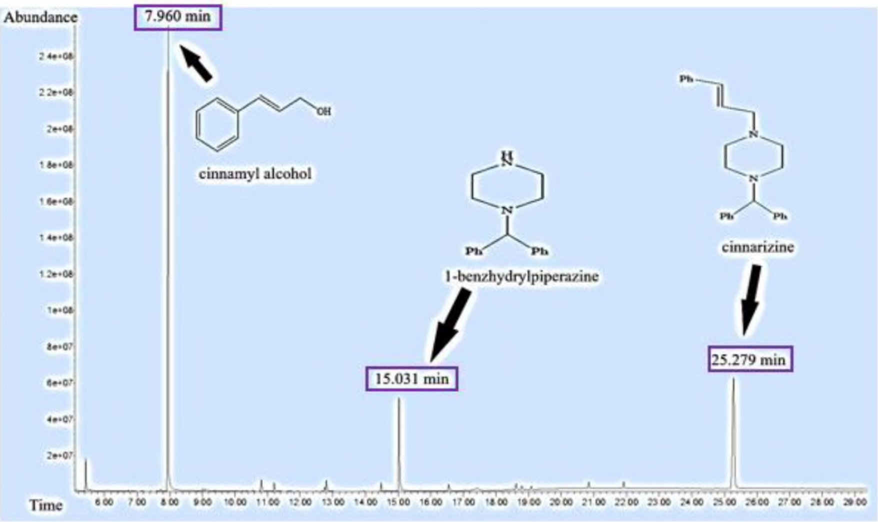

Figure 44: Experimental gas chromatogram of crude reaction mixture from the catalysis of the nucleophilic allylic substitution of cinnamyl alcohol with 1-benzhydrylpiperazine to form cinnarizine.

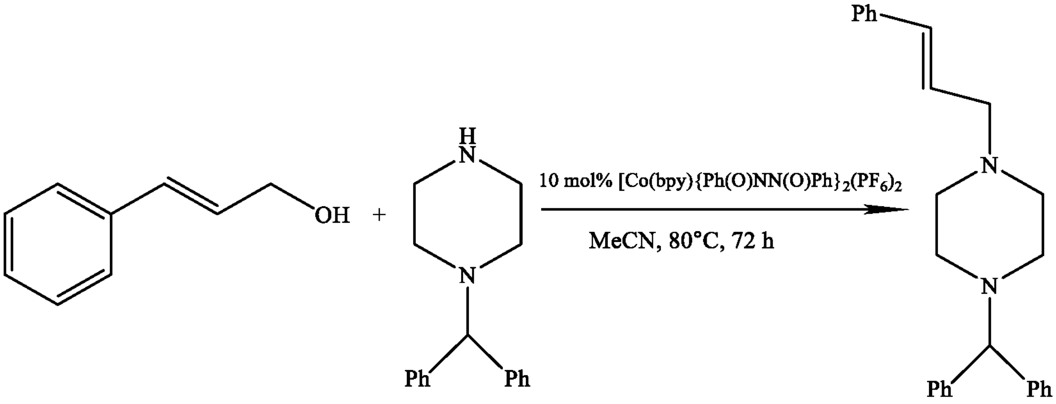

Figure 45: Synthesis of the allylic amine drug cinnarizine catalyzed by $[Co(bpy)\{Ph(O)NN(O)Ph\}_2](PF_6)_2$.

Based on the promising preliminary results from the catalytic synthesis of cinnarizine, I wished to continue the investigation of $[Co(bpy)\{Ph(O)NN(O)Ph\}_2](PF_6)_2$ as a catalyst in nucleophilic allylic substitution reactions that involve simpler substrates, so that I could potentially expand the substrate scope for the nucleophilic allylic substitution reaction involved in the synthesis of cinnarizine.[158] The simpler allylic alcohol substrate under investigation was *trans*-2-penten-1-ol, whereas the simpler amine substrates that were under investigation were piperidine (azacyclohexane) and azepane (azacycloheptane). Thus far, I have only been able to obtain promising preliminary GC-MS results for the catalysis of the nucleophilic substitution of *trans*-2-penten-1-ol with piperidine to form the desired allylic amine product $C_{10}H_{19}N$ (*m/z* 153). The *m/z* value of 153 corresponds to the molecular ion peak (M^+). The potential allylic amine peak in the gas chromatogram of the crude reaction mixture was identified by comparing its corresponding experimental mass spectrum to that in a NIST library and by extracting ion chromatograms. The experimental mass spectrum of the potential allylic amine product $C_{10}H_{19}N$ is depicted in Figure 46. The weak signals at *m/z* values greater than the molecular ion peak at 153 in the mass spectrum in Figure 46 possibly represent minor impurities from the GC column and/or mass spectrometer or noise. The experimental gas chromatogram of our crude reaction mixture with the potential allylic amine peak labeled is shown in Figure 47. Figure 47 shows that the retention time of the potential allylic amine product was 10.148 min. The unlabeled peaks in the gas chromatogram in Figure 47 possibly represent minor impurities from the instrument, silicon-containing species from the GC column, or noise. The preliminary catalytic scheme, including preliminary optimal reaction conditions is depicted in Figure 48. The optimization of reaction conditions for this reaction is still taking place. Unfortunately, as with the catalysis experiments for the synthesis of cinnarizine, attempts to separate and purify the potential allylic amine product by preparative column chromatography have been unsuccessful thus far, and therefore NMR spectra have not yet been acquired to confirm the catalytic synthesis of the desired allylic amine and a turnover number and isolated yield have not yet been determined. Hence, it cannot be reported with certainty that the desired allylic amine was synthesized. Efforts at column chromatography are still ongoing, but the preliminary GC-MS results show the potential of [Co(bpy){Ph(O)NN(O)Ph}$_2$](PF$_6$)$_2$ as a catalyst for two types of allylic amination: direct allylic amination with concomitant C–C double-bond transposition and nucleophilic allylic substitution.

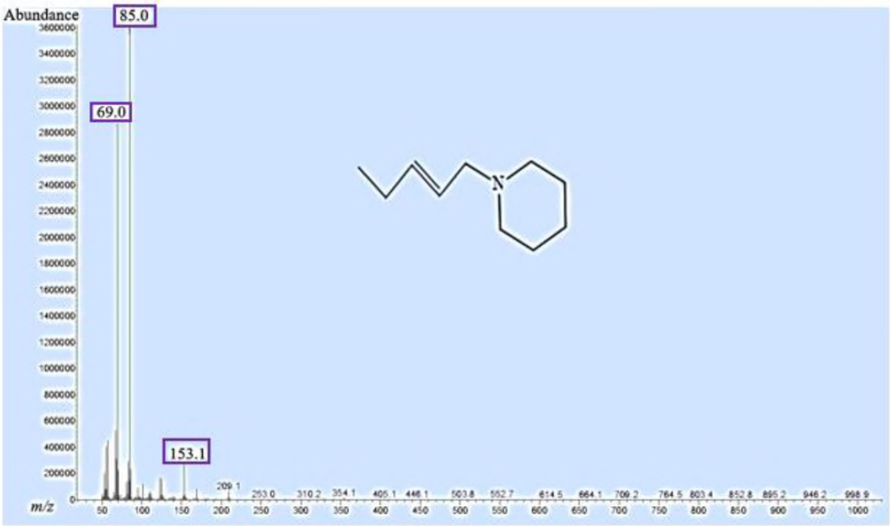

Figure 46: Experimental mass spectrum of potential allylic amine product.

Figure 47: Experimental gas chromatogram of crude reaction mixture from the catalysis of the nucleophilic substitution of *trans*-2-penten-1-ol with piperidine.

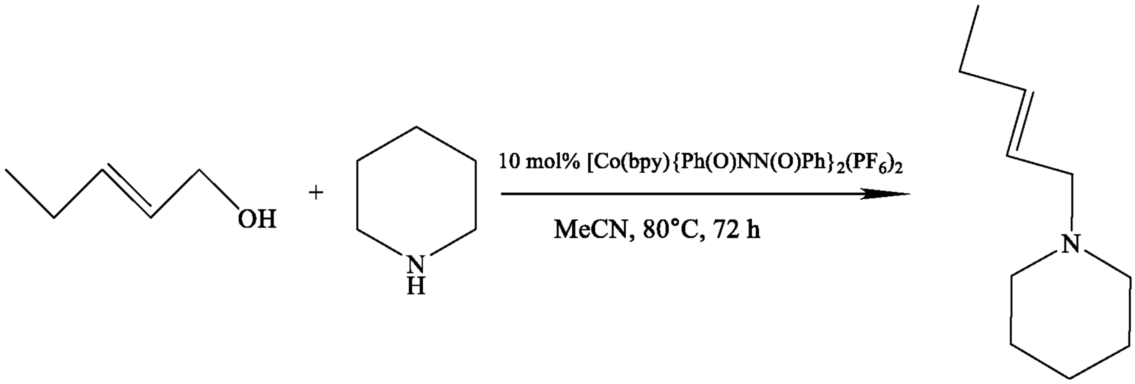

Figure 48: Nucleophilic allylic substitution of *trans*-2-penten-1-ol with piperidine catalyzed by [Co(bpy){Ph(O)NN(O)Ph}$_2$](PF$_6$)$_2$.

5.4 Experimental Methods

5.4.1 General Experimental Considerations

Both direct allylic amination and nucleophilic allylic substitution catalytic reactions were set up under an air- and moisture-free atmosphere (dry nitrogen) in an MBraun Labstar Pro glovebox. All glassware was dried at 160°C in an oven before use. Oxygen was removed from reaction solvents by sparging with nitrogen, and then moisture was removed from the solvents by passing them through activated alumina in an MBraun MB-SPS solvent purification system; air- and moisture-free solvents were kept in the glovebox. Preparative column chromatography was performed on crude reaction mixtures in a fume hood.[151] The preparation of [Co(bpy){Ph(O)NN(O)Ph}$_2$](PF$_6$)$_2$ is detailed in Chapter III and in our synthesis and characterization publication in *ACS Omega*.[170] The starting materials for the catalytic reactions were purchased from Sigma-Aldrich, Fisher, and Acros. Using the freeze-pump-thaw method, the liquid reagents were degassed; they were then dried over activated 4 Å molecular sieves. An Agilent GC-MS in which the GC was equipped with a silica column containing nonpolar groups and a mass spectrometer with an electron ionization source and a single quadrupole mass analyzer was utilized for our

GC-MS analyses. A NIST library of electron ionization mass spectra was used to compare all experimental mass spectra. ^{1}H NMR spectra were acquired for solutions of the purified allylic amine product from the direct allylic amination catalysis in $CDCl_3$ using a Bruker Avance III 400 MHz spectrometer.[151]

5.4.2 GC-MS Method Details

Before running any of our crude reaction mixtures, the GC column was conditioned for at least 1 hour at a temperature of 280°C to get rid of any analytes or species that previous GC-MS users might have injected. After conditioning the column, our crude reaction mixtures were analyzed on the instrument for a total run time of 29.4 min. The first 5 minutes of the method was dedicated to the solvent eluting before any potential organic products (solvent delay). The injection volume for each crude reaction mixture into the instrument was 1 μL. The column flow rate was 1 mL/min. The temperature of the GC column oven at the beginning and end of the run was 40°C and 280°C, respectively. In between sample runs, the column was kept at its final 280°C temperature for 10 minutes.

5.4.3 Direct Allylic Amination/C–C Double Bond Transposition Reactions

These reactions were set up in the glovebox, in which 0.073 mmol $[Co(bpy)\{Ph(O)NN(O)Ph\}_2](PF_6)_2$ (10 mol%) was dissolved in 2.5 mL of acetonitrile (MeCN) and transferred to a Schlenk tube with a stir bar. Then either 1.6 mmol 2-methyl-2-pentene or 2-methyl-2-hexene (alkene substrates) was added to the Schlenk tube, followed by a solution of 0.73 mmol phenylhydroxylamine (PhNHOH) in 5 mL MeCN. PhNHOH was the limiting reagent in these reactions. After the addition of the catalyst and reagents, the Schlenk tube was sealed with a Teflon stopcock before removing it from the glovebox. Once the Schlenk tube was removed from the glovebox, it was placed in an oil bath at 75°C for 72 hours. Once the reaction was done, the Schlenk tube was removed from the heated oil bath so that it could cool to room temperature. The reaction solvent MeCN was removed under reduced pressure, resulting in a brown solid that was extracted with diethyl ether (Et_2O).[151]

GC-MS was conducted on a small sample of the crude reaction mixture solution after running it through a miniature column that was composed of roughly 5 cm of silica gel atop a cotton ball in a Pasteur pipet. The pipet column step was necessary in order to remove any cobalt metal-containing species from the reaction mixture, since metal-containing species are nonvolatile and would stick to the GC column, fouling it. Preparative column chromatography was then performed in which the column consisted of silica gel and the mobile phase was a concentration gradient of petroleum ether and Et_2O. The collected fractions that contained the allylic amine product from column chromatography were determined by thin layer chromatography and UV light at a wavelength of 254 nm. These fractions were then combined to remove the solvent under reduced pressure to yield the allylic amine as a yellow oil.[151] The allylic amine identity and purity were confirmed by ^1H NMR spectroscopy as well as comparing to spectral data in the literature.[146,151]

5.4.4 Diels-Alder Trapping Experiment to Investigate Mechanism of Direct Allylic Amination Catalysis

The protocol described above for the direct allylic amination reactions (Section 5.4.3) was followed with slight modifications: PhNHOH was not used and 2,3-dimethyl-1,3-butadiene was used in place of the alkene 2-methyl-2-pentene or 2-methyl-2-hexene. GC-MS analysis was conducted on a Et_2O extract of the crude reaction mixture using the same method described in Section 5.4.2 in order to identify the reaction product.

Preparative column chromatography was not conducted, however, for this control experiment.[151]

5.4.5 Nucleophilic Allylic Substitution Reactions

This section discusses the experimental details that have thus far given the best preliminary results. (Refer back to the preliminary catalytic schemes in Figures 45 and 48.) The reactions were set up in the glovebox, in which 0.03 mmol $[Co(bpy)\{Ph(O)NN(O)Ph\}_2](PF_6)_2$ was dissolved in 5 mL of MeCN and transferred to a Schlenk tube with a stir bar. Then a solution of either 0.6 mmol cinnamyl alcohol or *trans*-2-penten-1-ol (allylic alcohol substrates) in 5 mL MeCN was added to the Schlenk tube, followed by a solution of either 0.3 mmol 1-benzhydrylpiperazine or piperidine (amine substrates) in 5 mL MeCN. (The amounts of reagents and catalyst used were based on the reported study that demonstrated iron-catalyzed nucleophilic allylic substitution in the synthesis of cinnarizine.[158]) The amine is the limiting reagent in these reactions. After the addition of the catalyst and reagents, the Schlenk tube was sealed with a Teflon stopcock before removing it from the glovebox. Once the Schlenk tube was removed from the glovebox, it was placed in an oil bath at 80°C for 72 hours. Once the reaction was finished, the Schlenk tube was removed from the heated oil bath so that it could cool to room temperature. The reaction solvent MeCN was removed under reduced pressure, resulting in a brown solid that was extracted into diethyl ether (Et_2O).

GC-MS analysis was conducted on a small sample of the crude reaction mixture solution after running it through a miniature column that was composed of roughly 5 cm of silica gel atop a cotton ball in a Pasteur pipet. Efforts to separate and purify the reaction products from these reactions are still ongoing.

CHAPTER VI

BIOLOGICAL ACTIVITY OF THE COBALT(II) BIPYRIDYL/DIPHENYLAZODIOXIDE COMPLEX SALT IN CELL STUDIES

6.1 Rationale

In addition to its catalytic applications, we became interested in the investigation of $[Co(bpy)\{Ph(O)NN(O)Ph\}_2](PF_6)_2$ as a potential anticancer drug, since its unusual trigonal prismatic coordination geometry suggested the possibility of its having novel biological effects in addition to novel reactivity outside of living systems. As was previously mentioned in Chapter I, Section 1.2, the use of transition metal complexes as anticancer drugs is a crucial pharmaceutical application. Interestingly, besides vitamin B_{12} (cobalamin),[171] there have not been any cobalt-based drugs in widespread clinical use. However, as mentioned in Chapter I, Section 1.2, the cobalt(III) imine complex Doxovir (CTC-96) has successfully completed phase II clinical trials in the treatment of herpes simplex virus[172] and phase I clinical trials in the treatment of two viral eye infections: ophthalmic herpetic keratitis[173] and adenoviral conjunctivitis[174].[175] Moreover, our interest was to see if the presence of the azodioxide ligand would lead to a change in anticancer effects, thus expanding the potential applications of azodioxide complexes. Prior to our work, no biological studies of azodioxide complexes had been reported.

6.2 Overview of Apoptosis

Apoptosis is a type of energy-dependent (requiring intracellular ATP) “programmed” cell death that usually occurs during developmental and aging processes.[176] Apoptosis occurs as both a homeostatic and a defense mechanism. As a homeostatic mechanism, apoptosis can preserve cell populations. Apoptosis as a defense mechanism can occur in immune reactions or when toxic agents damage cells.[176,177] When a cell undergoes apoptosis, the following structural characteristics or features of the cell are noticeable: a decrease in cell size, a bulging plasma membrane, cell rounding, the condensation of chromosomes, and the fragmentation of DNA. Additionally, apoptotic bodies appear containing the undamaged organelles and cytoplasm within the plasma membrane; these apoptotic bodies prevent cells undergoing apoptosis from releasing their components into nearby tissue, which would lead to inflammation.[176,178]

In contrast to apoptosis, necrosis is an energy-independent (not requiring intracellular ATP), uncontrolled form of cell death, also known as “accidental” cell death. Necrosis is usually considered a harmful process in which the following characteristics or features of a cell are noticeable: an increase in cell size, a disturbed plasma membrane, damage to organelles, and the release of cell components into nearby tissue, leading to inflammation. Necrosis usually occurs in cells as a result of extreme changes in physiological conditions, which include (but are not limited to) hypoxia, hypoglycemia, exposure to toxic substances, and extreme temperature changes. [176,179]

6.2.1 Major Proteins Involved in Apoptosis

During apoptosis, a very large number of proteins are involved, regardless of the pathway of apoptosis. (The different pathways of apoptosis will be discussed in the subsequent section.) Before explaining the major pathways of apoptosis, it is important to provide some background information on some of the major apoptotic proteins.

Caspases: One major class of proteins that play critical roles in apoptotic pathways is the caspases. These proteins are cysteine proteases that are targeted towards aspartate residues. Caspases exist in cells in inactive forms known as procaspases.[180] During apoptosis, however, these procaspases are cleaved at particular internal aspartate residues and thus become activated. The caspase family of proteins can be divided into two types: initiator caspases and effector caspases. Examples of initiator caspases are caspase-2, caspase-8, caspase-9, and caspase-10. Initiator caspases become activated (cleaved) once a death signal (regardless of the pathway) is received. These caspases then lead to the activation (cleavage) of effector caspases. Examples of effector caspases are caspase-3, caspase-6, and caspase-7. These effector caspases cleave important proteins such as cell cycle proteins, signal transduction proteins, and poly(ADP-ribose)polymerase (PARP). The cleavage of these proteins by effector caspases then results in apoptosis.[181]

Bcl-2 Family: In addition to caspases, the Bcl-2 (B-cell lymphoma-2) family of proteins play a major role in apoptosis. These proteins are primarily responsible for regulating the intrinsic apoptotic pathway (see Section 6.2.2 for the distinction between the intrinsic and extrinsic apoptotic pathways).[182] The Bcl-2 family contains both pro-apoptotic proteins as well as anti-apoptotic proteins. Two examples of pro-apoptotic proteins in this family are Bim and BAD. Bim is responsible for interacting with Bcl-2 proteins with anti-apoptotic activity and those with pro-apoptotic activity, especially with proteins Bax and Bak. The interaction of Bim with Bax and Bak results in conformational changes that are required for the mitochondrial outer membrane permeabilization (MOMP) complex to form, which is a critical step in the intrinsic pathway of apoptosis. BAD is a Bcl-2 binding protein that binds to anti-apoptotic protein members of the Bcl-2 family, leading to their inactivation.[182] An example of an important anti-apoptotic protein in the Bcl-2 family is Bcl-2 (B-cell lymphoma protein-2) itself. The Bcl-2 protein inhibits the activity of the pro-apoptotic protein members except for Bax and Bak.[182]

p53: Another important protein involved in apoptosis is p53, which is coded for by a tumor suppressor gene. This protein is responsible for activating gene transcription in genes whose products trigger apoptosis.[183] For example, p53 can regulate the transcription of the Bcl-2 family's pro-apoptotic proteins by ensuring that there are more pro-apoptotic proteins than anti-apoptotic proteins. Apoptosis that is mediated by p53 occurs mainly through the intrinsic pathway, although the possibility of this type of apoptosis occurring through the extrinsic pathway cannot be ruled out. The p53 protein is known for contributing to apoptosis that is induced by chemotherapy.[183]

PARP: A major event that is considered a hallmark or a classical indicator of apoptosis is the cleavage of the protein PARP. PARP is an enzyme with a molecular weight of 116 kDa that is useful in DNA replication and in cellular emergencies such as in DNA repair. During apoptosis, effector caspases cleave PARP into an 89 kDa C-terminal fragment and a 24 kDa N-terminal fragment, inactivating the enzyme.[184]

6.2.2 Apoptotic Pathways

There are a wide variety of stimuli that cause apoptosis, but not all forms of apoptotic cell death will occur in response to the same stimuli.[176] There are two possible pathways in which apoptosis can occur in a cell: the extrinsic, or death receptor, pathway and the intrinsic, or mitochondrial, pathway. A general outline of these apoptotic pathways is shown in Figure 49.

Extrinsic Pathway: The extrinsic pathway starts out with death ligands (cell death signals) binding to death receptors that belong to the tumor necrosis factor (TNF) family. These death receptors then acquire an adaptor protein. The initiator procaspases (procaspase-8 and procaspase-10) bind to the adaptor protein, resulting in the formation of the death-inducing signaling complex (DISC). DISC then activates the procaspases to caspase-8 and caspase-10. The effector procaspases (procaspase-3, procaspase-6, and procaspase-7) then become activated to caspases, leading to protein cleavage and ultimately apoptosis.[185,186]

Intrinsic Pathway: For the intrinsic pathway of apoptosis, stimuli such as damaged DNA in cells, oncogene upregulation, excess Ca^{2+}, and oxidants cause this pathway to occur. These stimuli first lead to the upregulation of the pro-apoptotic proteins Bim and BAD. Bim and BAD activate the pro-apoptotic proteins Bax and Bak, which, like Bim and BAD, are members of the Bcl-2 family. Once Bax and Bak are activated, mitochondrial outer membrane permeabilization (MOMP) occurs. This permeabilization leads to the release of cytochrome *c*, which then leads to the apoptosome being formed from cytochrome *c*, apoptotic protease-activating factor-1 (APAF-1), and procaspase-9. Within the apoptosome, procaspase-9 is activated to its caspase form, which then leads to the activation of effector procaspases (procaspase-3, procaspase-6, and procaspase-7), leading to protein cleavage and ultimately apoptosis.[185,187-189]

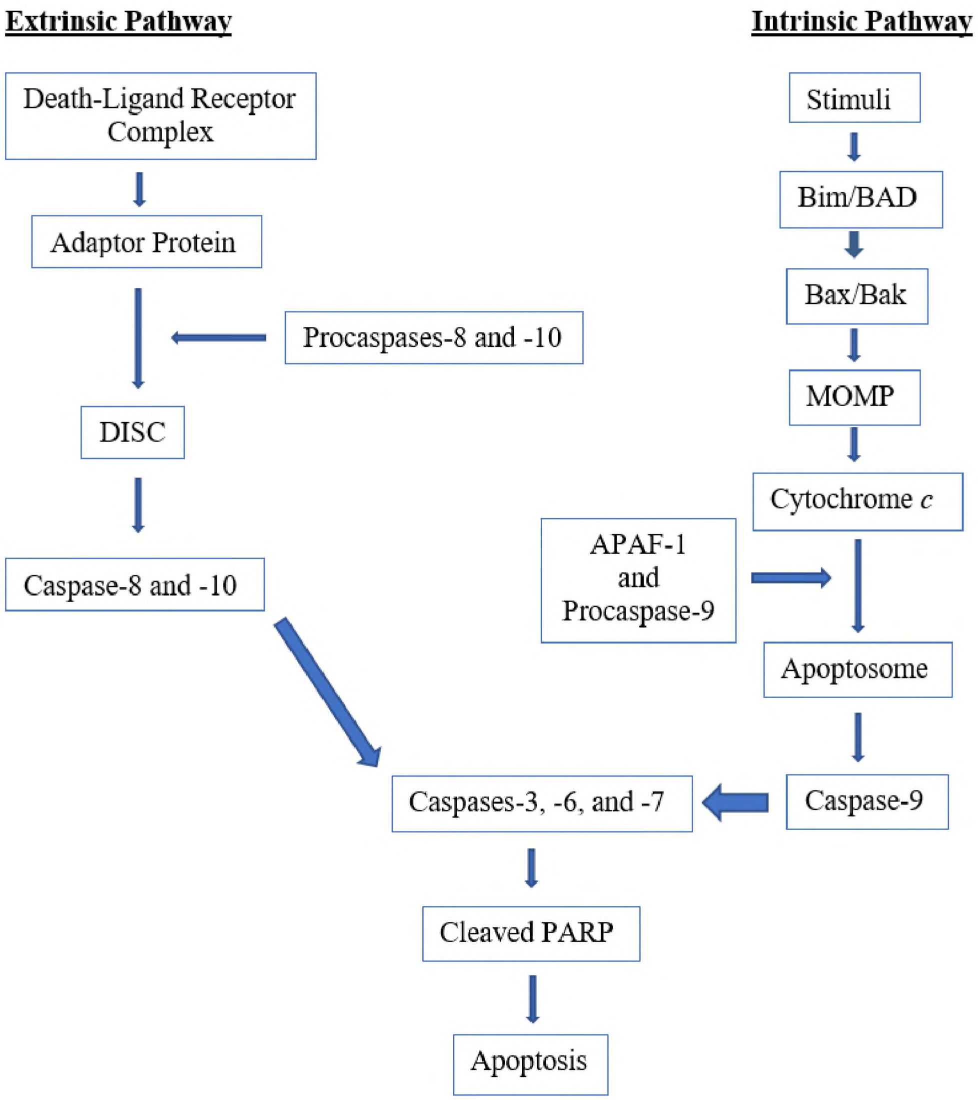

Figure 49: Extrinsic and Intrinsic Apoptotic Pathways.

6.3 Apoptosis in Cancer and Cancer Therapy

An important major role of apoptosis is cancer prevention. Therefore, the inhibition of apoptosis is an important indication of cancer, and it is nonspecific to the cancer type or cause of the cancer.[185,187,190,191] There are many ways in which apoptosis is inhibited in cancer cells. In many cases, however, the intrinsic pathway of apoptosis is inhibited, through the upregulation of anti-apoptotic protein members of the Bcl-2 family. The upregulation of these anti-apoptotic proteins is present in more than half of all cancers.

Another important, albeit less common, way in which the intrinsic pathway of apoptosis is inhibited is by the inhibition of caspase function after MOMP.[185,190] There are a wide variety of ways in which anti-apoptotic Bcl-2 proteins are upregulated and in which caspase function is inhibited.

Regarding cancer therapy, the most successful non-surgical treatment of cancer is the pharmaceutical targeting of apoptotic pathways. Different stages in both apoptotic pathways (intrinsic and extrinsic) have been targeted by several anticancer drugs.[185,192] Any stage in either pathway can be a target for cancer treatment, and there is currently no general consensus regarding which target is the most effective.[185] However, since the overexpression of anti-apoptotic Bcl-2 proteins occurs in many cancers, many apoptosis-targeting methods involve the suppression of anti-apoptotic Bcl-2 proteins and the stimulation of pro-apoptotic Bcl-2 proteins.[185,188]

6.4 Cisplatin

Since my project focuses primarily on transition metal chemistry, I would like to discuss as important background cisplatin, *cis*-$Pt(NH_3)_2Cl_2$,[193] an important example of a transition metal complex that acts as an anticancer agent by inducing apoptosis. Cisplatin is a neutral complex with platinum in the +2 oxidation state and a square-planar coordination geometry, whose structure is shown in Figure 50. Cisplatin was the first metal-based anticancer agent to reach global clinical use and remains today one of the most successful anticancer drugs.[175,194,195] Cisplatin can be used to treat a variety of different types of cancer, including testicular, ovarian, head and neck, and cervical cancers.[196]

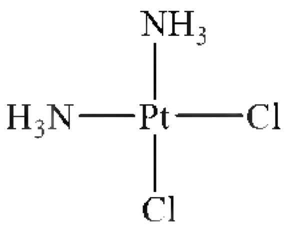

Cisplatin

Figure 50: Structure of cisplatin.

Cisplatin's mechanism of action involves its interaction with DNA. Before cisplatin can interact with DNA, it first needs to become activated by an aquation reaction, in which cisplatin's chloride (Cl^-) ligands are replaced with water (H_2O) ligands, becoming *cis*-$Pt(NH_3)_2(H_2O)_2^{2+}$.[197,198] Aquation usually takes place because of the high levels of water in cells. The N-7 sites of the DNA purine bases guanine or adenine, which are labeled in their structures shown in Figure 51, then displace the H_2O ligands from *cis*-$Pt(NH_3)_2(H_2O)_2^{2+}$, resulting in two portions of DNA becoming crosslinked to form cisplatin-DNA adducts.[197,199] The two types of crosslinking that can result are interstrand and intrastrand. Interstrand crosslinking occurs where two strands of DNA are connected by a Pt bridge. On the other hand, intrastrand crosslinking occurs where two purine bases of the same DNA strand are connected by a Pt bridge, a process in which a kink is introduced into the structure. The mechanism of action of cisplatin is very similar to that of alkylating agents, which are organic anticancer drugs that use an alkyl group to crosslink two purine bases of DNA rather than use a metal. Therefore, cisplatin is sometimes referred to as a "nonclassical alkylating agent," despite not actually containing any alkyl groups *per se*. Once the cisplatin-DNA adducts are formed, many signal transduction pathways become activated, which eventually lead to apoptosis.[197,200]

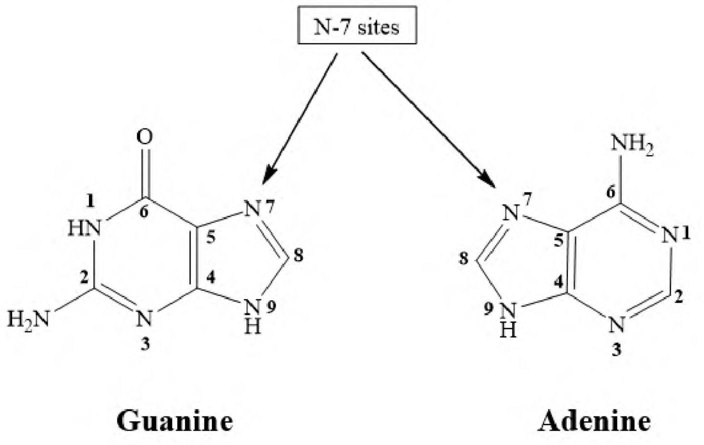

Figure 51: Structures of guanine and adenine with their corresponding numerical schemes.

Even though cisplatin is a successful drug in cancer treatment, it causes adverse effects in patients because of its high cytotoxicity. Some of those adverse effects include kidney damage, liver damage, nervous system damage, and ear damage. In order to lower cytotoxicity levels, further generations of Pt-containing drugs have been developed and are either FDA-approved (*e.g.* carboplatin and oxaliplatin) or are currently in U.S. clinical trials (*e.g.* satraplatin and lobaplatin).[175,194,201] Importantly, since complexes of 2nd- and 3rd-row transition metals are often more toxic than those of 1st-row transition metals,[202] and one important goal for metal-based drug development is reducing toxicity profiles,[203] the development of drugs containing 1st-row transition metals is desirable.

6.5 Background on Monometallic Cobalt(II) Complexes Shown to Induce Apoptosis

A variety of cobalt complexes, in which cobalt is either in the +2 or +3 oxidation state, have been demonstrated to be cytotoxic against particular cancer cell lines that have been reported to induce apoptosis.[204] For better comparison with our complex salt $[Co(bpy)\{Ph(O)NN(O)Ph\}_2](PF_6)_2$, which is monometallic with Co in the +2 oxidation state, I will give an overview of some examples of monometallic Co(II) complexes that have been shown to induce apoptosis in cancer cell lines. Klegeris and coworkers were able to show that a series of square-planar Co(II) complexes containing *β*-ketoaminato ligands increase caspase-3 activation and therefore induce apoptosis in prostate cancer cells.[204,205] Pombeiro and coworkers demonstrated that a series of Co(II) tris(pyrazolyl)-methane (also known as scorpionate) complexes induce apoptosis in liver and colorectal cancer cells. The mechanism of action for these scorpionate complexes was proposed to involve the production of reactive oxygen species (ROS).[204,206] Chiniforoshan and coworkers were able to show that a Co(II) complex containing 1,10-phenanthroline and the conjugate base of juglone (a natural product) as ligands induces apoptosis in colorectal, cervical, and liver cancer cells. The induction of apoptosis was proposed to involve DNA intercalation.[204,207] Gao and coworkers demonstrated the ability of a Co(II) complex containing the ligand tris(imidazolyl)benzene to induce apoptosis in oral epithelial carcinoma cells through DNA fragmentation and intercalation.[204,208] Simpson and coworkers were able to show that a series of Co(II) complexes containing benzyl carbazate-derived imines as ligands induce apoptosis in leukemia cells. Unfortunately, the mechanism of action of these complexes was not determined.[204,209] Chen and coworkers reported a Co(II) complex with oxoisoaporphine ligands as inducing apoptosis in ovarian cancer cells that happened to be resistant to cisplatin. Apoptosis induction involved an increase in ROS levels and caspase-3 and caspase-9 activation.[204,210] Filipovic and coworkers were able to show that a Co(II) complex containing an O-donor ligand of the (chalcogen)-semicarbazone type induces apoptosis in cervical cancer cells and in all-*trans* retinoic acid-resistant acute myeloid leukemia cells. Apoptosis induction involved the ROS-mediated damage of DNA.[204,211]

6.6 Results and Discussion

The biological activity of $[Co(bpy)\{Ph(O)NN(O)Ph\}_2](PF_6)_2$, in addition to the homoleptic $[Co\{Ph(O)NN(O)Ph\}_4](PF_6)_2$, was studied, with the results published in *ACS Omega*[204] in collaboration with Prof. Aimin Zhou of Cleveland State University and his former Ph.D. students, Drs. Norah Alghamdi and Ruhan Wei.

In this collaboration, we learned that $[Co(bpy)\{Ph(O)NN(O)Ph\}_2](PF_6)_2$ induced apoptosis in SK-HEP-1 human liver adenocarcinoma cells. These cells were treated with or without varying concentrations of $[Co(bpy)\{Ph(O)NN(O)Ph\}_2](PF_6)_2$ in DMSO for 12 hours, where DMSO was used as a vehicle to overcome the limited solubility of $[Co(bpy)\{Ph(O)NN(O)Ph\}_2](PF_6)_2$ in water. It is important to note here that UV-visible experiments confirmed good stability of 10 μM $[Co(bpy)\{Ph(O)NN(O)Ph\}_2](PF_6)_2$ in DMSO over a period of at least one week when storing the solution in a dark place at room temperature. Figure 52 shows that as the concentration of $[Co(bpy)\{Ph(O)NN(O)Ph\}_2](PF_6)_2$ increases, the cells become rounder and the number of viable cells decreases, meaning that higher concentrations have a greater apoptotic effect on the cells.[204]

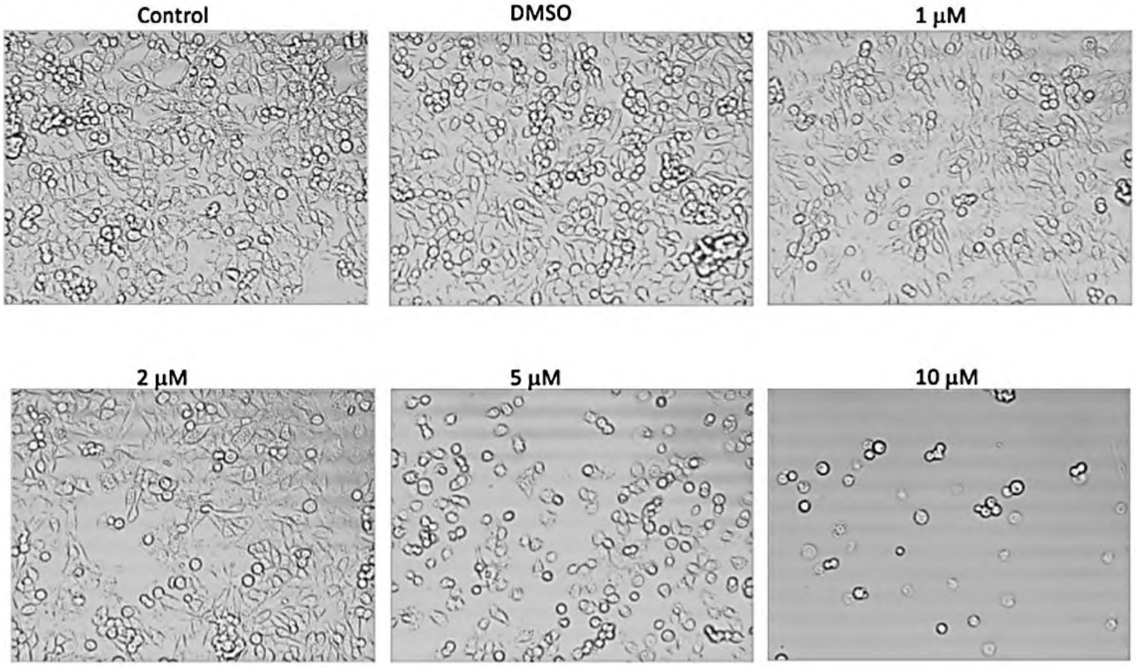

Figure 52: Cell morphology after 12 hour treatment with or without various $[Co(bpy)\{Ph(O)NN(O)Ph\}_2](PF_6)_2$ concentrations in DMSO. The control represents cells without any treatment. The DMSO morphology represents cells treated with only DMSO. For each well, images were taken under 20× magnification from five different fields at random using an inverted phase-contrast fluorescence microscope (Carl Zeiss).[204]

Furthermore, flow cytometry was performed on the SK-HEP-1 cells after they were treated with 10 μM $[Co(bpy)\{Ph(O)NN(O)Ph\}_2](PF_6)_2$ for 12 hours in relation to the control. Figure 53 shows the flow cytometry results.[204] An Annexin V fluorescein isothiocyanate (FITC)/propidium iodide (PI) apoptosis detection kit was used for flow cytometry experiments. In Figure 53, the first quadrant (Q1) represents necrotic cells, in which only PI stains these cells (Annexin V-FITC$^-$/PI$^+$); quadrant 2 (Q2) represents late apoptotic cells, in which both Annexin V-FITC and PI stain these cells (Annexin V-FITC$^+$/PI$^+$); quadrant 3 (Q3) represents viable cells, in which neither Annexin V-FITC nor PI stain these cells (Annexin V-FITC$^-$/PI$^-$); and quadrant 4 (Q4) represents early apoptotic cells, in which only Annexin V-FITC stains these cells (Annexin V-FITC$^+$/PI$^-$).[212] As Figure 53 shows, the percentage of cells that died from apoptosis was greatly increased from 4.8 to 16.6% after treatment with $[Co(bpy)\{Ph(O)NN(O)Ph\}_2](PF_6)_2$, indicating that cell death occurs primarily by apoptosis as opposed to necrosis. It is important to note that $[Co(bpy)\{Ph(O)NN(O)Ph\}_2](PF_6)_2$ is not capable of fluorescence; attempts to perform fluorescence spectroscopy on this compound did not yield emission spectra. Therefore, no fluorescence from this complex interfered with the flow cytometry results.[204]

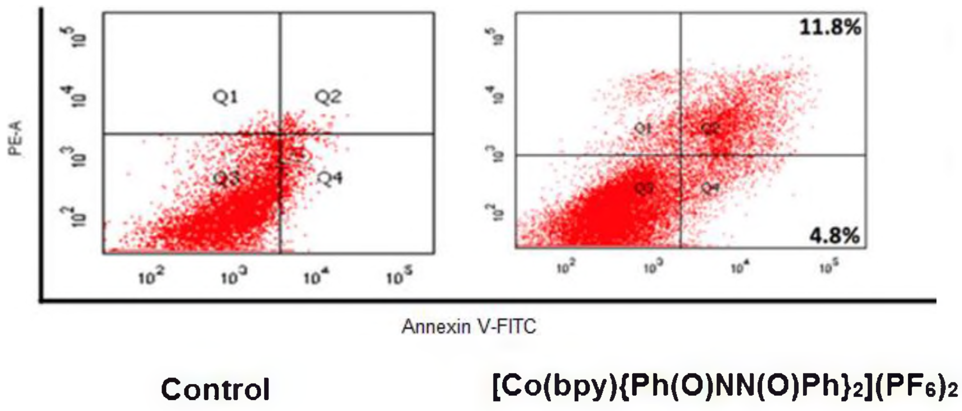

Figure 53: Flow cytometry results after treatment with 10 μM $[Co(bpy)\{Ph(O)NN(O)Ph\}_2](PF_6)_2$ for 12 hours. In a dark environment at 4°C, each sample was stained with 5 μL of Annexin V-FITC and 5 μL of PI for 15 minutes and 400 μL of 1× binding buffer was added. Using a flow cytometer with BD FACSDiva software, the cells were analyzed.[204] Annexin V-FITC$^-$/PI$^-$ cells were determined as being viable, Annexin V-FITC$^+$/PI$^-$ cells were identified as being early apoptotic. Annexin V-FITC$^+$/PI$^+$ cells were determined as being late apoptotic. Annexin V-FITC$^-$/PI$^+$ cells were identified as being necrotic.[212]

In addition to flow cytometry, Western blot analysis was also performed[204] in order to investigate the mechanism of apoptosis in the SK-HEP-1 cells caused by $[Co(bpy)\{Ph(O)NN(O)Ph\}_2](PF_6)_2$. Western blot analysis revealed that apoptosis in these cells involved the cleavage of PARP, which is a hallmark of apoptosis,[184] the activation (by cleavage) of procaspases (caspase-8 and caspase-9), the upregulation of pro-apoptotic proteins (BAD and Bim), and the downregulation of anti-apoptotic proteins (Bcl-2). The involvement of these species in apoptosis in a concentration- and time-dependent manner is depicted as a Western blot analysis[204] in Figure 54. For the concentration-dependent studies, the $[Co(bpy)\{Ph(O)NN(O)Ph\}_2](PF_6)_2$ concentration ranged from 0-10 μM, with the cells being treated with each concentration for 12 hours. For the time-dependent studies, the cells were incubated with 2 μM $[Co(bpy)\{Ph(O)NN(O)Ph\}_2](PF_6)_2$ for times ranging from 1-36 hours. In both concentration- and time-dependent studies, the results suggest apoptosis is induced through both the extrinsic and intrinsic pathways, with the extrinsic pathway of apoptosis being more favorable over the intrinsic pathway.[204] This conclusion is based on the greater expression of cleaved caspase-8, which is involved in the extrinsic pathway,[185,186] than that of cleaved caspase-9, which is involved in the intrinsic pathway.[185,187-189]

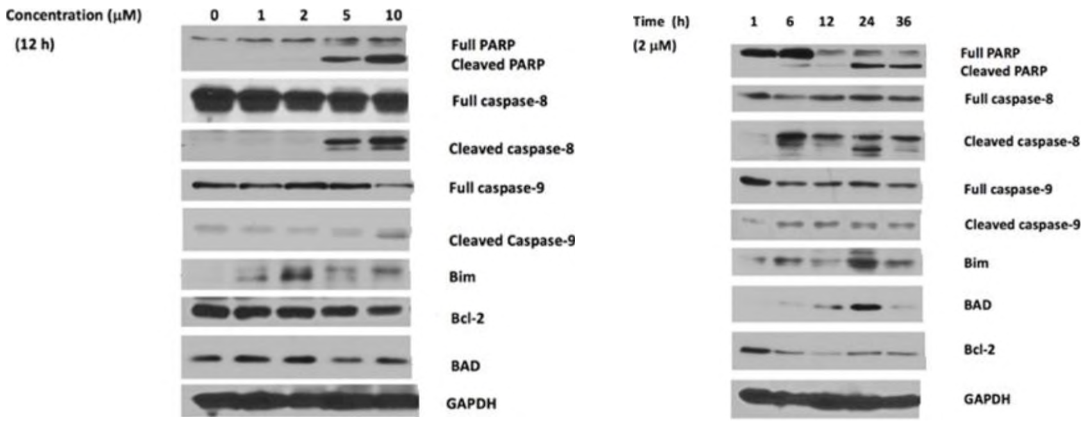

Figure 54: Concentration- and time-dependent protein levels after treating cells with $[Co(bpy)\{Ph(O)NN(O)Ph\}_2](PF_6)_2$. The preparation of total protein extracts involved suspending cell pellets in Triton-X 100 lysis buffer, which is composed of 50 mM *N*-(2-hydroxyethyl)piperazine-*N'*-ethanesulfonic acid, 150 mM NaCl, 1% Tris-X 100, and 5 mM ethylenediaminetetraacetic acid. The lysate mixture was then centrifuged at 20000*g* in a microcentrifuge for 10 minutes at 4°C. A Shimadzu UV-1280 UV-visible spectrometer was then used to measure the total protein content in the supernatant. The same amount of protein from each sample underwent 10% SDS-PAGE. The proteins were then transferred to a poly(vinylidene difluoride) membrane at a voltage of 100 for 80 minutes. Once the membrane was transferred, it was incubated for 1 hour at 25°C with 5% nonfat milk in TBST buffer, which is composed of 1 mM Tris at pH 7.4, 150 mM NaCl, and 0.2% Tween-20. The membrane was then incubated overnight at 4°C with a primary antibody in TBST. After washing the membrane with TBST several times, the membrane was incubated with a horseradish peroxidase-linked secondary antibody that was diluted 1:3000 and then washed three times with TBST. The membrane was processed using a Thermo Fisher Scientific Pierce ECL Plus Western Blotting Substrate by obtaining an enhanced chemiluminescence signal. GAPDH was used as a housekeeping protein or loading control.[204]

Moreover, since some Co(II) species are known for inducing apoptosis *via* the generation of ROS and oxidative DNA damage, akin to the iron(II)-catalyzed Fenton reactions[204,213] (in which Fe^{2+} catalyzes the production of $OH^{\cdot}$ from H_2O_2[214]), we were interested in determining whether or not ROS were involved in the apoptosis mechanism of $[Co(bpy)\{Ph(O)NN(O)Ph\}_2](PF_6)_2$. This assay involved treating the SK-HEP-1 cells with different concentrations of $[Co(bpy)\{Ph(O)NN(O)Ph\}_2](PF_6)_2$ for 14 hours and then running a fluorescence-based ROS assay that particularly measures the levels of the hydroxyl radical and superoxide, which are types of ROS. These assays showed that ROS levels greatly increased at high concentrations of [Co(bpy){Ph(O)NN(O)Ph}$_2$](PF$_6$)$_2$, but only modestly increased at the concentrations used in the flow cytometry and Western blot experiments. These results suggest that ROS-mediated DNA damage is not likely the main mechanism of apoptosis induced by [Co(bpy){Ph(O)NN(O)Ph}$_2$](PF$_6$)$_2$, though it cannot be ruled out entirely from making some contribution to apoptosis. These results are presented in Figure 55.[204]

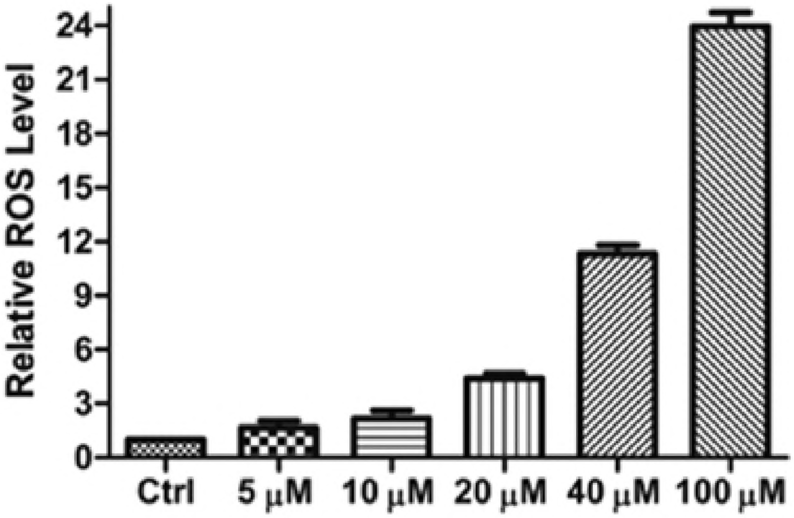

Figure 55: Effect of [Co(bpy){Ph(O)NN(O)Ph}$_2$](PF$_6$)$_2$ on ROS levels in SK-HEP-1 cells. The preparation of the master reaction mix followed the provided protocol by Sigma-Aldrich, and 100 μL of this mixture was added to each well. The cells were incubated with this mixture for 1 hour and were then treated with the different concentrations of [Co(bpy){Ph(O)NN(O)Ph}$_2$](PF$_6$)$_2$ with PBS buffer. The cells then underwent further incubation for 14 hours. With the use of a Hitachi F-7000 fluorescence spectrometer, the fluorescence intensity was measured using an excitation wavelength of 490 nm. The emission spectra showed an emission peak at 525 nm. Each treatment was conducted with 16 replicates.[204]

In order to assess the cytotoxicity of [Co(bpy){Ph(O)NN(O)Ph}$_2$](PF$_6$)$_2$ to SK-HEP-1 cells, a 3-(4,5-dimethylthiazol-2-yl)-2,5-diphenyl tetrazolium bromide (MTT) assay was conducted. The cells were incubated with [Co(bpy){Ph(O)NN(O)Ph}$_2$](PF$_6$)$_2$ at a series of concentrations ranging from 5.12 nM to 2 mM for 48 hours before the assay was performed. Interestingly, the results of the MTT assay revealed a substantial loss in cell viability only at the higher $[Co(bpy)\{Ph(O)NN(O)Ph\}_2](PF_6)_2$ concentrations of 400 μM and 2 mM, which are higher concentrations than those shown to induce apoptosis by our phase-contrast microscopy, flow cytometry, and Western blot experiments.[204] However, there has been evidence for MTT assays underestimating cytotoxicity and overestimating cell viability.[215] This may explain the inconsistency between our MTT results and the results from our other experiments.[204]

In addition to SK-HEP-1, other cell lines were treated with concentrations of $[Co(bpy)\{Ph(O)NN(O)Ph\}_2](PF_6)_2$ at 2 μM and 10 μM for 12 hours to see if it could induce apoptosis in more than one cell line. The other cell lines that were tested were HEK 293 (human embryonic kidney cells), HT-29 (colon cancer), MCF-7 (breast cancer), and PC-3 (prostate cancer). However, $[Co(bpy)\{Ph(O)NN(O)Ph\}_2](PF_6)_2$ did not cause substantial PARP cleavage in these lines as it did in SK-HEP-1 cells, suggesting that $[Co(bpy)\{Ph(O)NN(O)Ph\}_2](PF_6)_2$ is selective.[204] (See Figure 56.) The selectivity of $[Co(bpy)\{Ph(O)NN(O)Ph\}_2](PF_6)_2$ is encouraging and suggests that potential therapeutic use of this compound against liver cancer cells may largely spare cells in other organs.

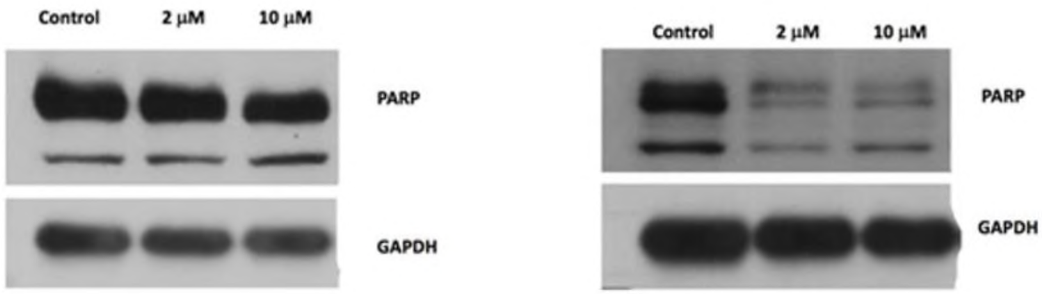

(a)

HEK 293 cells

(b)

HT-29 cells

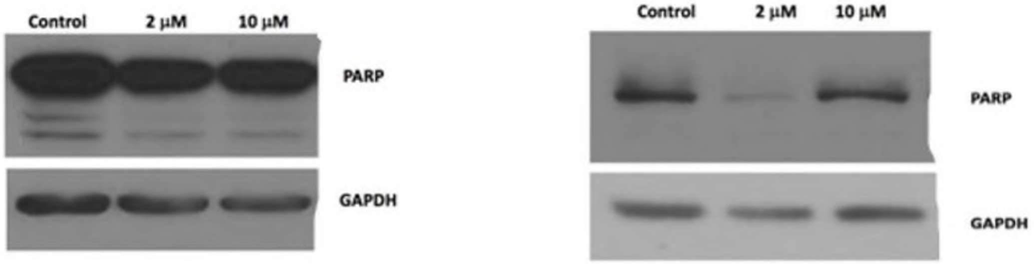

(c)

MCF-7 cells

(d)

PC-3 cells

Figure 56: Effect of 2 µM and 10 µM of $[Co(bpy)\{Ph(O)NN(O)Ph\}_2](PF_6)_2$ on PARP cleavage in (a) HEK 293 cells (b) HT-29 cells (c) MCF-7 cells (d) PC-3 cells after 12 hours.[204] See Figure 54 and Section 6.7.4 on how the Western blot analysis was conducted.

As an additional set of control experiments, we investigated the ability of the starting materials used in the synthesis of $[Co(bpy)\{Ph(O)NN(O)Ph\}_2](PF_6)_2$ to induce apoptosis in SK-HEP-1 cells independently. The starting materials that were analyzed were $Co(bpy)Cl_2$[216,217] and PhNO. (Refer to Chapter III, Section 3.2 for details on the synthesis of $[Co(bpy)\{Ph(O)NN(O)Ph\}_2](PF_6)_2$.) Additionally, the Co(II) complex $Co(phen)Cl_2$[218] (phen = 1,10-phenanthroline), a structurally similar compound to $Co(bpy)Cl_2$, and $CoCl_2$, a salt that dissociates to Co^{2+} and Cl^- ions in aqueous solution, were also analyzed. It is important to note that the free (uncoordinated) azodioxide ligand Ph(O)NN(O)Ph was not analyzed in this set of control experiments because free Ph(O)NN(O)Ph exists predominantly as a monomeric nitrosoarene, PhNO, in the solution phase, whereas dimeric azodioxides are generally favored in the solid phase.[219,220] SK-HEP-1 cells were treated with each of these four compounds at 10 μM for 12 hours. None of these compounds triggered substantial PARP cleavage in SK-HEP-1 cells as $[Co(bpy)\{Ph(O)NN(O)Ph\}_2](PF_6)_2$ did. (See Figure 57.) These results indicate that Co without azodioxide is not responsible for the induction of apoptosis, either by itself as aquated Co^{2+} or as part of a complex with aromatic diimine ligands. Therefore, we propose that the azodioxide ligand Ph(O)NN(O)Ph is critical to the biological activity of $[Co(bpy)\{Ph(O)NN(O)Ph\}_2](PF_6)_2$.[204] Importantly, the homoleptic complex salt $[Co\{Ph(O)NN(O)Ph\}_4](PF_6)_2$ showed very similar apoptotic activity to $[Co(bpy)\{Ph(O)NN(O)Ph\}_2](PF_6)_2$ in SK-HEP-1 cells,[204] which further supports our conclusion that the Ph(O)NN(O)Ph ligand plays an important role in the biological activity.

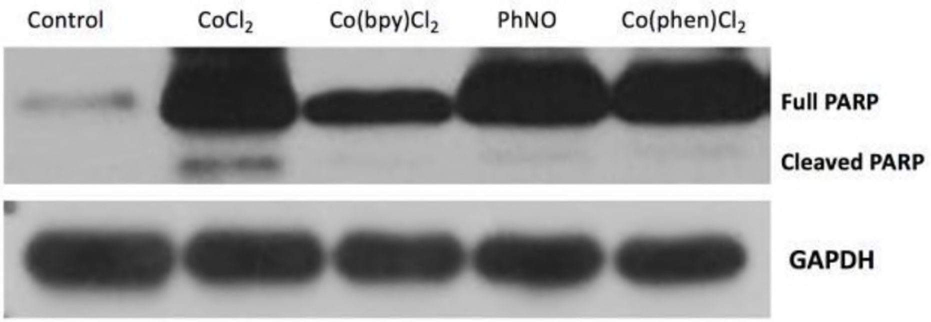

Figure 57: Effect of 10 μM of starting materials and $CoCl_2$ and $Co(phen)Cl_2$ on cleavage of PARP in SK-HEP-1 after 12 hours.[204] See Figure 54 and Section 6.7.4 on how the Western blot analysis was conducted.

6.7 Experimental Methods

6.7.1 Reagents and Antibodies

The preparations of $[Co(bpy)\{Ph(O)NN(O)Ph\}_2](PF_6)_2$ and $Co(bpy)Cl_2$[216] are detailed in Chapter III of this dissertation and in our synthesis and characterization

publication in *ACS Omega*.[217] The Co(II) complex $Co(phen)Cl_2$ was prepared following a procedure reported by Siddiqi and coworkers.[218] The antibodies used for procaspase-8, cleaved caspase-8, procaspase-9, cleaved caspase-9, Bcl-2, Bim, BAD, and PARP were obtained from Cell Signaling Technology, Inc. The antibody used for GAPDH was obtained from Santa Cruz Biotechnology.[204]

6.7.2 Cell Culture and Treatment

All cancer cell lines used for our studies were grown in RPMI-1640, which was obtained from Cleveland Clinic Foundation Core Facility, supplemented with 10% cosmic calf serum and 1% antibiotics. Cells were stored at 37°C in a humidified atmosphere with 5% CO_2. Cells were treated with or without varying concentrations of $[Co(bpy)\{Ph(O)NN(O)Ph\}_2](PF_6)_2$ for a given time frame once cell confluence reached 70%. Before being diluted in aqueous solution, $[Co(bpy)\{Ph(O)NN(O)Ph\}_2](PF_6)_2$ was dissolved in DMSO.[204]

6.7.3 Apoptotic Cell Morphology

An inverted phase-contrast fluorescence microscope (Carl Zeiss) was used to analyze all morphological changes in SK-HEP-1 cells after treating them with $[Co(bpy)\{Ph(O)NN(O)Ph\}_2](PF_6)_2$. These cells were seeded into 6-well plates (12×10^4 cells/well), cultured to the appropriate confluence, and treated for 12 hours at 37°C with relevant concentrations of $[Co(bpy)\{Ph(O)NN(O)Ph\}_2](PF_6)_2$. After the cells were treated, they were washed with phosphate-buffered saline (PBS). For each well, images were taken under 20× magnification from five different fields at random.[204]

6.7.4 Western Blot

After SK-HEP-1 cells were treated, they were first washed with cold PBS twice and then collected with a scraper. The preparation of total protein extracts involved suspending cell pellets in Triton-X 100 lysis buffer, which is composed of 50 mM *N*-(2-hydroxyethyl)piperazine-*N*'-ethanesulfonic acid, 150 mM NaCl, 1% Tris-X 100, and 5 mM ethylenediaminetetraacetic acid. The lysate mixture was then centrifuged at 20000*g* in a microcentrifuge for 10 minutes at 4°C. A Shimadzu UV-1280 UV-visible spectrometer was then used to measure the total protein content in the supernatant. The same amount of protein from each sample underwent 10% SDS-PAGE (sodium dodecyl sulfate-polyacrylamide gel electrophoresis). The proteins were then transferred to a poly(vinylidene difluoride) membrane with the use of a Bio-Rad Mini-PROTEAN 3 wet transfer unit at a voltage of 100 for 80 minutes. Once the membrane was transferred, it was incubated for 1 hour at 25°C with 5% nonfat milk in TBST buffer, which is composed of 1 mM Tris at pH 7.4, 150 mM NaCl, and 0.2% Tween-20. The membrane was then incubated overnight at 4°C with a primary antibody in TBST. After washing the membrane with TBST several times, the membrane was incubated with a horseradish peroxidase-linked secondary antibody that was diluted 1:3000 and then washed three times with TBST. Finally, the membrane was processed using a Thermo Fisher Scientific Pierce ECL Plus Western Blotting Substrate by obtaining an enhanced chemiluminescence signal.[204]

6.7.5 Flow Cytometry

A BD Biosciences Annexin V fluorescein isothiocyanate (FITC)/propidium iodide (PI) apoptosis detection kit was used. After the SK-HEP-1 cells were treated with $[Co(bpy)\{Ph(O)NN(O)Ph\}_2](PF_6)_2$, they were collected in cold PBS, centrifuged for 5 min at 4°C at a speed of 1500*g*, washed with PBS twice, and resuspended in 100 μL of 1× binding buffer per sample. In a dark environment at 4°C, each sample was stained with 5 μL of Annexin V-FITC and 5 μL of PI for 15 minutes and 400 μL of 1× binding buffer was added. Using a flow cytometer with BD FACSDiva software, the cells were analyzed.[204] Annexin $V\text{-}FITC^-/PI^-$ cells were determined as being viable, Annexin $V\text{-}FITC^+/PI^-$ cells were identified as being early apoptotic. Annexin $V\text{-}FITC^+/PI^+$ cells were determined as being late apoptotic. Annexin $V\text{-}FITC^-/PI^+$ cells were identified as being necrotic.[212] Fluorescence spectroscopy of $[Co(bpy)\{Ph(O)NN(O)Ph\}_2](PF_6)_2$ was performed using a Hitachi F-7000 fluorescence spectrometer.[204]

6.7.6 ROS Assay

A Sigma-Aldrich fluorometric intracellular ROS kit was used to assess any production of ROS while cells were being treated with $[Co(bpy)\{Ph(O)NN(O)Ph\}_2](PF_6)_2$. Before the assay was performed, cells were grown in medium in a 96-well plate at 4000 cells/well overnight. The preparation of the master reaction mix followed the provided protocol by Sigma-Aldrich, and 100 μL of this mixture was added to each well. The cells were incubated with this mixture for 1 hour and were then treated with the different concentrations of $[Co(bpy)\{Ph(O)NN(O)Ph\}_2](PF_6)_2$ with PBS buffer. The cells then underwent further incubation for 14 hours. Finally, with the use of a Hitachi F-7000 fluorescence spectrometer, the fluorescence intensity was measured using an excitation wavelength of 490 nm. The emission spectra showed an emission peak at 525 nm. Each treatment was conducted with 16 replicates.[204]

6.7.7 MTT Assay

In a 96-well plate at 3000 cells/well, SK-HEP-1 cells were grown in the medium overnight. The relevant $[Co(bpy)\{Ph(O)NN(O)Ph\}_2](PF_6)_2$ concentrations replaced the growth medium so that the cells could incubate for 48 hours. A 1:3 ratio of 5 mg/mL MTT and growth medium was prepared as the MTT solution, and 100 μL of this solution was added to each of the wells. The cells were then further incubated for 2 to 4 hours and then 200 μL DMSO was added to each of the wells. The absorbance at 570 nm was measured as soon as the precipitates had dissolved. A total of 8 replicates were conducted for each treatment.[204]

CHAPTER VII

FUTURE DIRECTIONS

7.1 Catalysis

Since the isolated yields and the turnover numbers reported for our catalysis experiments for the direct allylic amination/C–C double-bond transposition reactions are thus far low[221] (see Figure 29 in Chapter V, Section 5.3.1), one future goal is to improve the yield and scope of these reactions by modifying our $[Co(bpy)\{Ph(O)NN(O)Ph\}_2](PF_6)_2$ catalyst,[221] by preparing analogous catalysts containing substituted azodioxide ligands, which would include those with electron-donating and/or electron-withdrawing substituents on their aromatic rings. The synthesis of these types of azodioxide complexes with variable substituents on their ligands has the potential to enable a high degree of "tuning" of catalyst structure to enhance catalytic performance. It will also be interesting and informative to investigate and compare the catalytic ability of other azodioxide complexes prepared by our group in the future in direct allylic amination reactions.

Since only preliminary GC-MS results have thus far been obtained for our experiments on the catalysis of nucleophilic allylic substitution reactions (see Chapter V, Section 5.3.2), an ongoing effort will be to optimize reaction conditions. Optimizing reaction conditions may help reduce the presence of unreacted substrate molecules in the synthesis of the allylic amine drug cinnarizine after the reaction is complete[222] and improve the yields of nucleophilic allylic substitution reactions involving simpler substrates. Also, our efforts of purifying the desired allylic amine products (detected by GC-MS) from nucleophilic allylic substitution are ongoing. Once these allylic amines are purified and their syntheses are confirmed by NMR spectroscopy, we can then report with confidence that $[Co(bpy)\{Ph(O)NN(O)Ph\}_2](PF_6)_2$ is an active catalyst for two types of allylic amination reactions, hence expanding its catalytic applications.

Additional future work can involve studying the catalytic behaviors of the homoleptic complex salt $[Co\{Ph(O)NN(O)Ph\}_4](PF_6)_2$, prepared by former Boyd group Ph.D. student Dr. Lakshmi Balaraman, and other azodioxide complexes prepared by our group in the future, in the synthesis of allylic amine drugs and comparing their catalytic behaviors to that of $[Co(bpy)\{Ph(O)NN(O)Ph\}_2](PF_6)_2$. If further studies show evidence that $[Co(bpy)\{Ph(O)NN(O)Ph\}_2](PF_6)_2$ and our other azodioxide complexes can act as competent catalysts in the one-pot synthesis of cinnarizine,[222] and possibly in the synthesis of other allylic amine drugs, this will mean that $[Co(bpy)\{Ph(O)NN(O)Ph\}_2](PF_6)_2$ and other azodioxide complexes not only act as catalysts for different types of allylic amination, but also have the potential to be useful catalysts in the industrial production of allylic amine drugs.

7.2 Biological Studies

Future work in collaboration with Prof. Aimin Zhou and his students will involve investigating the therapeutic potential[223] of both $[Co(bpy)\{Ph(O)NN(O)Ph\}_2](PF_6)_2$ and $[Co\{Ph(O)NN(O)Ph\}_4](PF_6)_2$ in cancer through the use of liver cancer mouse models, as well as additional cellular studies to further elucidate the mechanism of their pro-apoptotic behavior. Additionally, future work will involve studying the interactions of both Co azodioxide species, both homoleptic and heteroleptic, with SK-HEP-1 cells as well as with other cell lines in order to explain the selectivity of these species to induce apoptosis in only SK-HEP-1 cells. Further stability studies on both Co azodioxide species will be conducted to gain more insight about their structural integrities as cells are being treated with them. It would also be interesting to study the potential antiviral activity of both Co azodioxide species, since the Co-containing species Doxovir[224] has shown to be a promising candidate as an antiviral agent. Another future goal is to study the potential biological activity of other azodioxide complexes prepared by our group in the future, with an eye toward identifying pro-apoptotic activity in SK-HEP-1 cells and other cell lines.[223] Biological studies on future azodioxide complexes will enable the construction of structure-activity relationships in which metals and ancillary ligands, as well as substituents on azodioxide ligands, can be varied in order to optimize biological activity.

REFERENCES

1. Senanayake, C. H., et al. Transition Metal Catalysis in the Pharmaceutical Industry. In *Applications of Transition Metal Catalysis in Drug Discovery and Development: An Industrial Perspective*; John Wiley & Sons, Inc: Hoboken, New Jersey, 2012; pp. 1-3.
2. Weller, M; Overton, T.; Rourke, J.; Armstrong, F. Catalysis. In *Inorganic Chemistry*; 6th ed.; Oxford University Press: Oxford, United Kingdom, 2014; pp. 735.
3. Hayler, J. D.; Leahy, D. K; Simmons, E. M. A Pharmaceutical Industry Perspective on Sustainable Metal Catalysis. *Organometallics*. **2018**, *38*, 36-46.
4. Senanayake, C. H., et al. Selected Applications of Pd- and Cu-Catalyzed Carbon-Heteroatom Cross-Coupling Reactions in the Pharmaceutical Industry. In *Applications of Transition Metal Catalysis in Drug Discovery and Development: An Industrial Perspective*; John Wiley & Sons, Inc: Hoboken, New Jersey, 2012; pp. 119.
5. (a) Fan, X.; Song, Y.; Long, Y. An Efficient and Practical Synthesis of the HIV Protease Inhibitor Atazanavir via a Highly Diastereoselective Reduction Approach. *Org. Process Res. Dev.* **2008**, *12*, 69-75. (b) Magano, J.; Dunetz, J. R. Large-Scale Applications of Transition Metal-Catalyzed Couplings for the Synthesis of Pharmaceuticals. *Chem. Rev.* **2011**, *111*, 2177-2250.
6. World Health Organization Model List of Essential Medicines; 21st ed.; World Health Organization, 2019.
7. Friedfeld, M. R.; Zhong, H.; Ruck, R. T.; Shevlin, M.; Chirik, P. J. Cobalt-Catalyzed Asymmetric Hydrogenation of Enamides Enabled by Single-Electron Reduction. *Science*. **2018**, *360*, 888-893.

8. (a) Sova, M.; Frlan, R.; Gobec, S.; Stavber, G.; Casar, Z. D-Glucosamine in Iron Catalyzed Cross-Coupling Reactions of Grignards with Allylic and Vinylic Bromides: Application to the Synthesis of a Key Sitagliptin Precursor. *Appl. Organometal. Chem*. **2015**, *29*, 528-535. (b) Piontek, A.; Bisz, E.; Szostak, M. Iron-Catalyzed Cross Couplings in the Synthesis of Pharmaceuticals: In Pursuit of Sustainability. *Angew. Chem. Int. Ed.* **2018**, *57*, 11116-11128.

9. Emayavaramban, B.; Roy, M.; Sundararaju, B. Iron-Catalyzed Allylic Amination Directly From Allylic Alcohols. *Chem. Eur. J.* **2016**, *22*, 3952-3955.

10. Ye, Z.; Brust, T. F.; Watts, V. J.; Dai, M. Palladium-Catalyzed Regio- and Stereoselective γ-Arylation of Tertiary Allylic Amines: Identification of Potent Adenylyl Cyclase Inhibitors. *Org. Lett*. **2015**, *17*, 892-895.

11. Mjos, K. D.; Orvig, C. Metallodrugs in Medicinal Inorganic Chemistry. *Chem. Rev.* **2014**, *114*, 4540-4563.

12. (a) Frezza, M.; Hindo, S.; Chen, D.; Davenport, A.; Schmitt, S.; Tomco, D.; Ping Dou, Q. Novel Metals and Metal Complexes as Platforms for Cancer Therapy. *Curr. Pharm. Des*. **2010**, *16* (16), 1813-1825. (b) Ndagi, U.; Mhlongo, N.; Soliman, M. E. Metal Complexes in Cancer Therapy-An Update from Drug Design Perspective. *Drug Des. Devel. Ther*. **2017**, *11*, 599-616.

13. Weller, M; Overton, T.; Rourke, J.; Armstrong, F. Inorganic Chemistry in Medicine. In *Inorganic Chemistry*; 6th ed.; Oxford University Press: Oxford, United Kingdom, 2014; pp. 820.

14. Sharma, V.; Piwnica-Worms, D. Metal Complexes for Therapy and Diagnosis of Drug Resistance. *Chem. Rev.* **1999**, *99* (9), 2545-2560.

15. Rosenberg, B.; VanCamp, L.; Trosko, J. E.; Mansour, V. H. Platinum Compounds: A New Class of Potent Antitumour Agents. *Nature*. **1969**, *222*, 385-386.

16. Gandeepan, P.; Müller, T.; Zell, D.; Cera, G.; Warratz, S.; Ackermann, L. 3*d* Transition Metals for C–H Activation. *Chem. Rev.* **2019**, *119*, 2192-2452.

17. (a) Melchior, M.; Rettig, S. J.; Liboiron, B. D.; Thompson, K. H.; Yuen, V. G.; McNeill, J. H.; Orvig, C. Insulin-Enhancing Vanadium(III) Complexes. *Inorg. Chem.* **2001**, *40* (18), 4686-4690. (b) Thompson, K. H.; Orvig, C. Metal Complexes in Medicinal Chemistry: New Vistas and Challenges in Drug Design. *Dalton Trans.* **2006**, 761-764.

18. Thompson, K. H.; Lichter, J.; LeBel, C.; Scaife, M. C.; McNeill, J. H.; Orvig, C. Vanadium Treatment of Type 2 Diabetes: A View to the Future. *J. Inorg. Biochem.* **2009**, *103* (4), 554-558.

19. Mayo Clinic Staff. "Vitamin B_{12}." *Mayo Clinic*, Mayo Foundation for Medical Education and Research, 2017, https://www.mayoclinic.org/drugs-supplements-vitamin-b12/art-20363663.

20. Hall, A. H.; Rumack, B. H. Hydroxycobalamin/Sodium Thiosulfate as a Cyanide Antidote. *J. Emerg. Med.* **1987**, *5* (2), 115-121.

21. Schwartz, J. A.; Lium, E. K.; Silverstein, S. J. Herpes Simplex Virus Type 1 Entry is Inhibited by the Cobalt Chelate Complex CTC-96. *J. Virol.* **2001**, *75* (9), 4117-4128.

22. Epstein, S. P.; Wallace, J. A.; Epstein, D.; Stewart, C. C.; Burger, R. M. Efficacy of Cobalt Chelates in the Rabbit Eye Model for Epithelial Herpetic Keratitis. *Cornea.* **1998**, *17* (5), 550-557.

23. Epstein, S. P.; Pashinsky, Y. Y.; Gershon, D.; Winicov, I.; Srivilasa, C.; Kristic, K. J.; Asbell, P. A. Efficacy of Topical Cobalt Chelate CTC-96 Against Adenovirus in a Cell

Culture Model and Against Adenovirus Keratoconjunctivitis in a Rabbit Model. *BMC Ophthalmol.* **2006**, *6* (22), 1-11.

24. Weller, M; Overton, T.; Rourke, J.; Armstrong, F. Inorganic Chemistry in Medicine. In *Inorganic Chemistry*; 6th ed.; Oxford University Press: Oxford, United Kingdom, 2014; pp. 827.
25. (a) Domarle, O.; Blampain, G.; Agnaniet, H.; Nzadiyabi, T.; Lebibi, J.; Brocard, J.; Maciejewski, L.; Biot, C.; Georges, A. J.; Millet, P. In Vitro Antimalarial Activity of a New Organometallic Analog, Ferrocene-Chloroquine. *Antimicrob. Agents Chemother.* **1998**, *42* (3), 540-544. (b) Dubar, F.; Khalife, J.; Brocard, J.; Dive, D.; Biot, C. Ferroquine, an Ingenious Antimalarial Drug-Thoughts on the Mechanism of Action. *Molecules.* **2008**, *13*, 2900-2907. (c) Anthony, E. J.; Bolitho, E. M.; Bridgewater, H. E.; Carter, O. W. L.; Donnelly, J. M.; Imberti, C.; Lant, E. C.; Lermyte, F.; Needham, R. J.; Palau, M.; Sadler, P. J.; Shi, H.; Wang, F.; Zhang, W.; Zhang, Z. Metallodrugs are Unique: Opportunities and Challenges of Discovery and Development. *Chem. Sci.* **2020**, *11*, 12888-12917.
26. Tinker, J. H.; Michenfelder, J. D. Sodium Nitroprusside: Pharmacology, Toxicology and Therapeutics. *Anestesiology.* **1976**, *45* (3), 340-354.
27. Antosova, M.; Plevkova, J.; Strapkova, A.; Buday, T. Nitric Oxide-Important Messenger in Human Body. *Open J. Mol. Integr. Physiol.* **2012**, *2*, 98-106.
28. Divakaran, S.; Loscalzo, J. The Role of Nitroglycerin and Other Nitrogen Oxides in Cardiovascular Therapeutics. *J. Am. Coll. Cardiol.* **2017**, *70* (19), 2393-2410.
29. Herzik Jr., M. A.; Jonnalagadda, R.; Kuriyan, J.; Marletta, M. A. Structural Insights into the Role of Iron-Histidine Bond Cleavage in Nitric Oxide-Induced Activation of

H-NOX Gas Sensor Proteins. *PNAS*. **2014**, *111* (40), 4156-4164.

30. Mayo Clinic Staff. “Sodium Nitroprusside.” *Mayo Clinic*, Mayo Foundation for Medical Education and Research, 2020, https://www.mayoclinic.org/drugs-supplements/sodium- nitroprusside-intravenous-route/proper-use/drg-20406115.
31. Ghofrani, H. A.; Osterloh, I. H.; Grimminger, F. Sildenafil: From Angina to Erectile Dysfunction to Pulmonary Hypertension and Beyond. *Nat. Rev. Drug Discov*. **2006**, *5*, 689-702.
32. Ford, P. C.; Lorkovic, I. M. Mechanistic Aspects of the Reactions of Nitric Oxide with Transition-Metal Complexes. *Chem. Rev*. **2002**, *102*, 993-1017.
33. Emhoff, K. A.; Balaraman, L.; Salem, A. M. H.; Mudarmah, K. I.; Boyd, W. C. Coordination Chemistry of Organic Nitric Oxide Derivatives. *Coord. Chem. Rev*. **2019**, *396*, 124-140.
34. Jiang, Y.; Schirmer, B.; Blacque, O.; Fox, T.; Grimme, S.; Berke, H. The “Catalytic Nitrosyl Effect”: NO Bending Boosting the Efficiency of Rhenium Based Alkene Hydrogenations. *J. Am. Chem. Soc*. **2013**, *135*, 4088-4102.
35. Lee, J.; Chen, L.; West, A. H.; Richter-Addo, G. B. Interactions of Organic Nitroso Compounds with Metals. *Chem. Rev*. **2002**, *102*, 1019-1065.
36. Weller, M; Overton, T.; Rourke, J.; Armstrong, F. An Introduction to Coordination Compounds. In *Inorganic Chemistry*; 6th ed.; Oxford University Press: Oxford, United Kingdom, 2014; pp. 229.
37. (a) Dieterich, D. A.; Paul, I. C.; Curtin, D. Y. Crystal Structure of Nitrosobenzene Dimer. *cis*-Azobenzene Dioxide. *J. Chem. Soc. D*. **1970**, 1710-1711. (b) Dieterich, D. A.; Paul, I. C.; Curtin, D. Y. Structural Studies on Nitrosobenzene and 2-

Nitrosobenzoic Acid. Crystal and Molecular Structures of *cis*-Azobenzene Dioxide and *trans*-2,2'-Dicarboxyazobenzene Dioxide. *J. Am. Chem. Soc.* **1974**, *96*, 6372-6380.

38. Cameron, M.; Gowenlock, B. G. The Coordination Complexes of Nitrosobenzene with Tin(IV) Chloride and Titanium(IV) Chloride. *Polyhedron* **1992**, *11* (21), 2781-2782.
39. Williams, K. C.; Imhoff, D. W. Syntheses of Organolead Compounds VI. Reaction of Dinitrogen Tetroxide with Organolead Compounds. *J. Organomet. Chem*. **1972**, *42* (1), 107-115.
40. Williams, K. C.; Imhoff, D. W. Concerning the Reaction of Dinitrogen Tetroxide with Tetramethyltin. *Inorg. Nucl. Chem. Lett.* **1973**, *9* (2), 227-231.
41. Lightfoot, A. P.; Pritchard, R. G.; Wan, H.; Warren, J. E.; Whiting, A. A Novel Scandium *ortho*-Methoxynitrosobenzene-Dimer Complex: Mechanistic Implications for the Nitroso Diels-Alder Reaction. *Chem. Comm.* **2002**, 2072-2073.
42. Fitts, L. S.; Bierschenk, E. J.; Hanusa, T. P.; Rheingold, A. L.; Pink, M.; Young Jr., V. G. Selective Modification of the Metal Coordination Environment in Heavy Alkaline Earth Iodide Complexes. *New J. Chem.* **2016**, *40*, 8229-8238.
43. Srivastava, R. S.;Khan, M. A.; Nicholas, K. M. A Novel Intermediate in Allylic Amination Catalyzed by Iron Salts. *J. Am. Chem. Soc*. **1996**, *118* (13), 3311-3312.
44. Srivastava, R. S.; Nicholas, K. M. On the Mechanism of Allylic Amination Catalyzed by Iron Salts. *J. Am. Chem. Soc*. **1997**, *119* (14), 3302-3310.
45. Emhoff, K. A.; Balaraman, L.; Simpson, S. R.; Stromyer, M. L.; Kalil, H. F.; Beemiller, J. R.; Sikatzki, P.; Eshelman, T. S.; Salem, A. M. H.; DeBord, M. A.; Panzner, M. J.; Youngs, W. J.; Boyd, W. C. Synthesis and Characterization of Cobalt(II) *N,N'*-

Diphenylazodioxide Complexes. *ACS Omega.* **2018**, *3* (11), 16021-16027.

46. Weller, M; Overton, T.; Rourke, J.; Armstrong, F. The *d*-Block Elements. In *Inorganic Chemistry*; 6th ed.; Oxford University Press: Oxford, United Kingdom, 2014; pp. 506.
47. (a) Bergman, J. G.; Cotton, F. A. The Crystal and Molecular Structure of Tetraphenylarsonium Tetranitratocobaltate(II); An Eight-Coordinate Cobalt(II) Complex. *Inorg. Chem.* **1966**, *5* (7), 1208-1213. (b) Koch, W. O.; Kaiser, J. T. First Structural Characterization of an Eight Coordinate Cobalt(II) Complex Containing Five-Membered Chelate Rings: Evidence for *d* Orbital σ-Stabilization Energy Favoring Eight- Over Six-Coordination at Cobalt(II) Ions. *Chem. Commun.* **1997**, 2237-2238. (c) Fiolka, C.; Pantenburg, I.; Meyer, G. Transition Metal(II)-Crown-Ether Polyiodides. *Cryst. Growth Des.* **2011**, *11* (11), 5159-5165.
48. Lyaskovskyy, V.; de Bruin, B. Redox Non-Innocent Ligands: Versatile New Tools to Control Catalytic Reactions. *ACS Catal.* **2012**, *2*, 270-279.
49. (a) Praneeth, V. K. K.; Ringenberg, M. R.; Ward, T. R. Redox-Active Ligands in Catalysis. *Angew. Chem. Int.* **2012**, *51*, 10228-10234. (b) Luca, O. R.; Crabtree, R. H. Redox-Active Ligands in Catalysis. *Chem. Soc. Rev.* **2013**, *42*, 1440-1459.
50. (a) Kalyanasundaram, K. Photophysics, Photochemistry, and Solar Energy Conversion with Tris(bipyridyl)ruthenium(II) and Its Analogues. *Coord. Chem. Rev.* **1982**, *46*, 159-244. (b) Juris, A.; Balzani, V.; Barigelletti, F.; Campagna, S.; Belser, P.; von Zelewsky, A. Ru(II) Polypyridine Complexes: Photophysics, Photochemistry, Electrochemistry, and Chemoluminescence. *Coord. Chem. Rev.* **1988**, *84*, 85-277. (c) Sullivan, B. P.; Salmon, D. J.; Meyer, T. J. Mixed Phosphine 2,2′-Bipyridine Complexes of Ruthenium. *Inorg. Chem.* **1978**, *17*, 3334-3341.

51. Weller, M; Overton, T.; Rourke, J.; Armstrong, F. *d*-Metal Complexes: Electronic Structure and Properties. In *Inorganic Chemistry*; 6th ed.; Oxford University Press: Oxford, United Kingdom, 2014; pp. 540-541.

52. (a) Harriman, A.; Richoux, M.-C.; Christensen, P. A.; Mosseri, S.; Neta, P. Redox Reactions with Colloidal Metal Oxides. Comparison of Radiation-generated and Chemically generated $RuO_2{\cdot}2H_2O$ and MnO_2 Colloids. *J. Chem. Soc., Faraday Trans. 1* **1987**, *83*, 3001-3014. (b) Hara, M.; Lean, J. T.; Mallouk, T. E. Photocatalytic Oxidation of Water by Silica-Supported Tris(4,4′-dialkyl-2,2′-bipyridyl)ruthenium Polymeric Sensitizers and Colloidal Iridium Oxide. *Chem. Mater.* **2001**, *13*, 4668-4675. (c) Fukuzumi, S.; Kato, S.; Suenobu,T. Combination of visible-light responsive heterogeneous and homogeneous photocatalysts for water oxidation. *Phys. Chem. Chem. Phys.* **2011**, *13*, 17960-17963. (d) Ryu, J.; Nam, D. H.; Lee, S. H.; Park, C. B. Biocatalytic Photosynthesis with Water as an Electron Donor. *Chem. Eur.* **2014**, *20*, 12020-12025.

53. (a) Du, J.; Yoon, T. P. Crossed Intermolecular [2+2] Cycloadditions of Acyclic Enones via Visible Light Photocatalysis. *J. Am. Chem. Soc.* **2009**, *131*, 14604-14605. (b) Ischay, M. A.; Lu, Z.; Yoon, T. P. [2+2] Cycloadditions by Oxidative Visible Light Photocatalysis. *J. Am. Chem. Soc.* **2010**, *132*, 8572-8574. (c) Hurtley, A. E.; Lu, Z.; Yoon, T. P. [2+2] Cycloaddition of 1,3-Dienes by Visible Light Photocatalysis. *Angew. Chem. Int. Ed.* **2014**, *53*, 8991-8994.

54. Buchanan, R. M..; Pierpont, C. G. Tautomeric Catecholate-Semiquinone Interconversion via Metal-Ligand Electron Transfer. Structural, Spectral, and Magnetic

Properties of (3,5-Di-tert-butylcatecholato)-(3,5-di-tertbutylsemiquinone)(bipyridyl)cobalt(III), a Complex Containing Mixed-Valence Organic Ligands. *J. Am. Chem. Soc.* **1980**, *102* (15), 4951- 4957.

55. Weller, M; Overton, T.; Rourke, J.; Armstrong, F. The *d*-Block Elements. In *Inorganic Chemistry*; 6th ed.; Oxford University Press: Oxford, United Kingdom, 2014; pp. 506.
56. Skoog, D. A.; Holler, F. J.; Crouch, S. R. Components of Optical Instruments. In *Principles of Instrumental Analysis*; 6th ed.; Cengage Learning: India, 2007; pp 169-173.
57. Blackmore, K. J.; Ziller, J. W.; Heyduk, A. F. "Oxidative Addition" to a Zirconium(IV) Redox-Active Ligand Complex. *Inorg. Chem.* **2005**, *44* (16), 5559-5561.
58. Haneline, M. R.; Heyduk, A. F. C–C Bond-Forming Reductive Elimination from a Zirconium(IV) Redox-Active Ligand Complex. *J. Am. Chem. Soc.* **2006**, *128* (26), 8410-8411.
59. Weller, M; Overton, T.; Rourke, J.; Armstrong, F. *d*-Metal Organometallic Chemistry. In *Inorganic Chemistry*; 6th ed.; Oxford University Press: Oxford, United Kingdom, 2014; pp. 617-618.
60. Srivastava, R. S.; Nicholas, K. M. On the Mechanism of Allylic Amination Catalyzed by Iron Salts. *J. Am. Chem. Soc.* **1997**, *119* (14), 3302-3310.
61. Friedman, H. L. The Visible and Ultraviolet Absorption of the Tetrachloroferrate(III) Ion in Various Media[1]. *J. Am. Chem. Soc.* **1952**, *74* (1), 5-10.
62. Rustad, D. S.; Gregory, N. W. Gas-Phase Ultraviolet and Visible Spectra of Sodium Tetrachloroferrate(III) and of Monomeric and Dimeric Iron(III) Chloride. *Inorg. Chem.* **1977**, *16* (12), 3036-3040.

63. Srivastava, R. S.; Nicholas, K. M. On the Mechanism of Allylic Amination Catalyzed by Iron Salts. *J. Am. Chem. Soc.* **1997**, *119* (14), 3302-3310.

64. Weller, M; Overton, T.; Rourke, J.; Armstrong, F. *d*-Metal Complexes: Electronic Structure and Properties. In *Inorganic Chemistry*; 6th ed.; Oxford University Press: Oxford, United Kingdom, 2014; pp. 529.

65. Mukhopadhyay, M.; Reddy, M. M.; Maikap, G. C.; Iqbal, J., Cobalt(II)-Catalyzed Conversion of Allylic Alcohols/Acetates to Allylic Amides in the Presence of Nitriles. *J. Org. Chem.* **1995**, *60*, 2670-2676.

66. Emhoff, K. A.; Balaraman, L.; Simpson, S. R.; Stromyer, M. L.; Kalil, H. F.; Beemiller, J. R.; Sikatzki, P.; Eshelman, T. S.; Salem, A. M. H.; DeBord, M. A.; Panzner, M. J.; Youngs, W. J.; Boyd, W. C. Synthesis and Characterization of Cobalt(II) *N,N′*-Diphenylazodioxide Complexes. *ACS Omega* **2018**, *3* (11), 16021-16027.

67. Barbour, C. J.; Cameron, J. H.; Winfield, J. M. Preparation of the Solvated Iron(II) Cation in Acetonitrile Using High Oxidation-State Fluorides and its Reaction with Trimethyl Phosphite. *J. Chem. Soc., Dalton Trans.* **1980**, *10*, 2001-2005.

68. Al-Sagher, H.; Fallis, I.; Farrugia, L. J.; Peacock, R. D. Trigonal Prismatic Geometry with Nonrigid Ligands: Cobalt(II) Complexes of Triaza-macrocycles with Pendant Alcohol Arms. *J. Chem. Soc., Chem. Commun.* **1993**, 1499-1500.

69. Weller, M; Overton, T.; Rourke, J.; Armstrong, F. *d*-Metal Complexes: Electronic Structure and Properties. In *Inorganic Chemistry*; 6th ed.; Oxford University Press: Oxford, United Kingdom, 2014; pp. 518.

70. Weller, M; Overton, T.; Rourke, J.; Armstrong, F. An Introduction to Coordination Compounds. In *Inorganic Chemistry*; 6th ed.; Oxford University Press: Oxford, United

Kingdom, 2014; pp. 216-217.

71. Stiefel, E. I.; Eisenberg, R.; Rosenberg, R. C.; Gray, H. B. Characterization and Electronic Structures of Six-Coordinate Trigonal-Prismatic Complexes. *J. Am. Chem. Soc.* **1966**, *88* (13), 2956−2966.

72. Eisenberg, R. Trigonal prismatic coordination in tris(dithiolene) complexes: Guilty or just non-innocent? *Coord. Chem. Rev.* **2011**, *255* (7-8), 825−836.

73. Haaland, A.; Hammel, A.; Rypdal, K.; Volden, H. V. The Coordination Geometry of Gaseous Hexamethyltungsten is not Octahedral. *J. Am. Chem. Soc.* **1990**, *112* (11), 4547-4549.

74. Weller, M; Overton, T.; Rourke, J.; Armstrong, F. The *d*-Block Elements. In *Inorganic Chemistry*; 6th ed.; Oxford University Press: Oxford, United Kingdom, 2014; pp. 506.

75. (a) Churchill, M. R.; Reis, A. H. Structural Studies on Clathro-chelate Complexes. Part III. Trigonal Prismatic Co-ordination of d^7 Cobalt(II) in Orthorhombic Crystalline $[\{FB(ONCHC_5H_3N)_3P\}Co^{II+}][BF_4^-]$, MeCN and a Single-Crystal Transformation of Unsolvated 6 Monoclinic $[\{FB(ONCHC_5H_3N)_3P\}Co^{II+}][BF_4^-]$. *J. Chem. Soc., Dalton Trans.* **1973**, 1570-1576. (b) Donaldson, P. B.; Tasker, P. A.; Alcock, N. W. Trigonal Prismatic versus Octahedral Co-ordination. Part 2. X-Ray Structure Determinations of Manganese(II), Cobalt(II), and Nickel(II) Complexes of Intermediate Geometry derived from the Ligand 1,1,1-Tris-(pyridine-2- aldiminomethyl)ethane. *J. Chem. Soc., Dalton Trans.* **1977**, 1160- 1165. (c) Voloshin, Y. Z.; Belaya, I. G.; Belov, A. S.; Platonov, V. E.; Maksimov, A. M.; Vologzhanina, A. V.; Starikova, Z. A.; Dolganov, A. V.; Novikov, V. V.; Bubnov, Y. N. Formation of the Second Superhydrophobic Shell Around an Encapsulated Metal Ion; Synthesis, X-ray Structure and

Electrochemical Study of the Clathrochelate and bis-Clathrochelate Iron(II) and cobalt (II, III) Dioximates with Ribbed Perfluoroalkylsulfide Substitutents. *Dalton Trans.* **2012**, *41*, 737-746. (d) Novikov, V. V.; Pavlov, A. A.; Belov, A. S.; Vologzhanina, A. V.; Savitsky, A.; Voloshin, Y. Z., Transition Ion Strikes Back: Large Magnetic Susceptibility Anisotropy in Cobalt(II) Clathrochelates. *J. Phys. Chem. Lett.* **2014**, *5* (21), 3799-3803.

76. (a) Wentworth, R. A. D.; Dahl, P. S.; Huffman, C. J.; Gillum, W. O.; Streib, W. E.; Huffman, J. C. Hindered-Ligand Systems. 9. Structure of the *cis,cis*-1,3,5-Tris(pyridine-2-carboxaldimino)cyclohexane Complexes of Cobalt(II) and Zinc(II) Ions. *Inorg. Chem.* **1981**, *21* (8), 3060-3063. (b) Paul, R. L.; Amoroso, A. J.; Jones, P. L.; Couchman, S. M.; Reeves, Z. R.; Rees, L. H.; Jeffery, J. C.; McCleverty, J. A.; Ward, M. D. Effects of Metal Co-ordination Geometry on Self-Assembly: A Monomeric Complex with Trigonal Prismatic Metal Co-ordination vs. Tetrameric Complexes with Octahedral Co-ordination. *J. Chem. Soc., Dalton Trans.* **1999**, 1563-1568. (c) Varzatskii, O. A.; Penkova, L. V.; Kats, S. V.; Dolganov, A. V.; Vologzhanina, A. V.; Pavlov, A. A.; Novikov, V.V.; Bogomyakov, A. S.; Nemykin, V. N.; Voloshin, Y. Z. Chloride Ion-Aided Self-Assembly of Pseudoclathrochelate Metal Tris-pyrazoloximates. *Inorg. Chem.* **2014**, *53* (6), 3062-3071. (d) Novikov, V. V.; Pavlov, A. A.; Nelyubina, Y. V.; Boulon, M.-E.; Varzatskii, O. A.; Voloshin, Y. Z.; Winpenny, R. E. P. A Trigonal Prismatic Mononuclear Cobalt(II) Complex Showing Single-Molecule Magnet Behavior. *J. Am. Chem. Soc.* **2015**, *137* (31), 9792-9795. (e) Peng, Y.; Bodenstein, T.; Fink, K.; Mereacre, V.; Anson, C. E.; Powell, A. K. Magnetic Anisotropy of a $\mathrm{Co^{II}}$ Single Ion Magnet with Distorted Trigonal Prismatic

Coordination: Theory and Experiment. *Phys. Chem. Chem. Phys.* **2016**, *18*, 30135-30143. (f) Ozumerzifon, T. J.; Bhowmick, I.; Spaller, W. C.; Rappé, A. K.; Shores, M. P. Toward Steric Control of Guest Binding Modality: A Cationic Co(II) Complex Exhibiting Cation Binding and Zero-Field Relaxation. *Chemical Commun.* **2017**, *53*, 4211-4214. (g) Pavlov, A. A.; Savkina, S. A.; Belov, A. S.; Nelyubina, Y. V.; Efimov, N. N.; Voloshin, Y. Z.; Novikov, V. V. Trigonal Prismatic Tris-Pyridineoximate Transition Metal Complexes: A Cobalt(II) Compound with High Magnetic Anisotropy. *Inorg. Chem.* **2017**, *56* (12), 6943-6951. (h) Belov, A. S.; Voloshin, Y. Z.; Pavlov, A. A.; Nelyubina, Y. V.; Belova, S. A.; Zubavichus, Y. V.; Avdeeva, V. V.; Efimov, N. N.; Malinina, E. A.; Zhizhin, K. Y.; Kuznetsov, N. T. Solvent-Induced Encapsulation of Cobalt(II) Ion by a Boron-Capped tris Pyrazoloximate. *Inorg. Chem.* **2020**, *59* (9), 5845-5853.

77. Schnidrig, S.; Bachmann, C.; Müller, P.; Weder, N.; Spingler, B.; Joliat-Wick, E.; Mosberger, M.; Windisch, J.; Alberto, R.; Probst, B. Structure-Activity and Stability Relationships for Cobalt Polypyridyl-Based Hydrogen-Evolving Catalysts in Water. *ChemSusChem.* **2017**, *10*, 4570-4580.
78. Jung, O-S.; Pierpont, C. G. Bistability and Low-Energy Electron Transfer in Cobalt Complexes Containing Catecholate and Semiquinone Ligands. *Inorg. Chem.* **1994**, *33* (10), 2227-2235.
79. Hoffmann, R. Building Bridges Between Inorganic and Organic Chemistry (Nobel Lecture). *Angew. Chem. Int. Ed.* **1982**, *21*, 711-724.
80. (a) Eisenberg, R.; Ibers, J. A. Trigonal Prismatic Coordination. The Molecular Structure of Tris(cis-1,2-diphenylethene-1,2- dithiolato)rhenium. *J. Am. Chem. Soc.* **1965**, *87*

(16), 3776−3778. (b) Eisenberg, R.; Stiefel, E. I.; Rosenberg, R. C.; Gray, H. B. Six Coordinate Trigonal-Prismatic Complexes of First-Row Transition Metals. *J. Am. Chem. Soc.* **1966**, *88* (12), 2874−2876. (c) Schrauzer, G. N.; Mayweg, V. P. Coordination Compounds with Delocalized Ground States. Tris(dithioglyoxal) and Related Prismatic α-Dithioketone Complexes of Transition Metals. *J. Am. Chem. Soc.* **1966**, *88* (14), 3235− 3242. (d) Al Mowali, A. H.; Porte, A. L. Electronic Ground States of the Trigonal-Prismatic Rhenium Complexes, Tris(cis-1,2-diphenylethene-1,2-dithiolato)rhenium, and Tris(toluene-3,4-dithiolato)- rhenium. *J. Chem. Soc., Dalton Trans.* **1975**, *3*, 250−252. (e) Sproules, S.; Benedito, F. L.; Bill, E.; Weyhermüller, T.; George, S. D.; Wieghardt, K. Characterization and Electronic Structures of Five Members of the Electron Transfer Series [Re(benzene-1,2-dithiolato)3] z (z = 1+,0,1−,2−,3−): A Spectroscopic and Density Functional Theoretical Study. *Inorg. Chem.* **2009**, *48* (23), 10926−10941.

81. Lightfoot, A. P.; Pritchard, R. G.; Wan, H.; Warren, J. E.; Whiting, A. A Novel Scandium *ortho*-Methoxynitrosobenzene-Dimer Complex: Mechanistic Implications for the Nitroso Diels-Alder Reaction. *Chem. Comm.* **2002**, 2072-2073.
82. Fitts, L. S.; Bierschenk, E. J.; Hanusa, T. P.; Rheingold, A. L.; Pink, M.; Young Jr., V. G. Selective Modification of the Metal Coordination Environment in Heavy Alkaline Earth Iodide Complexes. *New J. Chem.* **2016**, *40*, 8229-8238.
83. Weller, M; Overton, T.; Rourke, J.; Armstrong, F. Physical Techniques in Inorganic Chemistry. In *Inorganic Chemistry*; 6th ed.; Oxford University Press: Oxford, United Kingdom, 2014; pp. 237-238.

84. Pavia, D. L.; Lampman, G. M.; Kriz, G. S. Ultraviolet Spectroscopy. In *Introduction to Spectroscopy*; 3rd ed.; Thomson Learning, Inc: United States of America, 2001; pp. 356.
85. Coyle, J. D. What is Organic Photochemistry? In *Introduction to Organic Photochemistry*; John Wiley & Sons Ltd: New York, 1986; pp. 14.
86. Shah, R. S.; Shah, R. R.; Pawar, R. B.; Gayakar, P. P. UV-Visible Spectroscopy-A Review. *IJIPLS*. **2015**, *5* (5), 490-505.
87. Weller, M; Overton, T.; Rourke, J.; Armstrong, F. *d*-Metal Complexes: Electronic Structure and Properties. In *Inorganic Chemistry*; 6th ed.; Oxford University Press: Oxford, United Kingdom, 2014; pp. 540-543.
88. Lüttke, W. Spektroskopische Untersuchungen an Nitroso-Verbindungen 2. Mitteilung: Schwingungsfrequenz und Bindungscharakter von NO-Bindungen als Argumente zur Strukturbestimmug der Nitroso-Dimeren. *Z. Elektrochem*, **1957**, *61*, 976-986.
89. Pavia, D. L.; Lampman, G. M.; Kriz, G. S. Infrared Spectroscopy. In *Introduction to Spectroscopy*; 3rd ed.; Thomson Learning, Inc: United States of America, 2001; pp. 26.
90. Bain, G. A.; Berry, J. F. Diamagnetic Corrections and Pascal's Constants. *J. Chem. Educ.* **2008**, *85* (4), 532-536.
91. Weller, M; Overton, T.; Rourke, J.; Armstrong, F. *d*-Metal Complexes: Electronic Structure and Properties. In *Inorganic Chemistry*; 6th ed.; Oxford University Press: Oxford, United Kingdom, 2014; pp. 520-521.
92. Cotton, F. A.; Wilkinson, G. The Transition Elements and the Electronic Structures of Their Compounds. In *Advanced Inorganic Chemistry*; 4th ed.; John Wiley & Sons, Inc: New York, 1980; pp. 628.

93. Larsen, E.; La Mar, G. N.; Wagner, B. E.; Parks, J. E.; Holm, R. H. Three-Dimensional Macrocyclic Encapsulation Reactions. III. Geometrical and Electronic Features of Tris(141iamine) Complexes of Trigonal-Prismatic, Antriprismatic, and Intermediate Stereochemistry. *Inorg. Chem.* **1972**, *11* (11), 2652-2668.

94. Weil, J. A.; Bolton, J. R. Basic Principles of Paramagnetic Resonance. In *Electron Paramagnetic Resonance: Elementary Theory and Practical Applications*; 2nd ed.; Wiley-Interscience: Hoboken, New Jersey, 2007; pp. 1-3.

95. Weller, M; Overton, T.; Rourke, J.; Armstrong, F. Physical Techniques in Inorganic Chemistry. In *Inorganic Chemistry*; 6th ed.; Oxford University Press: Oxford, United Kingdom, 2014; pp. 253.

96. Weil, J. A.; Bolton, J. R. Systems with More Than One Unpaired Electron. In *Electron Paramagnetic Resonance: Elementary Theory and Practical Applications*; 2nd ed.; Wiley-Interscience: Hoboken, New Jersey, 2007; pp. 158-159.

97. Ball, D. W. Atoms and Molecules. In *Physical Chemistry*; India ed.; Cengage Learning: New Delhi, India, 2003; pp. 413-414.

98. (a) Dieterich, D. A.; Paul, I. C.; Curtin, D. Y., Crystal Structure of Nitrosobenzene Dimer. *cis*-Azobenzene Dioxide. *J. Chem. Soc. D.* **1970**, 1710-1711. (b) Dieterich, D. A.; Paul, I. C.; Curtin, D. Y., Structural Studies on Nitrosobenzene and 2-Nitrosobenzoic Acid. Crystal and Molecular Structures of *cis*-Azobenzene Dioxide and *trans*-2,2'-Dicarboxyazobenzene Dioxide. *J. Am. Chem. Soc.* **1974**, *96*, 6372-6380.

99. (a) Lightfoot, A. P.; Pritchard, R. G.; Wan, H.; Warren, J. E.; Whiting, A. A Novel Scandium *ortho*-Methoxynitrosobenzene-Dimer Complex: Mechanistic Implications

for the Nitroso-Diels-Alder Reaction. *Chem. Comm.* **2002**, 2072-2073. (b) Fitts, L. S.; Bierschenk, E. J.; Hanusa, T. P.; Rheingold, A. L.; Pink, M.; Young Jr., V. G. Selective Modification of the Metal Coordination Environment in Heavy Alkaline-Earth Iodide Complexes. *New J. Chem.* **2016**, *40*, 8229-8238. (c) Srivastava, R. S.; Nicholas, K. M. On the Mechanism of Allylic Amination Catalyzed by Iron Salts. *J. Am. Chem. Soc.* **1997**, *119* (14), 3302-3310. (d) Emhoff, K. A.; Balaraman, L.; Simpson, S. R.; Stromyer, M. L.; Kalil, H. F.; Beemiller, J. R.; Sikatzki, P.; Eshelman, T. S.; Salem, A. M. H.; DeBord, M. A.; Panzner, M. J.; Youngs, W. J.; Boyd, W. C. Synthesis and Characterization of Cobalt(II) *N,N′*-Diphenylazodioxide Complexes. *ACS Omega.* **2018**, *3* (11), 16021-16027.

100. Emhoff, K. A.; Balaraman, L.; Salem, A. M. H.; Mudarmah, K. I.; Boyd, W. C. Coordination Chemistry of Organic Nitric Oxide Derivatives. *Coord. Chem. Rev.* **2019**, *396*, 124-140.
101. Lee, J.; Chen, L.; West, A. H.; Richter-Addo, G. B. Interactions of Organic Nitroso Compounds with Metals. *Chem. Rev.* **2002**, *102*, 1019-1065.
102. Srivastava, R. S.; Khan, M. A.; Nicholas, K. M. Nitrosoarene-Cu(I) Complexes are Intermediates in Copper-Catalyzed Allylic Amination. *J. Am. Chem. Soc.* **2005**, *127*, 7278-7279.
103. (a) Tomson, N. C.; Labios, L. A.; Weyhermüller, T.; Figueroa, J. S.; Weighardt, K. Redox Noninnocence of Nitrosoarene Ligands in Transition Metal Complexes. *Inorg. Chem.* **2011**, *50*, 5763-5776. (b) Kundu, S.; Stieber, S. C. E.; Ferrier, M. G.; Kozimor, S. A.; Bertke, J. A.; Warren, T. H. Redox Non-innocence of Nitrosobenzene at Nickel. *Angew. Chem. Int. Ed.* **2016**, *55*, 10321-10325. (c) Askari, M. S.; Girard, B.;

Murugesu, M.; Ottenwaelder, X. The Two Spin States of an End-on Copper(II)-Superoxide Mimic. *Chem. Commun.* **2011**, *47*, 8055-8057.

104. Wiese, S.; Kapoor, P.; Williams, K. D.; Warren, T. H. Nitric Oxide Oxidatively Nitrosylates Ni(I) and Cu(I) C-organonitroso Adducts. *J. Am. Chem. Soc.* **2009**, *131*, 18105-18111.

105. (a) Kalyanasundaram, K. Photophysics, Photochemistry, and Solar Energy Conversion with Tris(bipyridyl)ruthenium(II) and Its Analogues. *Coord. Chem. Rev.* **1982**, *46*, 159-244. (b) Juris, A.; Balzani, V.; Barigelletti, F.; Campagna, S.; Belser, P.; von Zelewsky, A. Ru(II) Polypyridine Complexes: Photophysics, Photochemistry, Electrochemistry, and Chemoluminescence. *Coord. Chem. Rev.* **1988**, *84*, 85-277. (c) Sullivan, B. P.; Salmon, D. J.; Meyer, T. J. Mixed Phosphine 2,2′-Bipyridine Complexes of Ruthenium. *Inorg. Chem.* **1978**, *17*, 3334-3341.

106. Elgrishi, N.; Rountree, K. J.; McCarthy, B. D.; Rountree, E. S.; Eisenhart, T. T.; Dempsey, J. L. A Practical Beginner's Guide to Cyclic Voltammetry. *J. Chem. Educ.* **2018**, *95*, 197-206.

107. Kaim, W.; Fiedler, J. Spectroelectrochemistry: The Best of Two Worlds. *Chem. Soc. Rev.* **2009**, *38*, 3373-3382.

108. Huang, Y.; Lessard, J. Electrochemical Behavior of Nitrobenzene, Nitrosobenzene, Azobenzene, and Azoxybenzene on Hg, Pt, Cu, and Ni Electrodes in Aprotic Medium. *Electroanal.* **2016**, *28*, 2716-2727.

109. (a) Mann, C. K.; Barnes, K. K. Nitro and Nitroso Compounds. In *Electrochemical Reactions in Nonaqueous Systems*; Marcel Dekker Inc: New York, 1970; pp. 349-371. (b) Kemula, W.; Krygowski, T. M. Arsenic. In *Encyclopedia of the Electrochemistry*

of the Elements; 1st ed.; Vol. 2; Marcel Dekkar Inc: New York, 1973; pp. 21-51. (c) Lund, H. Cathodic Reduction of Nitro Compounds. In *Organic Electrochemistry*; Marcel Dekker Inc: New York, 1983; pp. 295-306.

110. Kemula, W.; Sioda, R. Polarography and Electrolysis of Nitrobenzene and Nitrosobenzene in Dimethylformamide. *Bull.Acad. Polon. Sci. Sér. Sci. Chim*. **1962**, *10*, 507 – 512.

111. (a) Lipsztajn, M.; Krygowski, T. M.; Laren, E.; Galus, Z. Electrochemical Investigations of Intermediates in Electroreduction of Aromatic Nitro and Nitroso Compounds in *N,N*-Dimethylformamide: Part II. Electrochemical Behavior of Nitrosobenzene. *J. Electroanal. Chem*. **1974**, *57*, 339-350. (b) Zuman, P.; Shah, B. Addition, Reduction, and Oxidation Reactions of Nitrosobenzene. *Chem. Rev*. **1994**, *94*, 1621-1641.

112. Hammerich, O. Reduction of Nitro Compounds and Related Substrates. In *Organic Electrochemistry*; 5th ed.; CRC Press, Taylor & Francis Group: Boca Raton, 2016; pp. 1149-1165.

113. Lipsztajn, M.; Krygowski, T. M.; Laren, E.; Galus, Z. Electrochemical Investigations of Intermediates in Electroreduction of Aromatic Nitro and Nitroso Compounds in DMF: Part I. Electrochemical Behavior of Azoxybenzene. *J. Electroanal. Chem*. **1974**, *54*, 313-320.

114. (a) Sadler, J. L.; Bard, A. J. The Electrochemical Reduction of Aromatic Azo Compounds. *J. Am. Chem. Soc*. **1968**, *90* (8), 1979-1989. (b) Troll, T.; Baizer, M. M. Synthetic Utilisation of Electrogenerated Bases-II Reduced Azobenzene as Base and Nucleophile. *Electrochim. Acta*. **1975**, *20* (1), 33-36. (c) Cheng, S.; Hawley, M. D.

Electrogenerated Bases: The Role of Weak Electroinactive Proton Donors and the Effect of Electrocatalysis on the Redox Behavior of Azobenzene. *J. Org. Chem.* **1985**, *50* (18), 3388-3392.

115. Askari, M. S.; Effaty, F.; Gennarini, F.; Orio, M.; Le Poul, N.; Ottenwaelder, X. Tuning Inner Sphere Electron Transfer in a Series of Copper/Nitrosoarene Adducts. *Inorg. Chem.* **2020**, *59*, 8678-8689.
116. Balaraman, L.; Emhoff, K. A.; Salem, A. M. H.; Hanna, J.; Alsabony, M. N.; Bayachou, M.; Mundell, J. J.; Boyd, W. C. Electrochemical Studies of Cobalt(II) Diphenylazodioxide Complexes. *Inorg. Chim. Acta* **2020**, *501*, 1-8.
117. Ferreira, H.; Conradie, M. M.; Conradie, J. Electrochemical and Electronic Properties of a Series of Substituted Polypyridine Ligands and their Co(II) Complexes. *Inorg. Chim. Acta* **2019**, *486*, 26-35.
118. Ferreira, H.; Conradie, M. M.; Conradie, J. Electrochemical Properties of a Series of Co(II) Complexes, Containing Substituted Phenanthrolines. *Electrochim. Acta* **2018**, *292*, 489-501.
119. Aroua, S.; Todorova, T. K.; Hommes, P.; Chamoreau, L.-M.; Reissig, H.-U.; Mougel, V.; Fontecave, M. Synthesis, Characterization, and DFT Analysis of bis-Terpyridyl Based Molecular Cobalt Complexes. *Inorg. Chem.* **2017**, *56*, 5930-5940.
120. Cabral, D.; Howlett, P. C.; Pringle, J. M.; Zhang, X.; MacFarlane, D. Electrochemistry of tris(2,2'-Bipyridyl) cobalt(II) in Ionic Liquids and Aprotic Molecular Solvents on Glassy Carbon and Platinum Electrodes. *Electrochim. Acta* **2015**, *180*, 419-426.
121. Monk, P. M. S. Analysis by Dynamic Measurement, A: Systems Under Diffusion Control. In *Fundamentals of Electroanalytical Chemistry*; John Wiley & Sons Ltd:

Chichester, UK, 2001; pp. 156-169.

122. Bard, A. J.; Faulkner, L. R. Potential Sweep Methods. In *Electrochemical Methods: Fundamentals and Applications*; 2nd ed.; John Wiley & Sons, Inc: Hoboken, NJ, 2001; pp. 236-239.

123. Bard, A. J.; Faulkner, L. R. Electrode Reactions with Coupled Homogeneous Chemical Reactions. In *Electrochemical Methods: Fundamentals and Applications*; 2nd ed.; John Wiley & Sons, Inc: Hoboken, NJ, 2001; pp. 509-512.

124. Nicholson, R. S. Theory and Application of Cyclic Voltammetry for Measurement of Electrode Reaction Kinetics. *Anal. Chem.* **1965**, *37*, 1351-1355.

125. Nadjo, L.; Saveant, J. M. Linear Sweep Voltammetry: Kinetic Control by Charge Transfer and/or Secondary Chemical Reactions: I. Formal Kinetics. *Electroanal. Chem. Interfac Electrochem.* **1973**, *48*, 113-145.

126. Heath, G. A.; Yellowlees, L. J.; Braterman, P. S. Spectro-electrochemical Studies on tris-Bipyridyl Ruthenium Complexes; Ultra-Violet, Visible, and Near-Infrared Spectra of the Series $[Ru(bipyridyl)_3]^{2+/1+/0/1-}$ *J. Chem. Soc. Chem. Commun.* **1981**, 287-289.

127. Gagne, R. R.; Koval, C. A.; Lisensky, G. C. Ferrocene as an Internal Standard for Electrochemical Measurements. *Inorg. Chem.* **1980**, *19*, 2854-2855.

128. (a) Praneeth, V. K. K.; Ringenberg, M. R.; Ward, T. R. Redox-Active Ligands in Catalysis. *Angew. Chem. Int.* **2012**, *51*, 10228-10234. (b) Luca, O. R.; Crabtree, R. H. Redox-Active Ligands in Catalysis. *Chem. Soc. Rev.* **2013**, *42*, 1440-1459.

129. Balaraman, L.; Emhoff, K. A.; Salem, A. M. H.; Hanna, J.; Alsabony, M. N.; Bayachou, M.; Mundell, J. J.; Boyd, W. C. Electrochemical Studies of Cobalt(II)

Diphenylazodioxide Complexes. *Inorg. Chim. Acta* **2020**, *501*, 1-8.

130. Akutagawa, K.; Tani, K. Asymmetric Isomerization of Allylamines. In *Catalytic Asymmetric Synthesis*; 2nd ed.; Wiley-VCH, Inc: New York, 2000; pp. 145-161.
131. Nicolaou, K. C.; Bulger, P. G.; Sarlah, D. Metathesis Reactions in Total Synthesis. *Angew. Chem. Int. Ed.* **2005**, *44*, 4490-4527.
132. Banerjee, D.; Jagadeesh, R. V.; Junge, K.; Junge, H.; Beller, M. An Efficient and Convenient Palladium Catalyst System for the Synthesis of Amines from Allylic Alcohols. *ChemSusChem*. **2012**, *5*, 2039-2044.
133. (a) Magnus, P.; Lacour, J.; Coldham, I.; Mugrage, B.; Bauta, W. B. New Trialkylsilyl Enol Ether Chemistry: α-N-tosylamination of Triisopropylsilyl Enol Ethers. *Tetrahedron*. **1995**, *51*, 11087-11110. (b) Trost, B. M. Cyclizations via Palladium Catalyzed Allylic Alkylations. *Angew. Chem. Int. Ed.* **1989**, *28* (9), 1173-1192. (c) Jamieson, A. G.; Sutherland, A. Ether-Directed, Stereoselective Aza-Claisen Rearrangements: Synthesis of the Piperidine Alkaloid, α-Conhydrine. *Org. Lett.* **2007**, *9* (8), 1609-1611. (d) Farwick, A.; Helmchen, G. Enantioselective Total Synthesis of (-)-α-Kainic Acid. *Org. Lett.* **2010**, *12* (5), 1108-1111.
134. (a) Trost, B. M.; Van Vranken D. L. A General Synthetic Strategy Toward Aminocyclopentitol Glycosidase Inhibitors. Application of Palladium Catalysis to the Synthesis of Allosamizoline and Mannostatin A. *J. Am. Chem. Soc.* **1993**, *115* (2), 444-458. (b) Friestad, G. K.; Jiang, T.; Mathies, A. K. Aldehyde-Selective Wacker Oxidation in a Thiyl-Mediated Vinyl Group Transfer Route to Daunosamine. *Org. Lett.* **2007**, *9* (5), 777-780.

135. (a) Hayashi, T.; Yamamoto, A.; Ito, Y.; Nishioka, E.; Miura, H.; Yanagi, K. Asymmetric Synthesis Catalyzed by Chiral Ferrocenylphosphine-Transition-Metal Complexes. 8. Palladium-Catalyzed Asymmetric Allylic Amination. *J. Am. Chem. Soc.* **1989**, *111* (16), 6301-6311. (b) Burgess, K.; Liu, L. T.; Pal, B. Asymmetric Syntheses of Optically Active .Alpha.,.Beta.-Disubstituted .Beta.-Amino Acids. *J. Org. Chem.* **1993**, *58* (17), 4758-4763. (c) Jumnah, R.; Williams, J. M. J.; Williams, A. C. Synthesis of *N*-Protected Amino Esters via Palladium-Catalyzed Allylic Substitution. *Tetrahedron Lett.* **1993**, *34* (41), 6619-6622. (d) Bower, J. F.; Jumnah, R.; Williams, A. C.; Williams, J. M. J. Palladium-Catalyzed Asymmetric Allylic Substitution: Synthesis of α- and β-Amino acids. *J. Chem. Soc., Perkin Trans. 1.* **1997**, 1411-1420.

136. Johannsen, M.; Jørgensen, K. A. Allylic Amination. *Chem. Rev.* **1998**, *98* (4), 1689-1708.

137. Selva, E.; Sempere, Y.; Ruiz-Martínez, D.; Pablo, O.; Guijarro, D. Synthesis of Allylic Amines by Asymmetric Transfer Hydrogenation or α,β-Unsaturated N-(tert-Butylsulfinyl)imines. *J. Org. Chem.* **2017**, *82* (24), 13693-13699.

138. Ye, Z.; Brust, T. F.; Watts, V. J.; Dai, M. Palladium-Catalyzed Regio- and Stereoselective γ-Arylation of Tertiary Allylic Amines: Identification of Potent Adenylyl Cyclase Inhibitors. *Org. Lett.* **2015**, *17*, 892-895.

139. Petranyi, G.; Meingassner, J. G.; Mieth, H. Antifungal Activity of the Allylamine Derivative Terbinafine In Vitro. *Antimicrob. Agents Chemother.* **1987**, *31* (9), 1365-1368.

140. World Health Organization Model List of Essential Medicines; 21st ed.; World Health Organization, 2019.

141. Hofmann, C.; Penner, U.; Dorow, R.; Pertz, H. H.; Jähnichen, S.; Horowski, R.; Latté, K. P.; Palla, D.; Schurad, B. Lisuride, a Dopamine Receptor Agonist with 5-HT$_{2B}$ Receptor Antagonist Properties: Absence of Cardiac Valvulopathy Adverse Drug Reaction Reports Supports the Concept of a Crucial Role for 5-HT$_{2B}$ Receptor Agonism in Cardiac Valvular Fibrosis. *Clin. Neuropharmacol.* **2006**, *29* (2), 80-86.

142. Connelly, J. F. Vigabatrin. *Ann. Pharmacother.* **1993**, *27* (2), 197-204.

143. Srivastava, A.; Ma, Y.; Pankayatselvan, R.; Dinges, W.; Nicholas, K. M. Molybdenum-Catalysed Allylic Amination. *J. Chem. Soc., Chem. Commun.* **1992**, 853-854.

144. Johannsen, M.; Jørgensen, K. A. Iron-Catalyzed Allylic Amination. *J. Org. Chem.* **1994**, *59* (1), 214-216.

145. Srivastava, R. S.; Nicholas, K. M. Regioselective Allylic Amination Catalyzed by Iron Salts. *Tetrahedron Lett.* **1994**, *35* (47), 8739-8742.

146. Srivastava, R. S.; Nicholas, K. M. On the Mechanism of Allylic Amination Catalyzed by Iron Salts. *J. Am. Chem. Soc.* **1997**, *119* (14), 3302-3310.

147. Srivastava, R. S.; Tarver, N. R.; Nicholas, K. M. Mechanistic Studies of Copper(I) Catalyzed Allylic Amination. *J. Am. Chem. Soc.* **2007**, *129* (49), 15250-15258.

148. Carey, F. A.; Giuliano, R. M. Structure and Preparation of Alkenes: Elimination Reactions. In *Organic Chemistry*; 9th ed.; McGraw-Hill: New York, 2014; pp. 190.

149. Leach, A. G.; Houk, K. N. Diels-Alder and Ene Reactions of Singlet Oxygen, Nitroso Compounds and Triazolinediones: Transition States and Mechanisms from

Contemporary Theory. *Chem. Commun.* **2002**, 1243-1255.

150. Emhoff, K. A.; Balaraman, L.; Salem, A. M. H.; Mudarmah, K. I.; Boyd, W. C. Coordination Chemistry of Organic Nitric Oxide Derivatives. *Coord. Chem. Rev.* **2019**, *396*, 124-140.
151. Emhoff, K. A.; Salem, A. M. H.; Balaraman, L.; Kingery, D. M.; Boyd, W. C. Allylic Amination and Carbon–Carbon Double Bond Transposition Catalyzed by Cobalt(II) Azodioxide Complexes. *Results in Chemistry*. **2020**, *2*, 1-5.
152. Srivastava, R. S.; Khan, M. A.; Nicholas, K. M. A Novel Intermediate in Allylic Amination Catalyzed by Iron Salts. *J. Am. Chem. Soc.* **1996**, *118* (13), 3311-3312.
153. Kürti, L.; Czakó, B. Alder (Ene) Reaction (Hydro-Allyl Addition). In *Strategic Applications of Named Reactions in Organic Synthesis: Background and Detailed Mechanisms*; Elsevier Academic Press: New York, 2005; pp. 6-7.
154. Weller, M; Overton, T.; Rourke, J.; Armstrong, F. *d*-Metal Organometallic Chemistry. In *Inorganic Chemistry*; 6th ed.; Oxford University Press: Oxford, United Kingdom, 2014; pp.585.
155. Butt, N. A.; Zhang, W. Transition Metal-Catalyzed Allylic Substitution Reactions with Unactivated Allylic Substrates. *Chem. Soc. Rev.* **2015**, *44*, 7929-7967.
156. Sundararaju, B.; Achard, M.; Bruneau, C. Transition Metal Catalyzed Nucleophilic Allylic Substitution: Activation of Allylic Alcohols via π-Allylic Species. *Chem. Soc. Rev.* **2012**, *41*, 4467-4483.
157. (a) Guérinot, A.; Serra-Muns, A.; Gnamm, C.; Bensoussan. C.; Reymond, S.; Cossy, J. $FeCl_3$-Catalyzed Highly Diastereoselective Synthesis of Substituted Piperidines and Tetrahydropyrans. *Org. Lett.* **2010**, *12* (8), 1808-1811. (b) Bricout, H.; Carpentier,

J. F.; Mortreux, A. Nickel vs. Palladium Catalysts for Coupling Reactions of Allyl Alcohol with Soft Nucleophiles: Activities and Deactivation Processes. *J. Mol. Catal. A Chem.* **1998**, *136* (3), 243-251.

158. Emayavaramban, B.; Roy, M.; Sundararaju, B. Iron-Catalyzed Allylic Amination Directly From Allylic Alcohols. *Chem. Eur. J.* **2016**, *22*, 3952-3955.
159. Weller, M; Overton, T.; Rourke, J.; Armstrong, F. Catalysis. In *Inorganic Chemistry*; 6th ed.; Oxford University Press: Oxford, United Kingdom, 2014; pp. 731.
160. Pavia, D. L.; Lampman, G. M.; Kriz, G. S. Mass Spectrometry. In *Introduction to Spectroscopy*; 3rd ed.; Thomson Learning, Inc: United States of America, 2001; pp. 394.
161. Smoluch, M.; Piechura, K. Basic Definitions. In *Mass Spectrometry: An Applied Approach*; 2nd ed.; John Wiley & Sons, Inc: Hoboken, New Jersey, 2019; pp. 10.
162. Günther, H. General Experimental Aspects of Nuclear Magnetic Resonance Spectroscopy. In *NMR Spectroscopy: Basic Principles, Concepts, and Applications in Chemistry*. 3rd ed.; Wiley-VCH: Weinheim, Germany, 2013; 74-78.
163. Pavia, D. L.; Lampman, G. M.; Kriz, G. S. Nuclear Magnetic Resonance Spectroscopy Part One: Basic Concepts. In *Introduction to Spectroscopy*; 3rd ed.; Thomson Learning, Inc: United States of America, 2001; pp. 124.
164. Pavia, D. L.; Lampman, G. M.; Kriz, G. S. Nuclear Magnetic Resonance Spectroscopy Part Three: Spin-Spin Coupling. In *Introduction to Spectroscopy*; 3rd ed.; Thomson Learning, Inc: United States of America, 2001; pp. 270.
165. Carey, F. A.; Giuliano, R. M. Chirality. In *Organic Chemistry*; 9th ed.; McGraw-Hill: New York, 2014; pp. 282.

166. Carey, F. A.; Giuliano, R. M. Chirality. In *Organic Chemistry*; 9th ed.; McGraw-Hill: New York, 2014; pp. 263.

167. Van Gorkom, M.; Hall, G. E. Equivalence of Nuclei in High-Resolution Nuclear Magnetic Resonance Spectroscopy. *Q. Rev. Chem. Soc.* **1968**, *22* (1), 14-29.

168. Gottlieb, H. E.; Kotlyar, V.; Nudelman, A. NMR Chemical Shifts of Common Laboratory Solvents as Trace Impurities. *J. Org. Chem.* **1997**, *62* (21), 7512-7515.

169. Pavia, D. L.; Lampman, G. M.; Kriz, G. S. Nuclear Magnetic Resonance Spectroscopy Part Three: Spin-Spin Coupling. In *Introduction to Spectroscopy*; 3rd ed.; Thomson Learning, Inc: United States of America, 2001; pp. 220.

170. Emhoff, K. A.; Balaraman, L.; Simpson, S. R.; Stromyer, M. L.; Kalil, H. F.; Beemiller, J. R.; Sikatzki, P.; Eshelman, T. S.; Salem, A. M. H.; DeBord, M. A.; Panzner, M. J.; Youngs, W. J.; Boyd, W. C. Synthesis and Characterization of Cobalt(II) *N,N′*-Diphenylazodioxide Complexes. *ACS Omega* **2018**, *3* (11), 16021-16027.

171. Mayo Clinic Staff. "Vitamin B_{12}." *Mayo Clinic*, Mayo Foundation for Medical Education and Research, 2017, https://www.mayoclinic.org/drugs-supplements-vitamin-b12/art-20363663.

172. Schwartz, J. A.; Lium, E. K.; Silverstein, S. J. Herpes Simplex Virus Type 1 Entry is Inhibited by the Cobalt Chelate Complex CTC-96. *J. Virol.* **2001**, *75* (9), 4117-4128.

173. Epstein, S. P.; Wallace, J. A.; Epstein, D.; Stewart, C. C.; Burger, R. M. Efficacy of Cobalt Chelates in the Rabbit Eye Model for Epithelial Herpetic Keratitis. *Cornea.* **1998**, *17* (5), 550-557.

174. Epstein, S. P.; Pashinsky, Y. Y.; Gershon, D.; Winicov, I.; Srivilasa, C.; Kristic, K. J.; Asbell, P. A. Efficacy of Topical Cobalt Chelate CTC-96 Against Adenovirus in a Cell Culture Model and Against Adenovirus Keratoconjunctivitis in a Rabbit Model. *BMC Ophthalmol.* **2006**, *6* (22), 1-11.

175. Mjos, K. D.; Orvig, C. Metallodrugs in Medicinal Inorganic Chemistry. *Chem. Rev.* **2014**, *114*, 4540-4563.

176. Elmore, S. Apoptosis: A Review of Programmed Cell Death. *Toxicol. Pathol.* **2007**, *35* (4), 495-516.

177. Norbury, C. J.; Hickson, I. D. Cellular Responses to DNA Damage. *Annu. Rev. Pharmacol. Toxicol.* **2001**, *41*, 367-401.

178. (a) Savill, J.; Fadok, V. Corpse Clearance Defines the Meaning of Cell Death. *Nature*. **2000**, *407*, 784-788. (b) Kurosaka, K.; Takahashi, M.; Watanabe, N.; Kobayashi, Y. Silent Cleanup of Very Early Apoptotic Cells by Macrophages. *J. Immunol.* **2003**, *171*, 4672-4679.

179. McConkey, D. J. Biochemical Determinants of Apoptosis and Necrosis. *Toxicol. Lett.* **1998**, *99* (3), 157-168.

180. Ventimiglia, R.; Lau, L.; Kinloch, R. A.; Hopkins, A.; Karran, E. H.; Petalidis, L. P.; Ward, R. V. Role of Caspases in Neuronal Apoptosis. *Drug Dev. Res.* **2001**, *52* (4), 515-533.

181. Widmann, C.; Gibson, S.; Johnson, G. L. Caspase-Dependent Cleavage of Signaling Proteins During Apoptosis. *J. Biol. Chem.* **1998**, *273* (12), 7141-7147.

182. (a) Siddiqui, W. A.; Ahad, A.; Ahsan, H. The Mystery of Bcl-2 Family: Bcl-2 Proteins and Apoptosis: An Update. *Arch. Toxicol.* **2015**, *89*, 289-317. (b) Knight, T.; Luedtke,

D.; Edwards, H.; Taub, J. W.; Ge, Y. A Delicate Balance-The Bcl-2 Family and its Role in Apoptosis, Oncogenesis, and Cancer Therapeutics. *Biochem. Pharmacol.* **2019**, *162*, 250-261.

183. (a) Fridman, J. S.; Lowe, S. W. Control of Apoptosis by p53. *Oncogene*. **2003**, *22*, 9030-9040. (b) Attardi, L. D.; Lowe, S. W.; Brugarolas, J.; Jacks, T. Transcriptional Activation by p53, but Not Induction of the p21 gene, is Essential for Oncogene Mediated Apoptosis. *EMBO J.* **1996**, *15*, 3693-3701. (c) Chen, X.; K. L. J.; Jayaraman, L.; Prives, C. p53 Levels, Functional Domains, and DNA Damage Determine the Extent of the Apoptotic Response of Tumor Cells. *Genes Dev.* **1996**, *10*, 2438-2451.
184. (a) Soldani, C.; Scovassi, A. I. Poly(ADP-ribose) Polymerase-1 Cleavage During Apoptosis: An Update. *Apoptosis*. **2002**, *7*, 321-328. (b) Kaufmann, S. H.; Desnoyers, S.; Ottaviano, Y.; Davidson, N. E.; Poirier, G. G. Specific Proteolytic Cleavage of Poly(ADP-ribose) Polymerase: An Early Marker of Chemotherapy-Induced Apoptosis. *Cancer Res.* **1993**, *53* (17), 3976-3985.
185. Pfeffer, C. M.; Singh, A. T. K. Apoptosis: A Target for Anticancer Therapy. *Int. J. Mol. Sci.* **2018**, *19*, 448-457.
186. (a) Zaman, S.; Wang, R.; Gandhi, V. Targeting the Apoptosis Pathway in Hematologic Malignancies. *Leuk. Lymphoma*. **2014**, *55*, 1980-1992. (b) Liu, H.; Su, D.; Zhang, J.; Ge, S.; Li, Y.; Wang, F.; Gravel, M.; Roulston, A.; Song, Q.; Xu, W.; Liang, J. G.; Shore, G.; Wang, X.; Liang, P. Improvement of Pharmacokinetic Profile of TRAIL via Trimer-Tage Enhances its Antitumor Activity In Vivo. *Sci. Rep.* **2017**, *7*, 8953-8963.

187. Xu, W.; Jing, L.; Wang, Q.; Lin, C. C.; Chen, X.; Diao, J.; Liu, Y.; Sun, X. Bas PGAM5L-Drp1 Complex is Required for Intrinsic Apoptosis Execution. *Oncotarget*. **2015**, *6*, 30017-30034.

188. Hassan, M.; Watari, H.; AbuAlmaaty, A.; Ohba, Y.; Sakuragi, N. Apoptosis and Molecular Targeting Therapy in Cancer. *BioMed Res. Int*. **2014**, *2014*, 1-23.

189. (a) Lomonosova, E.; Chinnadurai, G. BH_3-Only Proteins in Apoptosis and Beyond: An Overview. *Oncogene*. **2008**, *27*, S2-S19. (b) Hill, M. M.; Adrain, C.; Duriez, P. J.; Creagh, E. M.; Martin, S. J.; Analysis of the Composition, Assembly Kinetics and Activity of Native APAF-1 Apoptosomes. *EMBO J*. **2004**, *23*, 2134-2145. (c) Green, D. R.; Llambi, F. Cell Death Signaling. *Cold Spring Harb. Perspect. Biol*. 2015, 7, 1-24.

190. Lopez, J.; Tait, S. W. G. Mitochondrial Apoptosis: Killing Cancer Using the Enemy Within. *Br. J. Cancer*. **2015**, *112*, 957-962.

191. Arbiser, J. L.; Bonner, M. Y.; Gilbert, L. C. Targeting the Duality of Cancer. *NPJ Precis. Oncol*. **2017**, *1*, 1-7.

192. (a) Liu, Y.; Zhu, X. Endoplasmic Reticulum-Mitochondria Tethering in Neurodegenerative Diseases. *Transl. Neurodegener*. **2017**, *6*, 21-28. (b) Villa Pulgarín, J. A.; Gajate, C.; Botet, J.; Jimenez, A.; Justies, N.; Varela-M, R. E. Cuesta Marbán, A.; Müller, I.; Modolell, M.; Revuelta, J. L.; Mollinedo, F. Mitochondria and Lipid Raft-Located FoF1-ATP Synthase as Major Therapeutic Targets in the Antileishmanial and Anticancer Activities of Ether Lipid Edelfosine. *PLoS Negl. Trop. Dis*. **2017**, *11*, 1-31. (c) Bao, H.; Zhang, Q.; Zhu, Z.; Xu, H.; Ding, F.; Wang, M.; Du, S.; Du, Y.; Yan, Z. BHX, A Novel Pyrazoline Derivative, Inhibits Breast

Cancer Cell Invasion by Reversing the Epithelial Mesenchymal Transition and Down Regulating Wnt/β Catenin Signaling. *Sci. Rep.* **2017**, *7*, 9153-9162.

193. Rosenberg, B.; VanCamp, L.; Trosko, J. E.; Mansour, V. H. Platinum Compounds: A New Class of Potent Antitumour Agents. *Nature* **1969**, *222*, 385-386.
194. Alderden, R. A.; Hall, M. D.; Hambley, T. W. The Discovery and Development of Cisplatin. *J. Chem. Educ.* **2006**, *83* (5), 728-734.
195. Bruijnincx, P. C. A.; Sadler, P. J. New Trends for Metal Complexes with Anticancer Activity. *Curr. Opin. Chem. Biol.* **2008**, *12*, 197-206.
196. Jung, Y.; Lippard, S. J. Direct Cellular Responses to Platinum-Induced DNA Damage. *Chem. Rev.* **2007**, *107* (5), 1387-1407.
197. Siddik, Z. H. Cisplatin: Mode of Cytotoxic Action and Molecular Basis of Resistance. *Oncogene*. **2003**, *22*, 7265-7279.
198. (a) El-Khateeb, M.; Appleton, T. G.; Gahan, L. R.; Charles, B. G.; Berners-Price, S. J.; Bolton, A. M. Reactions of Cisplatin Hydrolytes with Methionine, Cysteine, and Plasma Ultrafiltrate Studied by a Combination of HPLC and NMR Techniques. *J. Inorg. Biochem*. **1999**, *77*, 13-21. (b) Kelland, L. R. Preclinical Perspectives on Platinum Resistance. *Drugs*. **2000**, *59*, 1-8.
199. Eastman, A. The Formation, Isolation and Characterization of DNA Adducts Produced by Anticancer Platinum Complexes. *Pharmacol. Ther*. **1987**, *34* (2), 155-166.
200. Wang, D.; Lippard, S. J. Cellular Processing of Platinum Anticancer Drugs. *Nat. Rev. Drug Discovery*. **2005**, *4*, 307-320.

201. (a) Cleare, M. J.; Hoeschele, J. D. Studies of the Antitumor Activity of Group VIII Transition Metal Complexes. Part I. Platinum(II) Complexes. *Bioinorg. Chem.* **1973**, *2* (3), 187-210. (b) Boulikas, T. Clinical Overview on Lipoplatin: A Successful Liposomal Formulation of Cisplatin. *Expert Opin. Invest. Drugs.* **2009**, *18* (8), 1-22.

202. Gandeepan, P.; Müller, T.; Zell, D.; Cera, G.; Warratz, S.; Ackermann, L. 3*d* Transition Metals for C–H Activation. *Chem. Rev.* **2019**, *119*, 2192-2452.

203. Ndagi, U.; Mhlongo, N.; Soliman, M. E. Metal Complexes in Cancer Therapy-An Update from Drug Design Perspective. *Drug Des. Devel. Ther.* **2017**, *11*, 599-616.

204. Alghamdi, N. J.; Balaraman, L.; Emhoff, K. A.; Salem, A. M. H.; Wei, R.; Zhou, A.; Boyd, W. C. Cobalt(II) Diphenylazodioxide Complexes Induce Apoptosis in SK-HEP-1 Cells. *ACS Omega.* **2019**, *4* (11), 14503-14510.

205. Gurley, L.; Beloukhina, N.; Boudreau, K.; Klegeris, A.; McNeil, W. S. The Synthesis and Characterization of a Series of Cobalt(II) β-Ketoaminato Complexes and Their Cytotoxic Activity Towards Human Tumor Cell Lines. *J. Inorg. Biochem.* **2011**, *105*, 858-866.

206. Silva, T. F. S.; Martins, L. M. D. R. S.; Guedes, da Silva, M. F. C.; Fernandes, A. R.; Silva, A.; Borralho, P. M.; Santos, S.; Rodrigues, C. M. P.; Pombeiro, A. J. L. Cobalt Complexes Bearing Scorpionate Ligands: Synthesis, Characterization, Cytotoxicity and DNA Cleavage. *Dalton Trans.* **2012**, *41*, 12888-12897.

207. Tabrizi, L.; Fooladivanda, M.; Chiniforoshan, H. Copper(II), Cobalt(II) and Nickel(II) Complexes of Juglone: Synthesis, Structure, DNA Interaction and Enhanced Cytotoxicity. *Biometals.* **2016**, *29*, 981-993.

208. Zhu, M.; Zhao, H.; Peng, T.; Su, J.; Meng, B.; Qi, Z.; Jia, B.; Feng, Y.; Gao, E. Structure and Cytotoxicity of Zinc(II) and Cobalt(II) Complexes Based on 1,3,5 Tris(1-imidazolyl)benzene. *Appl. Organomet. Chem*. **2019**, *33*, 1-12.

209. Nithya, P.; Rajamanikandan, R.; Simpson, J.; Ilanchelian, M.; Govindajaran, S. Solvent Assisted Synthesis, Structural Characterization and Biological Evaluation of Cobalt(II) and Nickel(II) Complexes of Schiff Bases Generated from Benzyl Carbazate and Cyclic Ketones. *Polyhedron*. **2018**, *145*, 200-217.

210. Qin, Q. P.; Qin, J. L.; Meng, T.; Lin, W. H.; Zhang, C. H.; Wei, Z. Z.; Chen, J. N.; Liu,Y. C.; Liang, H.; Chen, Z. F. High In Vivo Antitumor Activity of Cobalt Oxoisoaporphine Complexes by Targeting G-Quadruplex DNA, Telomerase and Disrupting Mitochondrial Function. *Eur. J. Med. Chem*. **2016**, *124*, 380-392.

211. Todorović, T. R.; Vukašinović, J.; Portalone, G.; Suleiman, S.; Gligorijević, N.; Bjelogrlić, S.; Jovanović, K.; Radulović, S.; Anđelković, K.; Cassar, A.; Filipović, N. R.; Schembri-Wismayer, P. (Chalcogen)semicarbazones and Their Cobalt Complexes Differentiate HL-60 Myeloid Leukaemia Cells and are Cytotoxic Towards Tumor Cell Lines. *Med. Chem. Commun*. **2017**, *8*, 103-111.

212. Zhou, J.; Qi, Y.; Diao, Q.; Wu, L.; Du, X.; Li, Y.; Sun, L. Cytotoxicity of Melittin and Apamin in Human Hepatic L02 and HepG2 Cells *In Vitro*. *Toxin Rev*. **2013**, *32*, 60-67.

213. (a) Beyersmann, D.; Hartwig, A. The Genetic Toxicology of Cobalt. *Toxicol. Appl. Pharmacol*. **1992**, *115*, 137-145. (b) Kasprzak, K. S.; Zastawny, T. H.; North, S. L.; Riggs, C. W.; Diwan, B. A.; Rice, J. M.; Dizdaroglu, M. Oxidative DNA Base Damage in Renal, Hepatic, and Pulmonary Chromatin of Rats After Intraperitoneal

Injection of Cobalt(II) Acetate. *Chem. Res. Toxicol.* **1994**, *7*, 329-335. (c) Beyersmann, D.; Hartwig, A. Carcinogenic Metal Compounds: Recent Insight into Molecular and Cellular Mechanisms. *Arch. Toxicol.* **2008**, *82*, 493-512.

214. Weller, M.; Overton, T.; Rourke, J.; Armstrong, F. The Group 16 Elements. In *Inorganic Chemistry*; 6th ed.; Oxford University Press: Oxford, United Kingdom, 2014; pp. 442.

215. (a) Jo, H. Y.; Kim, Y.; Park, H. W.; Moon, H. E.; Bae, S.; Kim, J.; Kim, D. G.; Paek, S. H. The Unreliability of MTT Assay in the Cytotoxic Test of Primary Cultured Glioblastoma Cells. *Exp. Neurobiol.* **2015**, *24*, 235−245. (b) Ś liwka, L.; Wiktorska, K.; Suchocki, P.; Milczarek, M.; Mielczarek, S.; Lubelska, K.; Cierpał, T.; Łyzwa, P.; Kie˙łbasinski, P.; Jaromin, A.; Flis, A.; Chilmonczyk, Z.´ The Comparison of MTT and CVS Assays for the Assessment of Anticancer Agent Interactions. *PLoS One.* **2016**, *11*, 1-17.

216. Mukhopadhyay, M.; Reddy, M. M.; Maikap, G. C.; Iqbal, J., Cobalt(II)-Catalyzed Conversion of Allylic Alcohols/Acetates to Allylic Amides in the Presence of Nitriles. *J. Org. Chem.* **1995**, *60*, 2670-2676.

217. Emhoff, K. A.; Balaraman, L.; Simpson, S. R.; Stromyer, M. L.; Kalil, H. F.; Beemiller, J. R.; Sikatzki, P.; Eshelman, T. S.; Salem, A. M. H.; DeBord, M. A.; Panzner, M. J.; Youngs, W. J.; Boyd, W. C. Synthesis and Characterization of Cobalt(II) *N,N′*-Diphenylazodioxide Complexes. *ACS Omega* **2018**, *3* (11), 16021-16027.

218. Nami, S. A. A.; Siddiqi, K. S. Unique Keto-Enol Tautomerism in Transition Metal Complexes of Cyanoimidodithiocarbonate. *J. Chem. Res.* **2006**, *2006*, 563-565.

219. Emhoff, K. A.; Balaraman, L.; Salem, A. M. H.; Mudarmah, K. I.; Boyd, W. C. Coordination Chemistry of Organic Nitric Oxide Derivatives. *Coord. Chem. Rev.* **2019**, *396*, 124-140.

220. Lee, J.; Chen, L.; West, A. H.; Richter-Addo, G. B. Interactions of Organic Nitroso Compounds with Metals. *Chem. Rev.* **2002**, *102*, 1019-1065.

221. Emhoff, K. A.; Salem, A. M. H.; Balaraman, L.; Kingery, D. M.; Boyd, W. C. Allylic Amination and Carbon–Carbon Double Bond Transposition Catalyzed by Cobalt(II) Azodioxide Complexes. *Results in Chemistry*. **2020**, *2*, 1-5.

222. Emayavaramban, B.; Roy, M.; Sundararaju, B. Iron-Catalyzed Allylic Amination Directly From Allylic Alcohols. *Chem. Eur. J.* **2016**, *22*, 3952-3955.

223. Alghamdi, N. J.; Balaraman, L.; Emhoff, K. A.; Salem, A. M. H.; Wei, R.; Zhou, A.; Boyd, W. C. Cobalt(II) Diphenylazodioxide Complexes Induce Apoptosis in SK-HEP-1 Cells. *ACS Omega*. **2019**, *4* (11), 14503-14510.

224. (a) Schwartz, J. A.; Lium, E. K.; Silverstein, S. J. Herpes Simplex Virus Type 1 Entry is Inhibited by the Cobalt Chelate Complex CTC-96. *J. Virol.* **2001**, *75* (9), 4117-4128. (b) Epstein, S. P.; Wallace, J. A.; Epstein, D.; Stewart, C. C.; Burger, R. M. Efficacy of Cobalt Chelates in the Rabbit Eye Model for Epithelial Herpetic Keratitis. *Cornea*. **1998**, *17* (5), 550-557. (c) Epstein, S. P.; Pashinsky, Y. Y.; Gershon, D.; Winicov, I.; Srivilasa, C.; Kristic, K. J.; Asbell, P. A. Efficacy of Topical Cobalt Chelate CTC-96 Against Adenovirus in a Cell Culture Model and Against AdenovirusKeratoconjunctivitis in a Rabbit Model. *BMC Ophthalmol.* **2006**, *6* (22), 1-11